INVESTIGATION OF THE OPTICAL PROPERTIES OF NOVEL ORGANIC MACROMOLECULES FOR SOLAR CELL APPLICATIONS

by

Oluwasegun Oluwasina Adegoke

A dissertation submitted in partial fulfillment
of the requirements for the degree of
Doctor of Philosophy
(Chemical Engineering)
in the University of Michigan
2015

Doctoral Committee:

Professor Theodore G. Goodson III, Co-Chair
Professor Emeritus Phillip E. Savage, Co-Chair
Associate Professor Lola Eniola-Adefeso
Associate Professor Jinsang Kim
Professor Michael J. Solomon

DEDICATION

This dissertation is dedicated to Almighty God, who gave me the grace to start the doctoral program and finish it successfully.

ACKNOWLEDGEMENTS

There are many people who have contributed immensely to my ascendancy to this point in my career and to these people I owe a heartfelt gratitude. Right from my time in INRI Experimental Nursery and Primary School, I have had teachers whose enthusiasm and passion to impact knowledge formed the bedrock of my education. Prominent among these teachers was Mr. Antwi who ensured that I had a good foundational knowledge in English Language and Mathematics through the organization of extra tutoring during weekends. He continued this gesture until I gained admission into high school and did not stop until he had to leave for his native country of Ghana. In my high school, efforts of teachers like Mrs Lala, Miss Gbadegesin and many others ensured that my interest in Science did not wane and this culminated in my choice of Chemical Engineering as a career path.

The most memorable time of my formative years as an engineer was spent in Obafemi Awolowo University, Ile-Ife where the all-encompassing training as an engineer was vital to my ability to pursue my engineering interest to the doctorate level. I particularly appreciate the efforts of Dr. Osunleke who served as my academic advisor for most of my time during the college years. His advice and willingness to help at difficult moments were unparalleled. My sincere gratitude also goes to Professor Femi Taiwo who was my research advisor when I had to write my undergraduate dissertation and he was

helpful in developing my computational skills. I am also grateful to Dr. Ayoka who was always very receptive when I come to his office to do internet search on my final year dissertation and helped to save printing cost when I had to deliver my final drafts to the College of Engineering.

In addition, I will not forget to express my sincere gratitude to the staff and faculty of the Departments of Chemistry and Chemical Engineering in the University of Michigan. I am particularly thankful to Professor Lola Eniola-Adefeso who convinced me to pick University of Michigan over the University of Pennsylvania. Having spent the last five years in Ann Arbor, I have no regret over the choice. I am grateful to the excellent service offered by Susan Hamlins. She was always ready to help on any graduate program-related problem during my stay in the University of Michigan. I will like to express my sincere appreciation to my dissertation committee: Professors Phillip Savage, Lola Eniola-Adefeso, Michael Solomon and Jinsang Kim. I appreciate all the suggestions and feedbacks towards my dissertation. I owe a great debt of gratitude to my graduate advisor Ted Goodson III who did not consider my limited background in Chemistry in admitting me into his research group. His advice and constant push towards scientific excellence are crucial to who I am today. I would not have been able to finish my thesis without the support of my colleagues in my research group. My gratitude goes to Meghan Orr and Dr. Oleg Varnavski who put me through the process of alignment of laser set up when I joined the research group. The constant critique of Sunny, Joe, Nerangha, Leslie, Phi, and Brad were helpful in shaping my ideas and thoughts.

Lastly, my appreciation also goes to my family and the families of Champoux and Adunbi in Ann Arbor who were pillars of support during my stay in Ann Arbor. My

appreciation goes to my wife and my mom who supported me during the course of my program. I am thankful to Professor Adunbi and his wife who ensured that I was never lonely during the holidays. I am grateful to Larry, Lucy, Ginny and Paul Champoux for the constant show of love. It is unfortunate that Paul will not be around when I eventually finish my program but I take solace in the fact that he has gone to rest in the bosom of the Lord. I appreciate you all.

TABLE OF CONTENTS

LIST OF FIGURES

LIST OF TABLES

LIST OF SCHEMES

ABSTRACT

The search for renewable energy sources to replace fossil fuel has been a major research focus in the energy sector. The sun, with its vast amount of energy, remains the most abundant and ubiquitous energy source that far exceeds the world energy demand. The ability to effectively capture and convert energy from the sun in the form of photons will be the key to its effective utilization. Of the many materials researched, organic macromolecules have tremendous potential to replace and out-perform existing materials, due to their low-cost, ease of tunability, high absorption coefficient and "green" nature.

In this thesis, zinc phthalocyanine (ZnPc) functionalized with oligothiophene was investigated. ZnPc is known for its chemical and thermal stability. There is efficient charge transfer in ZnPc because of its conjugated π-electrons. The power conversion efficiency (PCE) in ZnPc-based solar devices is however, very low because of the poor absorption of ZnPc in the 300 – 550 nm region of the solar spectrum. Oligothiophenes have good absorption in the spectral region where the absorption of ZnPc is poor. By functionalizing ZnPc with oligothiophene using ethynylene linkage, it is possible to capture the solar energy in the entire visible spectrum. Spectroscopic techniques of steady state absorption and time-resolved fluorescence spectroscopy were used to show the improved absorption of the oligothiophene-functionalized ZnPc. The steady-state fluorescence result showed an energy transfer from the oligothiophene units to the ZnPc and the efficiency of energy transfer increases as the number of oligothiophene groups attached to ZnPc increases. The ultrafast energy transfer was found to

occur in a time of 300 fs.

Other groups of organic compounds that have gained prominence in the study for the design of efficient active materials for photovoltaic cells are the polymers. Over the years, the efficiency of devices fabricated from organic polymers has increased steadily. For organic polymers to compete favorably with inorganic counterparts, the fundamental correlation between the structure and performance of polymers has to be investigated. In this dissertation, PTB7 which once had the world solar efficiency record of ~ 7.4% was investigated using steady state spectroscopy, nonlinear optical spectroscopy and time-resolved fluorescence techniques were used to investigate the structure-function relationship in the polymer. The steady state measurement showed a good absorption of PTB7 over the entire visible region because of strong electronic coupling between electron-donating benzodithiophene (BDT) and electron-withdrawing thienothiophene (TT). The large two-photon cross-section found in PTB7 suggests that there is an efficient charge transfer between the BDT and TT co-monomers of PTB7. The electronic structure calculation of PTB7 indicates that the HOMO was localized in the BDT co-monomer and the LUMO was localized in the TT co-monomer. Four other promising conjugated polymers based on thieno[2′,3′:5′,6′]pyrido[3,4-g]thieno[3,2-c]isoquinoline-5,11(4H,10H)-dione (TPTI) and fluorenedicyclopentathiophene dimalononitrile (FDCPT-CN) were also investigated and their photophysical properties were compared with the properties of PTB7. The results of the four polymers showed that a strong coupling between electron-donating co-monomer and electron-withdrawing co-monomer is essential for good solar cell performance. This conclusion agrees with the results obtained for PTB7

Chapter 1

Introduction and Background

1.1 The Scope of this Dissertation

The search for efficient and new forms of energy is one of the most exciting and challenging areas of research.[1–4] Historically, the world has depended on energy sources from fossil fuels such as coal, natural gas and oil.[5–10] These energy sources were formed from gradual decay of prehistoric plants and animals that died and are buried under layers of rocks which are over millions of years old. These energy sources are non-renewable and are known to be a major source of emissions. According to United States Department of Energy, 75% of human-caused emissions have come from the burning of fossil fuels in the past twenty years.[11] Some drawbacks that are associated with the over-reliance on fossil fuels include production of acidic gas such as sulphur dioxide and carbon dioxide which can result in acid rain, greenhouse effect which is the gradual warming of the earth and the destruction of the landscape when mining for the fossil fuels.[12–15] The continued rise in the world energy consumption which has culminated in increased environmental pollution has led to the intensification of research into alternative energy forms of energy.

Hydroelectric, geothermal, nuclear, wind, biofuels and solar forms of energy are some of optional sources of energy available to the world.[6,16–20] Hydroelectric power generation involves the generation of electrical power from the gravitational force of falling or flowing water.[21,22] For this source of energy to be viable, there has to be large volume of water in different seasons. Because of this reason, its use is limited to countries which have large bodies

of water that can be dammed for hydroelectric power generation. There is usually fluctuation of the power generation during the dry season when the volume of water in the water bodies reduces. China is the largest producer of hydroelectric power.[23,24]

Geothermal energy is a more recent source of energy which involves the conversion of thermal energy inside the earth crust into usable energy. Heat is constantly being produced below the earth's crust as a result of the decay of naturally radioactive materials such as uranium.[25–29] The heat from geothermal energy source can be used to heat houses during the winter season by using ground-source heat pumps comprising of piping system buried under the ground. This piping system is used to circulate air on anti-freeze liquid into buildings for heating purpose.[30] Additionally, steam can be produced in the earth crust through contacts of underground water with layer of hot and molten rock. Electricity can be generated when the produced steam is used to turn turbines. Only few countries are presently making use of geothermal energy sources on a large scale and these countries include United States of America, Philippines, Italy, Iceland, Mexico, Indonesia and El Salvador.[31,32] There are research collaborations on this alternative energy source to better harness its utilization and make its usage commercially viable.[33–36]

Nuclear power generation makes use of the exothermic energy generated from nuclear processes to generate useful heat and electricity.[37,38] The energy generation process takes place via nuclear fission. Nuclear fission is the breaking up of the nuclei of radioactive materials into smaller nuclei accompanied by the production of large amount of energy usually in the form of heat.[39–41] The process of generation of electricity in nuclear plants is similar to that used by geothermal processes. The heat generated from nuclear fission is used to produce steam in boiling water reactors through a physical process. The generated steam is piped to drive

turbines whose mechanical energy is converted to electricity. The nuclear energy alternative source is widely used by most industrialized countries but there have been recent call for its use to be limited because of the Fukushima Daiichi nuclear disaster in Japan in 2011. There have been rigid regulations as a result of the accident and a few countries including Germany and Italy have shut down their nuclear power plants.[42,43]

Wind power generation involves the use of large draft of air to drive wind turbines and wind mills to produce electrical power.[44] This form of energy is very unreliable as there could be a significant variation in the generated power over a short time.[45–47] For effective utilization of the energy, there has to be the capacity to store produced energy during the peak period of air draft for use during the off-peak periods.[48–50]

Recently, there has been some focus on biofuels.[51,52] Biofuels are energy derived from living organisms mostly plants and micro-organisms. Biofuels are produced through thermal or chemical conversion of plants into other forms of products which have higher calorific values.[53–55] One disadvantage of this form of energy is that some of the plants that are often used to generate biofuels also serve as food to humans. Bioethanol has been produced from crops such as sugarcane, soy bean, corn and sorghum through fermentation. Over-reliance on these food crops for biofuel production can lead to the increase in the prices of food and this reason has led to the shift of focus into non-food sources such as trees, grasses and algae.[56–61] These non-food sources are subjected to several chemical processes to extract bioethanol. There has also been an intense research into how to improve the production of these non-food sources to make biofuels to be commercially viable. Presently, biofuels are used to supplement fossil fuel in order to reduce the world's fossil fuel use.[62,63]

The sun is a stable source of energy with a vast amount of energy in the region of 3.86

10^{26} J released every second from the core of the sun.[64] The solar energy is the most plentiful and ubiquitous out of all the alternative energy sources. Some of the energy released from the core of the sun is lost as a result of absorption by the air mass in the atmosphere and the earth receives over 100,000 TW of energy from the sun annually.[65,66] An hour of energy from the sun is enough to power the earth for one year.[67,68] In spite of the enormous amount of energy received from the sun, it has only been possible to capture a small fraction of the energy reaching the earth from the sun. The limitation has reduced effective utilization of this energy source to power the earth. The energy from the sun could be harnessed by using solar thermal electricity, solar architecture, artificial photosynthesis and solar photovoltaics.[69–74] The solar photovoltaic is the most common method of harvesting solar energy from the sun. This study is focused on the characterization of new organic materials for the effective conversion of solar energy into electricity. The most essential properties that a material must meet before it can be used for photovoltaic applications include (a) strong light absorption over a large spectral range, (b) good carrier collection properties, (c) low cost of production, (d) stability over time when subjected to illumination, (e) high abundance of source materials and (f) environmentally friendly technology.[75–77]

The first step in photovoltaic process is the absorption of light. It is therefore essential that photovoltaic materials exhibit good absorption in the visible region of the solar spectrum. The incident photon passes through transparent electrodes and area absorbed by the active material in the photovoltaic cells. The energy from the incident photon is passed to the active material to generate electron-hole pair known as excitons. Organic semiconductor materials have better absorption coefficient than their inorganic counterparts. Organic materials can have absorption coefficient in the order of 10^5 M^{-1} cm^{-1} which ensures that only thin layer of organic

materials are needed to absorb significant fraction of light.[78] The absorption coefficient of organic materials is two orders of magnitude more than that of silicon.[79] Another approach that can be used to increase solar absorption is the increase in the thickness of the active layer. However, there is a limit to which the thickness of the active layer can be increased because of the low charge mobilities in organic polymers. Charge mobilities in organic materials can be as low as 10^{-4} cm^2/Vs. Hence, the advantage of increased absorption due to increased thickness of the active layer will be lost in reduced short-circuit current because of the low charge mobilities. Modulation of the chemical structure of the organic materials to ensure that their absorption spectrum matches the solar spectrum is therefore a better approach to improve solar absorption.[80] There have been significant efforts to design low bandgap materials which are capable of absorbing solar energy in the near-infrared region of the solar spectrum.[64,81–83]

Generated charge carriers after photon absorption will have to diffuse through the active layers of the photovoltaic cells to the electrodes. The electrons diffuse to the cathode while the holes diffuse to the anode. The interfacial barrier between the active materials and the electrodes will have to be surmounted before the charge carrier can be collected by the electrodes. The electrodes are usually coated by materials such as poly(3,4-ethylenedioxythiophene) polystyrene sulfonate (PEDOT:PSS), graphene oxide and metal oxides to improve the hole collection in the anode.[81,84,85]

For a solar cell material to be used commercially, the cost of production must be low. That was the initial incentive for the search for alternatives to the use of silicon as active material in photovoltaic cell. The fabrication process for crystalline silicon is expensive because of the need for high purity in the silicon.[78] Organic polymers are soluble in most organic solvents and this has ensured that organic solar cells can be produced through solution

processing by spin-coating, ink-jet printing and roll-to-roll processing. These processing techniques have reduced the manufacturing cost of organic photovoltaic cells.[86]

A solar cell material must be stable when subjected to illumination over a long period of time to be useful as active material for commercial solar device. At the moment, Si-based solar cells are more durable than organic solar cells. For organic solar cells to be able to compete favorably, it is essential that researchers re-engineer organic materials to be resistant to oxidation when exposed to air and humidity; and reaction with electrode material. The approach presently used to reduce oxidation of active layers of solar cell materials is to the modulation of the high occupied molecular orbital (HOMO) energy level below the oxidation threshold (-5.27 eV).[87,88]

Solar cell materials must also be abundant to be used as active materials in photovoltaic cells. Silicon is one of the most abundant elements on earth.[89] That is one of the factors responsible for its use in manufacturing active materials in solar cell. In spite of its abundance, the manufacturing cost of pure form of silicon is expensive.[78] On the other hand, newer materials like cadmium telluride (CdTe) and copper indium gallium selenide (CIGS) depend on rare elements like tellurium and indium. The rarity of the source materials of these materials has limited their applications.[90] Organic solar cells have the advantage of being able to be processed from small molecules and polymers using well-developed synthetic processes.[91–93]

The manufacturing technology for the production of solar cell material must be environmentally-friendly for it to be generally acceptable. The world is gradually shifting towards green technology. There is a growing interest in the environmental-friendliness of the processes involved in manufacturing alternative green energy. Any solar cell material will have to be able to surmount this scrutiny for it to be useful in photovoltaic applications in the long

run.[94,95]

1.2 Silicon-based Photovoltaic Solar Cell Mechanisms

Semiconductor materials can either be inorganic compounds (such as silicon) or organic compounds. Photovoltaic cells based on inorganic compounds presently have efficiency between 12 – 25%[96–100] while photovoltaic cells based on organic compounds have efficiency in the region of 12%.[101–104] The solar cell market is still dominated by silicon-based photovoltaic technology because of the abundant supply of silicon as raw material and the established technology.[105,106] The silicon technology has been well developed before the advent of photovoltaics and high quality material was already being produced for the use in transistors and integrated circuit. The first silicon solar cell was reported by Bell Laboratories in 1954 with a power conversion efficiency of 6%.[107] Significant progress in the silicon-based solar cell industry has contributed in no small measure to the current power conversion efficiency that stands at a maximum of ~ 25%.[108,109] When light with appropriate energy is incident on silicon, electrons are promoted from the valence band into the conduction band. The valence band is the region with the highest probability of finding electrons and it is located below the conduction band. On the other hand, the conduction band is the region that an electron that is already freed from the electron affinity of the valence bound is free to move to. Materials can be categorized by the amount of energy required to free electrons from the valence band to the conduction band known as the band gap. Figure 1.1 shows a schematic of the band structure of a typical semi-conductor material.

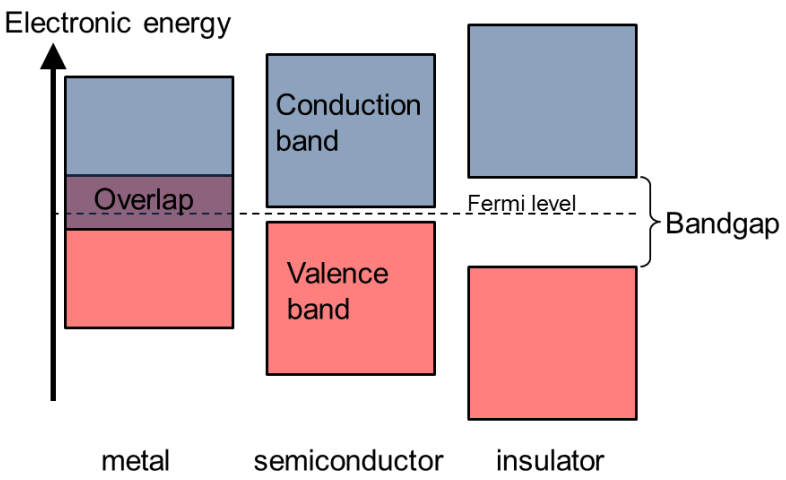

Figure 1.1 Schematic of the band structure of a typical semiconductor compared to metal and insulator

For metals, the conduction band and the valence band overlap and this is the reason why metals are very conductive. The bandgap of a semi-conductor material is between that of a conductor and an insulator. Silicon is an example of a semi-conductor with an indirect bandgap because the crystal momentum (k-vector) in the minimum energy state of the conduction band and the maximum energy state in the valence band are the different.[110–112] In an indirect bandgap material, an electron can only emit a photon through an intermediate state. This has the implication of limitation of absorption in silicon-based materials because light has to penetrate the silicon materials much farther before being absorbed. Consequently, it requires more materials to make silicon-based solar cells as light absorption cannot effectively take place over thin active layer. The weak absorption of light in silicon-based material has implication on its cost from the material stand point. Silicon will require 100 μm of thickness to absorb 90% of incident light compared to 1 μm GaAs which is a direct bandgap material.[113]

High purity silicon crystals are usually required to manufacture solar cells. Silicon atoms have four electrons in its outermost electrons and the electrons are locked in the valence band. Pure silicon can be doped by ‘impurities’ (dopant) to modulate its electrical properties

and therefore make it conductive. Charge carriers can be introduced into the lattice of silicon by introducing suitable extrinsic materials. The charge carriers can either be electrons or holes. Group III and V elements are usually used as dopants. When group III elements (such as boron) having three electrons in their valence bands are used as dopants, p-type of semiconductor having excess holes is produced. Alternatively, when group V elements having five electrons (such as phosphorus) in their valence bands are used as dopants, n-type of semiconductor having excess electrons are produced. When a p-type semiconductor is placed near an n-type semiconductor, a p-n junction is produced. Light of adequate intensity and energy can generate a free electron which is attracted to the n-region of the p-n semiconductor through the p-n junction. This creates an imbalance of charge between the n-type semiconductor and the p-type semiconductor. The imbalance in charge promotes the flow of electrons from the n-type semiconductor to an external load thereby generating electricity.

Crystalline silicon still dominates the silicon solar cell market but there have been tremendous progress in the thin-film materials which require only small amounts of material. In the emerging markets of thin-film materials are amorphous silicon, cadmium telluride, copper indium gallium diselenide and organic polymers.[114]

1.3 The Principle of Organic Photovoltaic Systems

Photovoltaic is the method by which electrical power is generated by converting energy from the sun using semiconductor materials into direct current. In order to understand the principle of photovoltaics, it is important to define some terminologies that will be encountered throughout this dissertation.

The molecular orbital of an organic system is the region in the molecule where the probability of finding an electron is highest. Because molecules are made up of atoms,

molecular orbital is formed from the overlap of atomic orbitals. Molecular orbital gives the spatial representation of electrons in the organic system. In organic systems, the molecular orbital is formed from the overlap of the σ- and π-orbitals. There are two types of molecular orbitals in organic systems which are the highest orbital molecular orbital and the lowest unoccupied molecular orbital which are often referred to as HOMO and LUMO. HOMO is the region of the orbital with the highest probability of finding bonding electrons. The HOMO is equivalent to the valence band of inorganic semiconductors. On the other hand, the LUMO is the orbital with the least probability of electron occupation is the LUMO. The LUMO is the anti-bonding molecular orbital (π* orbital). The occupation of the LUMO by electrons weakens the bonding in the organic polymer and raises the overall energy of the polymer. The LUMO is equivalent to conduction band in inorganic semiconductors. The bandgap is the difference in the energy between the LUMO and the HOMO. The bandgap is usually given in the unit of electron Volt (eV). For optimum harvest of solar energy from the sun, the bandgap has to be in the region of 1.1 - 1.5 eV.[115–117] At this bandgap, the polymer is able to absorb energy from the sun in the near infrared region of the electromagnetic spectrum. This is the region of the electromagnetic spectrum where the energy from the sun is most intense. Figure 1.2 shows the relative intensity of the radiation from the sun at different wavelengths.

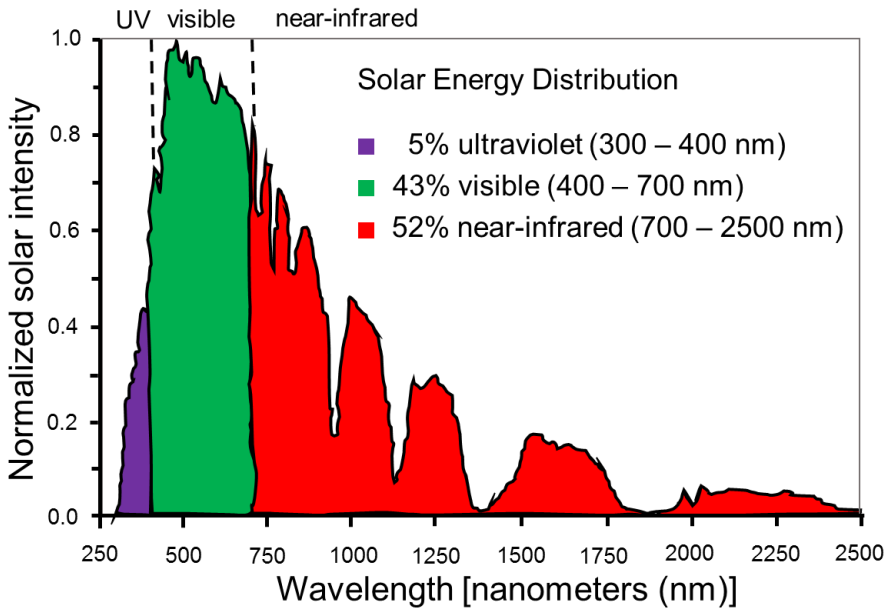

Figure 1.2 Intensity of sunlight at different wavelengths for AM1.5 conditions.[118]

The open-circuit voltage (V_{oc}) is the potential difference between the terminals of the solar cell under illumination when there is no external load connected to it. At the instant when the measurement of the open-circuit voltage is made, there is no current flowing through the solar cell. It is the maximum voltage that can be obtained from the solar cell. The short-circuit current (I_{sc}) is the current flowing the solar cell under illumination when there is no potential between its terminals. It is the maximum current obtainable from the solar cell. Figure 1.3 shows a typical current density-voltage (J-V) characteristic curve for organic photovoltaic device.

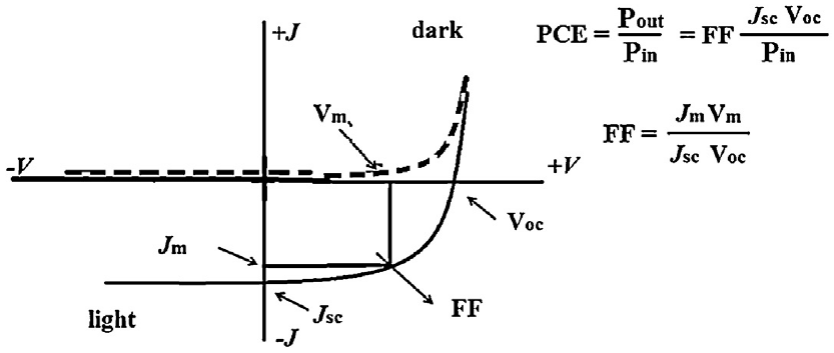

Figure 1.3 Typical current-voltage characteristic curve for an organic solar cell[81]

The fill factor (FF) is the ratio of the maximum obtainable power (P_{out}) from the solar cell and the power obtainable from the cell when the voltage and the current have values equivalent to the open-circuit voltage and the short-circuit current. To have a high fill factor, it is important for the solar cell to have a very low resistive loss. The fill factor is given by Equation 1.1.

$$FF = \frac{P_{out}}{V_{oc} \cdot I_{sc}} = \frac{V_m \cdot I_m}{V_{oc} \cdot I_{sc}} \qquad \textbf{Equation 1.1}$$

In Equation 1.1, V_m and I_m are the voltage and current in the solar cell at maximum power point. Due to the limitation of the ability of semiconductor materials to absorb incident light from the sun and the internal loss of energy as heat in the solar cell, all the energy from the sun cannot be converted into electrical power. The power conversion efficiency (PCE) is the performance metric of solar cell and it is the percentage of the incident radiant energy from the sun that can be converted to electrical energy. For the sake of comparison of the efficiencies of different solar cells, power conversion efficiencies are measured under standard test conditions (STC) at temperature of 25^{o}C, irradiance of 1000 W/m^2 and an air mass 1.5 (AM1.5) spectrum.[118] The PCE can be expressed algebraically in terms of measurable parameters of V_{oc} (in Volt), I_{sc} (in Ampere) and FF as shown in Equation 1.2.

$$PCE = \frac{P_{out}}{P_{in}} = \frac{V_{oc} \times I_{sc} \times FF}{E \times s}$$ **Equation 1.2**

In Equation 1.2, E is the intensity of the energy from the sun (in W/m^2) and s is the surface area (in m^2) of the solar cell being evaluated. The short-circuit current is as a result of the generation of charge carriers (electrons and holes). The movement of the charge carriers in the solar cell materials leads to the flow of current. To ensure a high short-circuit current, it is essential that the solar cell material must have good absorption in the entire solar spectrum, good charge carrier mobility, and low recombination rate.[119] Solar cell materials are required to have low bandgap for their spectra to match the intensity peak of the solar spectrum. The intensity peak of the solar spectrum is near infrared region and the lower the bandgap, the more the shift of the spectrum of the organic solar material to the red region of the electromagnetic spectrum (see Figure 1.2). It has been reported that good morphology of solar cell materials also improves the I_{sc} because the charge carrier mobility in solar cell is dependent on morphology.[120,121] The V_{oc} is dependent on the potential difference between the LUMO and the HOMO of the donor (p-type semiconductor) and acceptor (n-type semiconductor) materials of the solar cell respectively. V_{oc} can be viewed as the driving force needed to transfer electron from the HOMO of the donor organic molecule to the LUMO of the acceptor molecule. If the incident light cannot provide energy more than this driving force, photovoltaic effect will not take place. Deep-lying HOMO level favors increased V_{oc}.[122,123] The addition of highly electromagnetic elements like fluorine to organic polymers has been reported to decrease the HOMO level.[124–126] Low equivalent series resistance and a high equivalent shunt resistance are requirements for high fill factor.[127] This ensures that the internal losses in the solar cell as heat are minimized. Typical commercial solar cells have fill factor greater than 0.70 while most solar cell materials have fill factors between 0.4 and 0.8.[128,129]

Quantum efficiency is a parameter used to characterize the extent of conversion of the incident photon to electrical current. The quantum efficiency can be categorized into two: internal and external quantum efficiency. The internal quantum efficiency (IQE) is the ratio of the charge carriers generated by the solar cell to the number of photons absorbed by the solar cell while the external quantum efficiency (EQE) is the ratio of the charge carriers generated by the solar cell to the number of photons that are actually incident on the solar cell. Generally, the number of photons absorbed by the solar cell is less than the number of photons incident on the solar cell, therefore the internal quantum efficiency is greater than the external quantum efficiency. The external quantum efficiency depends on the absorption of light by the solar cell and the ability to successfully separate the generated charge carriers. Charge recombination reduces the external quantum efficiency because it limits the number of flowing electrons. The formula for IQE and EQE are given in Equation 1.3.

$$IQE = \frac{generated\ electrons\ per\ unit\ time}{number\ of\ absorbed\ photons\ per\ unit\ time}$$

$$EQE = \frac{generated\ electrons\ per\ unit\ time}{number\ of\ incident\ photons\ per\ unit\ time}$$

Equation 1.3

Figure 1.4 shows the schematics for the mechanisms by which the photovoltaic process takes place. The processes involved in the conversion of incident light to electrical power are (1) absorption of incident light by the solar cell material. (2) the promotion of electrons from the HOMO to the LUMO of the donor organic material to generate electron-hole pair known as exciton. The energy of the incident light needs to be equivalent or greater than the band gap of the donor material in order for the exciton to be generated. If the energy of the incident light is greater than the bandgap, some of the energy will be lost through internal conversion. (3) diffusion of the exciton to the interface of the donor and acceptor polymers. It is essential that

the exciton diffuses to the interface before the lifetime of the exciton. The diffusion length of excitons is around 10 nm (4) exciton dissociation and charge carrier generation at the donor/acceptor interface. The generated holes and electrons are still coulombically attracted to each other; therefore, they would have to be dissociated before they can be transported to the electrodes (5) transportation of charges to the electrodes. The PCE of the solar cell changes if any of these five processes is altered. Therefore, the solar cell has to be optimized such that all the processes run at optimum levels.

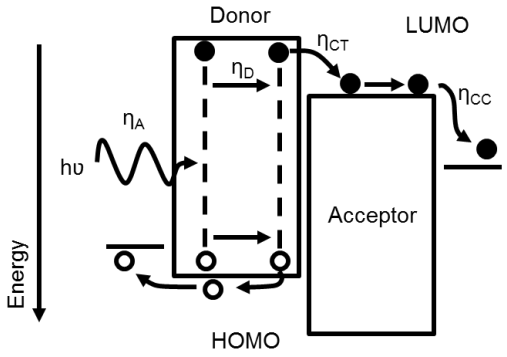

Figure 1.4 Schematic of photovoltaic processes showing photon absorption (η_A), exciton diffusion (η_D), exciton dissociation by charge transfer (η_{CT}) and exciton charge carrier collection (η_{CC})[129]

1.4 The Development of First Generation of Solar Cell

Silicon-based solar cells still dominate the solar cell market but there have been intense research into solar cells based on organic materials. For solar cell to be a commercially viable source of electricity, it is important for it to be affordable. The high cost of production of silicon has limited the usage of silicon-based solar cell.[130–132] Organic materials have the advantages of low production costs in high volumes, high optical absorption coefficient, and flexibility in the molecular engineering of organic materials.[101,133,134] Unlike silicon, only a thin film of organic material is required to absorb considerable amount of solar energy.[135,136] More importantly, the flexibility in the molecular engineering of organic materials enables the

bandgap to be modulated by changing the length or functional groups of the polymers. In spite of all the advantages that organic polymers offer over silicon in the manufacture of solar cells, the commercialization of organic solar cells has not reached the peak because of low power conversion efficiency and low stability of organic polymers.

The development of organic photovoltaic cell was first reported as early as 1959 by Kallmann and Pope.[78,137,138] A single layer anthracene was developed with a solar efficiency below 0.1%. The exciton was strongly bound and needed to be split in order to generate electrical current. The molecular structure of anthracene is shown in Figure 1.5. Later, the major breakthrough in organic solar cell design occurred in 1985 when C. W. Tang used a bilayer structure to produce a solar cell device based on copper phthalocyanine (CuPc) and 3,4,9,10-perylene tetracarboxylic-bis-benzimidazole (PTCBI).[139] CuPc acted as the electron donor while PTCBI was the electron acceptor in the bilayer system. This design configuration resulted in a short-circuit density of 2.3 mA/cm^2, open-circuit voltage of 0.24 V and fill factor of 0.65. The power conversion efficiency was around 1% and this was a significant milestone at the time.[139] The bilayer design improved the charge separation process in the solar cell device.

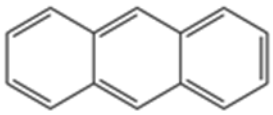

Figure 1.5 Structure of anthracene

It is important that the polymers are soluble in organic solvents for easy processability. Thus, the polymers are usually synthesized with alkyl side chain to improve solubility. The solubility of the polymers can be limited if shorter side chains are used but shorter side chains enhance molecular packing and charge transfer. If the side chain is too bulky, that could cause the precipitation of the polymers during preparation. It is therefore essential to determine the

side chain that will give the optimum result for each polymer.[140,141]

1.5 Design Architectures for Organic Photovoltaics

Different design architectures have been employed in order to ensure the separation of electron-hole pair to generated free electrons and holes. Some of these configurations are the single layer, bilayer and bulk heterojunction (BHJ).[133,142,143] In the single layer organic photovoltaic cell, the organic material is sandwiched between two electrodes of different work functions. When organic materials absorb light, the electric potential created by the different electrodes drive the electrons and holes to the appropriate electrodes. There is a strong possibility of a recombination between the electrons and holes before arriving at the electrodes.[144] This limits the power conversion efficiency from organic photovoltaic cells based on a single layer junction. Another configuration that could be used is the bilayer junction in which two organic materials of different electron affinities are sandwiched between two electrodes. One of the organic materials will be an electron-donor while the other will be an electron-acceptor. The difference in the electron affinities of the organic materials improves the efficiency of separation of the electron-hole pairs in the exciton. The electron donor and electron acceptor in the bilayer configuration are arranged in a planar configuration. The diffusion length of exciton is in the order of 10 nm, which is very small compared to the length of the active layer required for significant absorption of photons. For there to be a significant absorption in the active layer, the thickness would have to be in the order of 100 nm. This has the implication of most of the excitons not reaching the bilayer interface.[144]

The most widely used configuration is the bulk heterojunction in which the two organic materials acting as the donor and acceptor are dispersed in the bulk of the active layer. The invention of the bulk heterojunction (BHJ) increased the region of charge generation. The BHJ

architecture was invented by Yu *et al.*[145] The BHJ is formed from the self-assembling of donor and acceptor components of the solar cell to form continuous interpenetrating networks. The length scale of the assembly must be in the region of 10 – 20 nm to avoid recombination which typically occurs within 10 nm. The BHJ approach is still being used till today and this approach has largely been successful. Organic polymers are usually used as electron donor with C_{60} fullerene derivatives as electron acceptor. This design architecture ensures that the generated excitons are able to diffuse to the interface of the organic materials before the end of the lifetimes of the excitons. Figure 1.6 shows the various design architectures explored in organic solar cells.

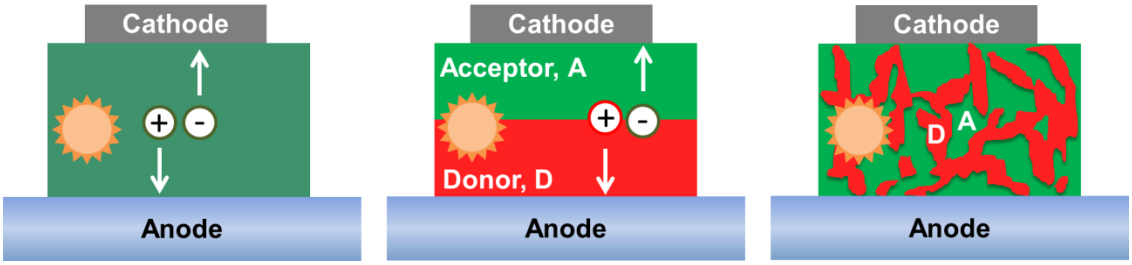

Figure 1.6 Schematics of single layer (left), bilayer (middle) and bulk heterojunction organic photovoltaic cells[146]

Fullerene derivatives, 6,6-phenyl-C_{61}-butyric acid methyl ester ($PC_{61}BM$) and 6,6-phenyl-C_{71}-butyric acid methyl ester ($PC_{71}BM$) are usually explored as electron acceptor in the various design configurations. Fullerenes are used because of the high electron affinity and good solubility in most organic solvents.[134,147]

1.6 Different Organic Materials used as Active Materials in Organic Photovoltaic Cells

1.6.1 Poly(3-hexylthiophenes)

Poly(3-hexylthiophene) (P3HT) is one of the most studied polymers used as active materials in polymer-based solar cells. P3HT has an absorption spectrum that spans 350 to 650

nm. Figure 1.7 shows the structure and absorption spectrum of P3HT. P3HT is the best performing solar cell organic polymer in the group of polythiophene polymers. P3HT has advantages of easy synthesis, high charge carrier mobility and regioregularity. The performance of P3HT as solar cell active layer has been partly attributed to its regioregularity. Regioregularity of P3HT improves its crystallinity and its charge-carrier ability. It can easily assume a planar structure leading to highly conjugated polymer. A twist in the backbone of P3HT can lead to increase in its bandgap and affect its conducting properties. Therefore, high regioregularity is essential for good photoconversion of P3HT.[148,149] The molecular weight of P3HT is also important to its performance. The molecular weight of polymers is generally controlled by the technique of preparation. The hole mobility of P3HT increases with increasing molecular weight.[150–152] Solar cell devices based on P3HT with efficiencies of 4 – 5% have been achieved.[149,153,154] There have also been attempts to improve the efficiencies of P3HT-based solar cells by modifying the morphology, electron acceptor and device architecture. Therefore efficiencies around 7% have been obtained for P3HT-based solar cells.[155–157] P3HT, however, has disadvantages of relatively large bandgap (~1.9 eV) and high HOMO level.[158] The large bandgap limits the absorption of the near-infrared region of the solar spectrum and the high HOMO level limits the V_{oc}. The V_{oc} of P3HT/PCBM-based solar cells are usually in the region of 0.6 eV.[82]

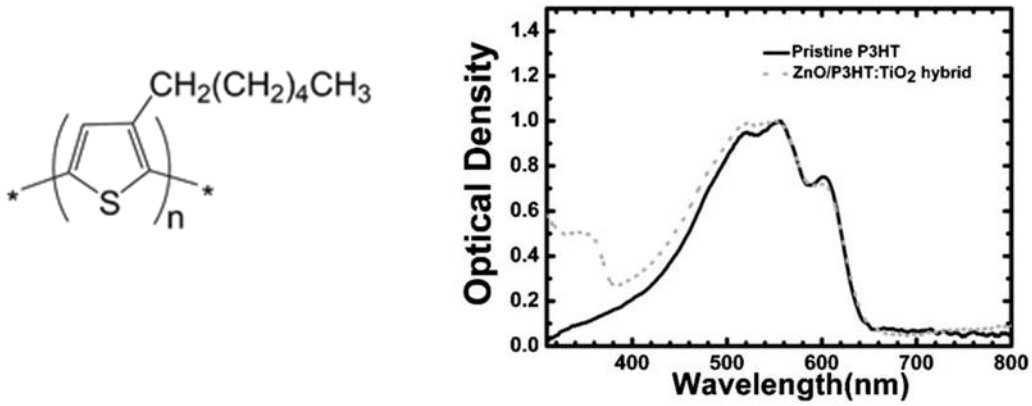

Figure 1.7 Structure of P3HT and the absorption spectrum of P3HT and hybrid ZnO/P3HT:TiO_2 thin films[159]

1.6.2 Poly(phenylene vinylene)

Poly(phenylene vinylene) is used for light-emitting diodes (LED) and as solar cell materials.[160] Poly(phenylene vinylene) (PPV)-based organic compounds are commonly used as donor materials in organic solar cell. Poly[2-methoxy-5-(2-ethylhexyloxy)-1,4-phenylene vinylene] (MEH-PPV) and poly[2-methoxy-5-(3′,7′-dimethyloctyloxy)-1,4-phenylene vinylene] (MDMO-PPV) are two representatives of PPV-based organic compounds that have exhibited efficiencies of ~2% in organic solar cells when used in combination with PCBM as electron acceptor.[161–164] The bandgap of PPV-based organic materials is in the region of 2.3 eV, therefore it does not capture the near-infrared region of the electromagnetic spectrum.[165,166] This limits the short-circuit current of PPV-based organic solar cells and ultimately the power conversion efficiency. Figure 1.8 shows the two widely used examples of PPV-based organic materials.

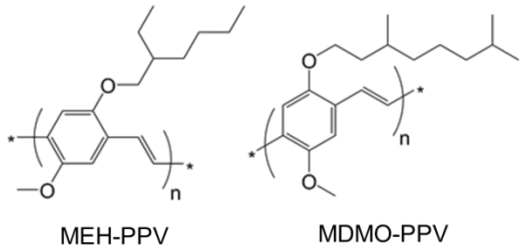

Figure 1.8 Structures of MEH-PPV and MDMO-PPV which are the most common poly(phenyl vinylene) materials

1.6.3 Porphyrins

Porphyrins are other groups of materials that have been studied as active layers of organic solar cell. Figure 1.9 shows the structure of porphyrin with a metal center. Porphyrins have conjugated π-electron system that is suitable for electron transfer in solar cell materials. Porphyrins have the advantages of fast electron transfer to the acceptor, good absorption in the visible region (especially in the blue-green region), and tenability of the redox potential by the insertion of metal into their cavities.[167,168] While porphyrins are commonly used as donor materials in the organic solar cells, they have often been used as acceptors depending on the substituents or metal center attached to them.[169–172] Porphyrins have the disadvantages of short exciton diffusion less than 10 nm and low charge carrier mobility which limit the efficiencies of porphyrin-based devices.[171,173] Hole mobility values between 10^{-10} to 10^{-1} $cm^2/(V\ s)$ have been reported for porphyrins.[174–176] These values are too low to achieve efficient charge transport in solar cells. Sun *et al.* was able to achieve an efficiency of 0.775% with annealed BHJ porphyrin:PCBM based solar cells.[170] Porphyrins also find their uses as photosensitizer to absorb photons that are not absorbed by other active materials in ternary systems.[177]

Figure 1.9 General structure of metallic porphyrins

1.6.4 Pthalocyanines

Phthalocyanines are closely related to porphyrins in structure. Phthalocyanines are planar and aromatic compounds with 18 π-electrons in one aromatic ring. Phthalocyanines comprise of four isoindole units connected by N-linkage. Phthalocyanines are known for good thermal and chemical stability.[178–180] The stability of phthalocyanines has contributed in no small measure to their use as active materials in organic solar cells. The optical and electronic properties of phthalocyanines are flexible as they could be easily tuned through synthetic modification by the addition of different functional groups to their molecules. More than 70 metallic and non-metallic ions can be added into the phthalocyanine cavity but copper phthalocyanine (CuPc) and zinc phthalocyanine (ZnPc) are the most studied form of the compounds till date.[181] The advantages of phthalocyanines over porphyrins are longer exciton diffusion lengths, wider spectral range and higher hole mobility.[182] CuPc and ZnPc have the highest exciton diffusion length out of all phthalocyanines and that is why they are commonly used as active materials. The exciton diffusion length of CuPc has been found to vary between 8 and 68 nm.[183,184] Phthalocyanines have intense absorption in the near-infrared region of the electromagnetic spectrum. The intense absorption especially near the infrared region leads to increase in photocurrent generation. Measurements of hole mobilities of CuPc-based organic solar cell device show mobilities in the range of $10^{-7} – 10^{-2}$ $cm^2/(V\ s)$.[185–187] Tang *et al.* in 1986

used CuPc in the construction of a bilayer architecture with CuPc acting as the donor material and PTCBI acting as the acceptor material and a solar efficiency of 1% was achieved.[139] Peumans and Forrest achieved an efficiency of 3.6% with a bilayer device based on CuPc as the donor and PTCBI as the acceptor.[188] Figure 1.10 shows the structure of a metallic phthalocyanine.

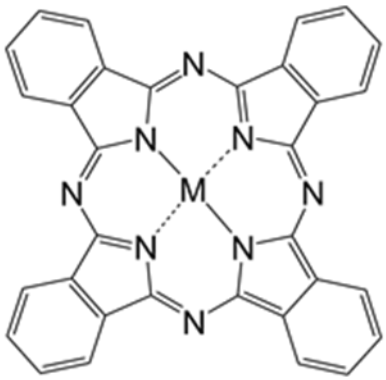

Figure 1.10 General structure of metallic phthalocyanines

1.6.5 Development of donor-acceptor co-polymers resulting in 5% solar efficiency in organic solar devices

Common problems to the materials already discussed above are the large bandgap and high-lying HOMO level. In order to harvest a greater fraction of energy from the sun and also improve the V_{oc}, it is essential that the bandgap of the solar materials is reduced and the HOMO level is lowered. One strategy that has been used successfully to achieve this is to construct organic materials with backbone having alternating electron-donor and electron-acceptor units forming D-A co-polymers.[83,189,190] Other approaches adopted are the stabilization of the quinoid resonance structure of the organic materials in order to maintain planarity, incorporation of strong electron-withdrawing substituents like fluorine atom or esters for induced dipole moment and attachment of conjugated side chain in order to increase conjugation.[124,191] One polymer that was designed based on the repeating alternating electron-

donor and electron-acceptor units is poly[N-9′-heptadecanyl-2,7-carbazole-alt-5,5-(4′,7′-di-2-thienyl-2′,1′,3′-benzothiadiazole)] (PCDTBT).[192] PCDTBT contains repeating units of electron-donating carbazole and electron-withdrawing benzothiadiazole. PCDTBT has a bandgap of 1.88 eV and HOMO level of 5.50 eV. The device made from PCDTBT showed a PCE of 3.6%. The V_{oc}, J_{sc} and FF were 0.89 V, 6.92 mA/cm^2 and 63% respectively. By modifying PCDTBT-based device through addition of optical spacer, solution processing and device engineering, the efficiency has been raised to ~ 7%.[193,194] Polymers based on repeating units of cyclopenta[2,1-b:3,4-b′]dithiophene (CPDT) and dithieno[3,2-b:2′,3′-d]silole (DTS) showed lower bandgaps of approximately 1.5 eV.[195,196] The polymers, poly[(4,4-bis(2-ethylhexyl)-cyclopenta-[2,1-b:3,4-b′]dithiophene)-2,6-diyl-alt-(2,1,3-benzothiadiazole-4,7-diyl)] (PCPDTBT) and poly[(4,4′-bis(2-ethylhexyl)dithieno[3,2-b:2′,3′-d]silole)-2,6-diyl-alt-(2,1,3-benzothiadiazole-4,7-diyl)] (PSBTBT) synthesized from these units showed absorption up to 850 nm and showed PCE of ~ 5%. The performance of the polymers can be related to the strong intramolecular interactions between the donor and acceptor units. The structures of PCPDTBT and PSBTBT are shown in Figure 1.11.

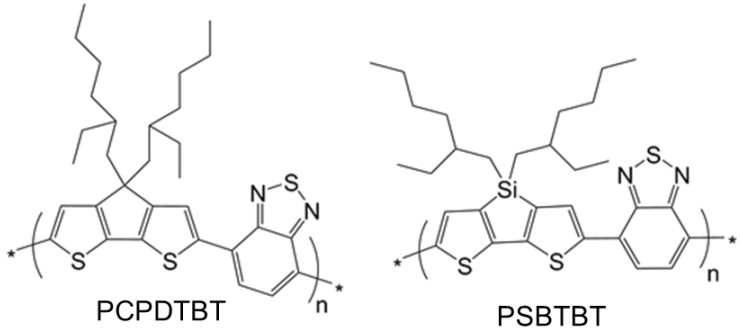

Figure 1.11 Structures of PCPDTBT and PSBTBT which gave PCE of 5% in organic photovoltaic cell

1.6.6 Introduction to PTB polymer series

A major breakthrough in the search for polymer organic materials as active materials in

photovoltaic cell came with the synthesis of the PTB series of polymers by the research group of Luping Yu.[126,190,197,198] The polymers contain co-monomers of conjugated benzo[1,2-b:4,5-b′]dithiophene (BDT) and electron-rich thieno[3,4-b]thiophene (TT) that was stabilized by electron-withdrawing ester group. TT co-monomer has the ability to support the quinodal structure of the PTB polymers which lead to enhanced planarity and the reduction of bandgaps.[190] Different polymers were designed by altering the side chains attached to the BDT and TT co-monomer. Alkyl and alkoxyl groups were explored as side chains for the BDT co-monomer while fluorine was explored as side chain for the TT co-monomer. It was observed that by using alkoxyl group and fluorine as side chains for the BDT and TT co-monomers respectively, it has the effect of lowering the HOMO energy level. PTB polymer series exhibited approximately 1.6 eV as bandgaps. The hole mobilities of the polymers were between 2.6×10^{-4} and 7.7×10^{-4} $cm^2/(V\ s)$. All the polymers had similar absorption in the visible spectrum which covered wavelength range of 300 nm to > 800 nm. Through the optimization of the solar device made from these polymers by using different solvents for preparation, it was possible to obtain highest values of 0.76 V, 14.50 mA/cm^2 and 68.97 as V_{oc}, J_{sc} and FF. The different solvents modified the morphology of the composite films of the PTB polymers and fullerene acceptor prepared by spin-coating. The films were produced in mixed solvent of dichloromethane/1,8-diiodomethane in volume ratio of 97:3 to improve morphology.

The best performing polymer in the PTB polymer series was poly[[4,8-bis[(2-ethylhexyl)oxy]benzo[1,2-b:4,5-b′]dithiophene-2,6-diyl][3-fluoro-2-[(2-ethylhexyl) carbonyl] thieno[3,4-b]thiophenediyl]] (PTB7). PTB7 had fluorine and ester substituent in the TT co-monomer and an alkoxyl substituent in the BDT co-monomer. The solar cell device fabricated from PTB7 once held a world record efficiency of 7.4%.[198] Poly[(4,8-bis-(2-ethylhexy-

thiophene-5-yl)-benzo[1,2-b:4,5-b′]dithiophene-2,6-diyl)-alt-(2-(2′-ethylhexanoyl)-thieno[3,4-b]thiophene-4,6-diyl)] (PBDTTT-C-T) and poly[(((2-hexyldecyl)sulfonyl)-4,6-di(thiophene-2-yl)thieno[3,4-b]thiophene-2,6-diyl)-alt-(4,8-bis((2-ethylhexyl)oxy)benzo[1,2-b:4,5-b′] dithiophene-2,6-diyl)] (PBDTDTTT-S-T) are other polymers that have been synthesized based on repeating units of TT and BDT. They have been shown to have efficiencies of 8% and 9% in solar cell device.[199–201] The polymers were obtained by replacing the alkoxyl side chain in the BDT co-monomer of PTB7 by alkylcarbonyl-substituted thieno[3,4-b]thiophene. PBDTDTTT-S-T also had a thiophene linkage between the BDT and the TT units and a sulphonyl group attached to the TT unit. Figure 1.12 shows the structures of PTB7, PBDTTT-C-T and PBDTDTTT-S-T.

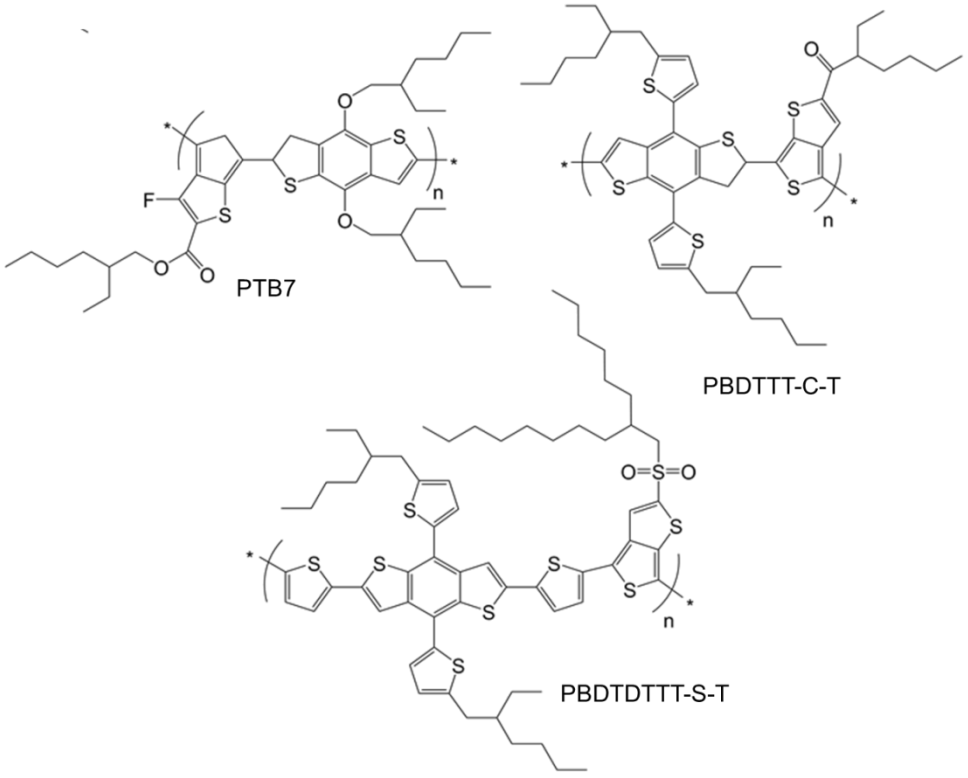

Figure 1.12 Structures of PTB7, PBDTTT-C-T and PBDTDTTT-S-T. The PTB polymer series heralded the solar efficiency above 7% in organic solar cell

1.6.7 Development of electron-accepting organic materials

There has been tremendous progress in the development of electron-accepting materials (n-type semiconductor) for use in solar cell device. The most commonly used n-type semiconductor materials are the fullerenes. The solubility of fullerenes is not quite good but can be improved by the addition of substituents. C-60 fullerene derivative [6,6]-phenyl-C_{61}-butyric acid methyl ester ($PC_{61}BM$) which was synthesized by Wudl *et al.*[145] and [6,6]-phenyl-C_{71}-butyric acid methyl ester ($PC_{71}BM$), first reported by Janssen *et al.*[202] are the most commonly used fullerenes. $PC_{71}BM$ has a better absorption in the visible region than $PC_{61}BM$ but it is more costly due to a more difficult purification process. The two organic materials have been used in conjunction with many high-performing electron-donating polymers in the solar cell device fabrication. Fullerenes possess high degree of symmetry. Attempts have been made to shift the LUMO level of the fullerene derivatives in order to increase the V_{oc} of their solar cell device. One approach is the utilization of trimetallic nitride fullerenes. The LUMO level of Lu_3N@C80-PCBH was 0.28 eV higher than that of $PC_{61}BM$ and the PCE of device developed with P_3HT reached 4.2%.[203] The expensive synthetic method of obtaining the trimetallic nitride fullerenes has limited their commercial use.

There have been attempts to use small polymers as electron-accepting unit in BHJ systems because of their better absorption than PCBM in the visible region. In addition, it is easier to synthesize polymers than fullerenes. Derivatives of perylene diimides (PDI) have been explored as electron-accepting units because of their high electron affinity. More work has to be done in the development of other small molecule polymers because the efficiency offered by these polymers is presently low.[204–206] Figure 1.13 shows the structures of some common organic compounds used as electron-acceptors in organic photovoltaic cells.

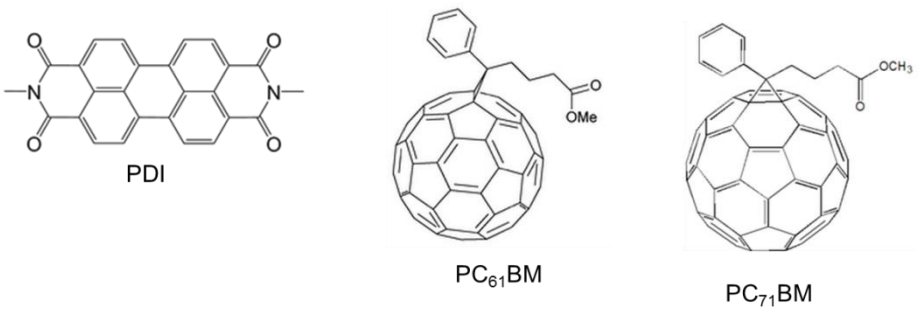

Figure 1.13 Organic materials which have been used as electron-acceptors in organic photovoltaic cells

1.7 The Big Picture of the Dissertation

As described in the earlier sections, there have been significant works on the development of new organic polymers that can be used as active materials in organic photovoltaic cells. The new polymers have contributed to the solar efficiency of approximately 12% which presently exists in tandem solar cell.[102–104] For polymer solar cells to be able to compete favorably with their inorganic counterparts, the efficiency of organic solar cells need to increase. Continuous design and testing of new polymers in organic photovoltaic cells requires significant efforts. It is therefore essential to determine the fundamental properties that the organic polymers need to have in order to be able to convert solar energy to electricity efficiently in organic photovoltaic cells.

In this thesis, the work on the use of spectroscopic techniques of steady state measurement, two-photon absorption measurement and time-resolved fluorescence measurement to correlate the structure and performance of organic materials will be presented. The results of the work can help in the design of new materials with potential to outperform the present materials available in the literature. The steady state measurement can give insight into the structural requirements of the organic materials to be able to absorb photons over a wide spectral range. The two-photon absorption technique can be used to determine the two-photon

absorption cross-section which is related to the transition dipole moment of organic materials. Efficient charge transfer is a key requirement in organic photovoltaic materials and measurable property like two-photon absorption cross-section and transition dipole moment can be used to determine how the structure of the organic polymers contribute to charge transfer. The fluorescence lifetime measurement gives information about the dynamics of exciton decay and energy transfer between different energy states. The lifetime of exciton decay must be more than the exciton diffusion time in organic solar cell in order for the generated charge carriers to reach the electrode.

Two different groups of organic materials were used in the thesis to show how spectroscopic techniques can be used to relate the structure-function properties. In the first project presented in Chapter 3, two zinc phthalocyanine dyads functionalized with oligothiophene were used to illustrate the improvement of the spectral window of absorption of zinc phthalocyanine by the combination of two materials with complementary absorption. The energy transfer process in the dyads was illustrated through the steady state absorption and fluorescence lifetime measurements.

PTB7, one of the best-performing polymers, was studied in Chapter 4. The spectroscopic techniques were used to illustrate how the structures of PTB7 contributed to its performance in organic photovoltaic cells. Four other promising conjugated polymers were also studied and their results were compared to those of PTB7. The chapter illustrates the effect of the alteration of the conjugation and donor-acceptor group on the photophysical properties of organic systems and ultimately the performance of the organic systems in organic photovoltaics.

The effect of different linkages and alkyl side chains on the photophysical properties of

polymers was illustrated in Chapter 5. Four different conjugated polymers based on 3,7-didodecyl-2,6-di(thiophen-2-yl)benzo[1,2-b:4,5-b′]difuran (BDF) as donor and either 3,6-di(2-furanyl)-1,4-diketopyrrolo[3,4-c]pyrrole (FDPP) or 3,6-di(2-thienyl)-1,4-diketopyrrolo[3,4-c]pyrrole (TDPP) as the acceptor were used in the study. The result of the chapter illustrates how the alteration of heteroatoms and alkyl side chain in organic systems influence the photophysical properties and ultimately the performance of the organic systems in organic photovoltaics.

1.8 Outline of the Dissertation

The body of the remaining part of the dissertation is organized as follows. Chapter 2 includes the relevant experimental techniques used in the experiments presented in this dissertation. The new techniques discussed include the steady state spectroscopy which comprises measurement of the absorption spectrum, emission spectrum and the quantum yield; two-photon spectroscopy which comprises of the two-photon excited fluorescence excitation measurement and the nonlinear transmission method; and the time-domain lifetime measurement which comprises the time-resolved fluorescence upconversion spectroscopy and the time-correlated single photon counting.

Chapter 3 presents the work published in the Journal of Physical Chemistry on the characterization of zinc phthalocyanine functionalized with oligothienylene-ethynylene subunits. The chapter will focus on the application of ultrafast spectroscopic techniques to understand how the addition of oligothienylene-ethynylene subunits affected the optical properties of the zinc phthalocyanine. The steady state spectroscopy and the time-resolved fluorescence upconversion techniques were used for this study. The compounds that were studies were synthesized by the group of Peter Bäuerle and Tomas Torrés. The synthesis of the

compounds was briefly summarized and the photovoltaic studies were presented.

Chapter 4 gives the spectroscopic characterization work on PTB7 polymer which once had the world best solar efficiency. Other promising polymers based on the repeating units of alternating donor and acceptor co-polymers were also considered. The steady state spectroscopy, two-photon spectroscopy and time-domain lifetime measurements of the polymers were measured and compared with that of PTB7. The results of the electronic structure calculations of the polymers were shown and the correlation with the experimental results was analyzed. The work was presented at the American Chemical Society National Meeting between August 10 – 14 and the manuscript has been submitted for publication in a peer-reviewed journal.

In Chapter 5, the spectroscopic characterization of novel donor-acceptor conjugated polymers based on donor 3,7-didodecyl-2,6-di(thiophen-2-yl)benzo[1,2-b:4,5-b′]difuran (BDF) and either 3,6-di(2-furanyl)-1,4-diketopyrrolo[3,4-c]pyrrole (FDPP) or 3,6-di(2-thienyl)-1,4-diketopyrrolo[3,4-c]pyrrole (TDPP) as the acceptor, was presented. The polymers were first synthesized by the research laboratory of Professor Malika Jeffries-EL in Iowa State University. The steady state spectroscopy, two-photon spectroscopy and lifetime measurements were carried out on the polymers. The linear and nonlinear spectroscopic results were analyzed and correlated with the performance of the polymers in organic photovoltaics.

Chapter 6 gives an overall summary of the research and also suggests future research direction on the investigated organic macromolecules.

References

(1) Ors, O.; Sinayuc, C. An Experimental Study on the CO2–CH4 Swap Process between Gaseous CO2 and CH4 Hydrate in Porous Media. *J. Pet. Sci. Eng.* **2014**, *119*, 156–162.

(2) Soloiu, V.; Covington, A. Performance of a Direct Injection Diesel Engine Fueled by a Heavy Oil With the Addition of Low Density Polyethylene (LDPE) Polymer. *J. Eng. Gas Turb. Power* **2012**, *134*, 1–4.

(3) Lim, M.; Zhou, Y.; Guo, Y.; Sun, C.; Wood, B.; Wang, L.; Hulicova-Jurcakova, D.; Zou, J.; Rudolph, V.; Lu, G. Q. M. Visible-Light Photoresponsive Heterojunctions of (Nb–Ti–Si) and (Bi/Bi-O) Nanoparticles. *Electrochem. Commun.* **2009**, *11*, 509–514.

(4) (IFRC), I. F. R. C. Status Report on Fusion Research. *Nucl. Fusion* **2005**, *45*, A1–A28.

(5) Haseeb, A. S. M. A.; Fazal, M. A.; Jahirul, M. I.; Masjuki, H. H. Compatibility of Automotive Materials in Biodiesel: A Review. *Fuel* **2011**, *90*, 922–931.

(6) Woods, J.; Williams, A.; Hughes, J. K.; Black, M.; Murphy, R. Energy and the Food System. *Phil. Trans. R. Soc. B* **2010**, *365*, 2991–3006.

(7) Fadeyi, S.; Ustadi, I.; Fath, H.; Abu-Zahra, M. R. M. Evaluation of CO2 Post Combustion Capture Integration with Combined Cycle Power and Desalination Co-Generation Plant. *Energy Procedia* **2013**, *37*, 2595–2601.

(8) Mancaruso, E.; Sequino, L.; Vaglieco, B. M. First and Second Generation Biodiesels Spray Characterization in a Diesel Engine. *Fuel* **2011**, *90*, 2870–2883.

(9) Rosatella, A. A.; Simeonov, S. P.; Frade, R. F. M.; Afonso, C. A. M. 5-Hydroxymethylfurfural (HMF) as a Building Block Platform: Biological Properties, Synthesis and Synthetic Applications. *Green Chem.* **2011**, *13*, 754–793.

(10) Olah, G. A. Towards Oil Independence Through Renewable Methanol Chemistry. *Angew. Chem. Int. Ed.* **2013**, *52*, 104–107.

(11) United States Department of Energy. Http://energy.gov/science-Innovation/energy-Sources/fossil.

(12) Motasemi, F.; Ani, F. N. A Review on Microwave-Assisted Production of Biodiesel. *Renew. Sust. Energ. Rev.* **2012**, *16*, 4719–4733.

(13) Shamsul, N. S.; Kamarudin, S. K.; Rahman, N. A.; Kofli, N. T. An Overview on the Production of Bio-Methanol as Potential Renewable Energy. *Renew. Sust. Energ. Rev.* **2014**, *33*, 578–588.

(14) Shahir, S. A.; Masjuki, H. H.; Kalam, M. A.; Imran, A.; Fattah, I. M. R.; Sanjid, A. Feasibility of Diesel–biodiesel–ethanol/bioethanol Blend as Existing CI Engine Fuel: An Assessment of Properties, Material Compatibility, Safety and Combustion. *Renew. Sust. Energ. Rev.* **2014**, *32*, 379–395.

(15) Kiran, B.; Kumar, R.; Deshmukh, D. Perspectives of Microalgal Biofuels as a Renewable Source of Energy. *Energy Convers. Manag.* **2014**.

(16) Trancik, J. E. Back the Renewables Boom. *Nature* **2014**, *507*, 300–302.

(17) Gude, G. V.; Patil, P.; Martinez-Guerra, E.; Deng, S.; Nirmalakhandan, N. Microwave Energy Potential for Biodiesel Production. *Sustain. Chem. Process.* **2013**, *1*, 1–31.

(18) Gross, M. Looking for Alternative Energy Sources. *Curr. Biol.* **2012**, *22*, R103–R106.

(19) Williams, L. O. Alternative Energy Sources. *Appl. Energ.* **1994**, *47*, 123–146.

(20) Schiermeier, Q.; Kohnert, K. Renewables Revolution. *Nature* **2011**, *480*, 279–280.

(21) Glasnovic, Z.; Margeta, J. The Features of Sustainable Solar Hydroelectric Power Plant. *Renew. Energ.* **2009**, *34*, 1742–1751.

(22) Premalatha, M.; Tabassum-Abbasi; Abbasi, T.; Abbasi, S. A. A Critical View on the Eco-Friendliness of Small Hydroelectric Installations. *Sci. Total Environ.* **2014**, *481*, 638–643.

(23) Hu, Y.; Cheng, H. The Urgency of Assessing the Greenhouse Gas Budgets of Hydroelectric Reservoirs in China. *Nat. Clim. Chang.* **2013**, *3*, 708–712.

(24) Jiao, N.; Zhang, Y.; Zeng, Y.; Gardner, W. D.; Mishonov, A. V; Richardson, M. J.; Hong, N.; Pan, D.; Yan, X.-H.; Jo, Y.-H.; et al. Ecological Anomalies in the East China Sea: Impacts of the Three Gorges Dam? *Water Res.* **2007**, *41*, 1287–1293.

(25) Choi, J.; Kang, B.; Cho, H. Performance Comparison between R22 and R744 Solar-Geothermal Hybrid Heat Pumps according to Heat Source Conditions. *Renew. Energ.* **2014**, *71*, 414–424.

(26) Younger, P. L. Missing a Trick in Geothermal Exploration. *Nat. Geosci.* **2014**, *7*, 479–480.

(27) Majorowicz, J.; Grasby, S. E. Geothermal Energy for Northern Canada: Is It Economical? *Nat. Resour. Res.* **2013**, *23*, 159–173.

(28) Putra, D. D.; Lelawati, I. Finding Geothermal Energy Based on Radioisotopes Technology. *Energy Procedia* **2014**, *47*, 71–75.

(29) Wildemeersch, S.; Jamin, P.; Orban, P.; Hermans, T.; Klepikova, M.; Nguyen, F.; Brouyère, S.; Dassargues, A. Coupling Heat and Chemical Tracer Experiments for Estimating Heat Transfer Parameters in Shallow Alluvial Aquifers. *J. Contam. Hydrol.* **2014**, *169*, 90–99.

(30) Kalogirou, S. A. Seawater Desalination Using Renewable Energy Sources. *Prog. Energy Combust. Sci.* **2005**, *31*, 242–281.

(31) Fridleifsson, I. B. Geothermal Energy for the Benefit of the People. *Renew. Sust. Energ. Rev.* **2001**, *5*, 299–312.

(32) Wright, P. M. Geothermal Energy — A Sustainable Resource of Enormous Potential. *JOM* **1998**, *50*, 38–40.

(33) Barbier, E. Nature and Technology of Geothermal Energy: A Review. *Renew. Sust. Energ. Rev.* **1997**, *1*, 1–69.

(34) Barbier, E. Geothermal Energy Technology and Current Status: An Overview. *Renew. Sust. Energ. Rev.* **2002**, *6*, 3–65.

(35) Awerbuch, L.; Lindemuth, T. E.; May, S. C.; Rogers, A. N. Geothermal Energy Recovery Process. *Desalination* **1976**, *19*, 325–336.

(36) Bourouni, K.; Deronzier, J. C.; Tadrist, L. Experimentation and Modelling of an Innovative Geothermal Desalination Unit. *Desalination* **1999**, *125*, 147–153.

(37) Ko, W. I.; Lee, H. H.; Choi, S.; Kim, K. H.; Kim, S.-K.; Park, B. H.; Lee, H. J.; Kim, I. T.; Lee, H. S. Preliminary Conceptual Design and Cost Estimation for SFR Fuel Manufacturing Facility (SFMF). *Nucl. Eng. Des.* **2014**, *277*, 225–233.

(38) Marques, J. G. Environmental Characteristics of the Current Generation III Nuclear Power Plants. *WIREs Energy Env.* **2014**, *3*, 195–212.

(39) Dekker, L.; Osborne, T. H.; Santini, J. M. Isolation and Identification of Cobalt- and Caesium-Resistant Bacteria from a Nuclear Fuel Storage Pond. *FEMS Microbiol. Rev. Lett.* **2014**, *359*, 81–84.

(40) Dominiczak, M. H. Science, Art, and the Discovery of Nuclear Fission. *Clin. Chem.* **2014**, *60*, 1247–1248.

(41) Ricotti, M. E. Nuclear Energy: Basics, Present, Future. *EPJ Web Conf.* **2013**, *54*, 01005.

(42) Winter, C.-J. SUNRISE – A Caesura after Nuclear Has Gone: Energy in Germany (and in Other Potentially de-Nuclearizing Countries). *Int. J. Hydrog. Energy* **2012**, *37*, 7317–7342.

(43) Cesari, F. G.; Rogante, M.; Giostri, A. Results of the Experimental Campaign on Contaminated Metal Components Parameters and Suggestions for Safely NPP Component Dismantling. *Nucl. Eng. Des.* **2008**, *238*, 2801–2810.

(44) Bohrer, G.; Zhu, K.; Jones, R. L.; Curtis, P. S. Optimizing Wind Power Generation While Minimizing Wildlife Impacts in an Urban Area. *PLoS One* **2013**, *8*, 1–8.

(45) Xiaoa, X.; Yib, H.; Kang, Q.; Nie, J. A Two-Level Energy Storage System for Wind Energy Systems. *Procedia Environ. Sci.* **2012**, *12*, 130–136.

(46) Gu, W.; Du, Z. Simulation of Aluminum Electrolysis by Non-Grid-Connection Wind Power. *Adv. Mat. Res.* **2012**, *503-504*, 144–147.

(47) Hemmes, K.; Guerrero, J. M.; Zhelev, T. Highly Efficient Distributed Generation and High-Capacity Energy Storage. *Chem. Eng. Prog.* **2012**, *51*, 18–31.

(48) Tiang, T. L.; Ishak, D. Novel MPPT Control in Permanent Magnet Synchronous Generator System for Battery Energy Storage. *Appl. Mech. Mater.* **2011**, *110-116*, 5179–5183.

(49) Wang, K.; Jiang, K.; Chung, B.; Ouchi, T.; Burke, P. J.; Boysen, D. A.; Bradwell, D. J.; Kim, H.; Muecke, U.; Sadoway, D. R. Lithium–antimony–lead Liquid Metal Battery for Grid-Level Energy Storage. *Nature* **2014**, *514*, 348–350.

(50) Chen, L.; Shaw, L. L. Recent Advances in Lithium–sulfur Batteries. *J. Power Sources* **2014**, *267*, 770–783.

(51) Aho, P. Impact on the World Poultry Industry of the Global Shift to Biofuels. *Poult. Sci.* **2007**, *86*, 2291–2294.

(52) Galadima, A.; Muraza, O. Biodiesel Production from Algae by Using Heterogeneous Catalysts: A Critical Review. *Energy* **2014**, 1–12.

(53) Chomvong, K.; Kordi, V.; Li, X.; Bauer, S.; Gillespie, A. E.; Ha, S.; Oh, E. J.; Galazka, J. M.; Jin, Y.; Cate, J. H. D. Overcoming Inefficient Cellobiose Fermentation by Cellobiose Phosphorylase in the Presence of Xylose. *Biotechnol. Biofuels* **2014**, *85*, 1–11.

(54) Zaki, A. M.; Wimalasena, T. T.; Greetham, D. Phenotypic Characterisation of Saccharomyces Spp. for Tolerance to 1-Butanol. *J. Ind. Microbiol. Biotechnol.* **2014**, *41*, 1627–1636.

(55) Blumer-Schuette, S. E.; Brown, S. D.; Sander, K. B.; Bayer, E. A.; Kataeva, I.; Zurawski, J. V; Conway, J. M.; Adams, M. W. W.; Kelly, R. M. Thermophilic Lignocellulose Deconstruction. *FEMS Microbiol. Rev.* **2014**, *38*, 393–448.

(56) Faeth, J. L.; Valdez, P. J.; Savage, P. E. Fast Hydrothermal Liquefaction of Nannochloropsis Sp. To Produce Biocrude. *Energy Fuels* **2013**, *27*, 1391–1398.

(57) Savage, P. E.; Hestekin, J. a. A Perspective on Algae, the Environment, and Energy. *Environ. Prog. Sustain. Energy* **2013**, *32*, 877–883.

(58) Wen, B.; Yuan, X.; Li, Q. X.; Liu, J.; Ren, J.; Wang, X.; Cui, Z. Comparison and Evaluation of Concurrent Saccharification and Anaerobic Digestion of Napier Grass after Pretreatment by Three Microbial Consortia. *Bioresour. Technol/* **2015**, *175*, 102–111.

(59) Lindsey, K.; Johnson, A.; Kim, P.; Jackson, S.; Labbé, N. Monitoring Switchgrass Composition to Optimize Harvesting Periods for Bioenergy and Value-Added Products. *Biomass Bioenerg.* **2013**, *56*, 29–37.

(60) Murphy, T. E.; Fleming, E.; Berberoglu, H. Vascular Structure Design of an Artificial Tree for Microbial Cell Cultivation and Biofuel Production. *Transp. Porous Med.* **2014**, *104*, 25–41.

(61) Tang, W.; Tang, A. Y. Transgenic Woody Plants for Biofuel. *J. For. Res.* **2014**, *25*, 225–236.

(62) Bastian, S.; Liu, X.; Meyerowitz, J. T.; Snow, C. D.; Chen, M. M. Y.; Arnold, F. H. Engineered Ketol-Acid Reductoisomerase and Alcohol Dehydrogenase Enable Anaerobic 2-Methylpropan-1-Ol Production at Theoretical Yield in Escherichia Coli. *Metab. Eng.* **2011**, *13*, 345–352.

(63) Sureshkumar, K.; Velraj, R.; Ganesan, R. Performance and Exhaust Emission Characteristics of a CI Engine Fueled with Pongamia Pinnata Methyl Ester (PPME) and Its Blends with Diesel. *Renew. Energ.* **2008**, *33*, 2294–2302.

(64) Bundgaard, E.; Krebs, F. Low Band Gap Polymers for Organic Photovoltaics. *Sol. Energy Mater. Sol. Cells* **2007**, *91*, 954–985.

(65) Grätzel, M. Recent Advances in Sensitized Mesoscopic Solar Cells. *Acc. Chem. Res.* **2009**, *42*, 1788–1798.

(66) Grätzel, M. Photovoltaic and Photoelectrochemical Conversion of Solar Energy. *Phil. Trans. R. Soc. A* **2007**, *365*, 993–1005.

(67) Goldin, E.; Erickson, L.; Natarajan, B.; Brase, G.; Pahwa, A. Solar Powered Charge Stations for Electric Vehicles. *Environ. Prog. Sustain. Energy* **2014**, *33*, 1298–1308.

(68) Thirugnanasambandam, M.; Iniyan, S.; Goic, R. A Review of Solar Thermal Technologies. *Renew. Sust. Energ. Rev.* **2010**, *14*, 312–322.

(69) Romero, M.; González-Aguilar, J. Solar Thermal CSP Technology. *WIREs Energy Env.* **2014**, *3*, 42–59.

(70) Kribus, A. A High-Efficiency Triple Cycle for Solar Power Generation. *Sol. Energy* **2002**, *72*, 1–11.

(71) DeLaquil, P. Prospects for Solar Thermal Electricity Generation - an Introduction. *Sol. Energ. Mater.* **1991**, *24*, 78–81.

(72) Metz, W. D. Solar Thermal Electricity: Power Tower Dominates Research. *Science (80-.).* **1977**, *197*, 353–356.

(73) Berardi, S.; Drouet, S.; Francas, L.; Gimbert-Surinach, C.; Guttentag, M.; Richmond, C.; Stoll, T.; Llobet, A. Molecular Artificial Photosynthesis. *Chem. Soc. Rev.* **2014**, *43*, 7501–7519.

(74) Peer, A.; Biswas, R. Nanophotonic Organic Solar Cell Architecture for Advanced Light Trapping with Dual Photonic Crystals. *ACS Photonics* **2014**, *1*, 840–847.

(75) Vigil-Galán, O.; Courel, M.; Andrade-Arvizu, J. A.; Sánchez, Y.; Espíndola-Rodríguez, M.; Saucedo, E.; Seuret-Jiménez, D.; Titsworth, M. Route towards Low Cost-High Efficiency Second Generation Solar Cells: Current Status and Perspectives. *J. Mater. Sci. Mater. Electron.* **2014**.

(76) Liang, Y.; Yu, L. Development of Semiconducting Polymers for Solar Energy Harvesting. *Polym. Rev.* **2010**, *50*, 454–473.

(77) Schoijet, M. Possibilities of New Materials for Solar Photovoltaic Cells. *Sol. Energ. Mater.* **1979**, *1*, 43–57.

(78) Kaur, N.; Singh, M.; Pathak, D.; Wagner, T.; Nunzi, J. M. Organic Materials for Photovoltaic Applications: Review and Mechanism. *Synth. Met.* **2014**, *190*, 20–26.

(79) Green, M. A.; Keevers, M. J. Optical Properties of Intrinsic Silicon at 300. *Prog Photovoltaics Res Appl* **1995**, *3*, 189–192.

(80) Brabec, C. J.; Sariciftci, N. S.; Hummelen, J. C. Plastic Solar Cells. *Adv. Funct. Mater.* **2001**, *11*, 15–26.

(81) Xu, T.; Yu, L. How to Design Low Bandgap Polymers for Highly Efficient Organic Solar Cells. *Mater. Today* **2014**, *17*, 11–15.

(82) Kroon, R.; Lenes, M.; Hummelen, J. C.; Blom, P. W. M.; de Boer, B. Small Bandgap Polymers for Organic Solar Cells (Polymer Material Development in the Last 5 Years). *Polym. Rev.* **2008**, *48*, 531–582.

(83) Boudreault, P.-L. T.; Najari, A.; Leclerc, M. Processable Low-Bandgap Polymers for Photovoltaic Applications. *Chem. Mater.* **2011**, *23*, 456–469.

(84) Murray, I. P.; Lou, S. J.; Cote, L. J.; Loser, S.; Kadleck, C. J.; Xu, T.; Szarko, J. M.; Rolczynski, B. S.; Johns, J. E.; Huang, J.; et al. Graphene Oxide Interlayers for Robust, High-Efficiency Organic Photovoltaics. *J. Phys. Chem. Lett.* **2011**, *2*, 3006–3012.

(85) Tokito, S.; Noda, K.; Taga, Y. Metal Oxides as a Hole-Injecting Layer for an Organic Electroluminescent Device. *J. Phys. D Appl. Phys.* **1996**, *29*, 2750–2753.

(86) Brabec, C. J.; Durrant, J. R. Solution-Processed Organic Solar Cells. *MRS Bull.* **2008**, *33*, 670–675.

(87) Thompson, B. C.; Kim, Y.-G.; Reynolds, J. R. Spectral Broadening in MEH-PPV:PCBM-Based Photovoltaic Band Gap via Blending with a Narrow Band Gap Cyanovinylene-Dioxythiophene Polymer. *Macromolecules* **2005**, *38*, 5359–5362.

(88) Jørgensen, M.; Norrman, K.; Krebs, F. C. Stability/degradation of Polymer Solar Cells. *Sol. Energy Mater. Sol. Cells* **2008**, *92*, 686–714.

(89) Reece, S. Y.; Hamel, J. A.; Sung, K.; Jarvi, T. D.; Esswein, A. J.; Pijpers, J. J. H.; Nocera, D. G. Wireless Solar Water Splitting Using Silicon-Based Semiconductors and Earth-Abundant Catalysts. *Science (80-.).* **2011**, *334*, 645–648.

(90) Mitzi, D. B.; Gunawan, O.; Todorov, T. K.; Wang, K.; Guha, S. The Path towards a High-Performance Solution-Processed Kesterite Solar Cell. *Sol. Energy Mater. Sol. Cells* **2011**, *95*, 1421–1436.

(91) Mativetsky, J. M.; Loo, Y.-L. Modular Construction and Deconstruction of Organic Solar Cells. *AIChE* **2012**, *58*, 3280–3288.

(92) Mishra, A.; Bäuerle, P. Small Molecule Organic Semiconductors on the Move: Promises for Future Solar Energy Technology. *Angew. Chem. Int. Ed.* **2012**, *51*, 2020–2067.

(93) Liu, Y.; Chen, C.-C.; Hong, Z.; Gao, J.; Michael Yang, Y.; Zhou, H.; Dou, L.; Li, G.; Yang, Y. Solution-Processed Small-Molecule Solar Cells: Breaking the 10% Power Conversion Efficiency. *Sci. Rep.* **2013**, *3*, 3356.

(94) Bag, M.; Gehan, T. S.; Renna, L. a.; Algaier, D. D.; Lahti, P. M.; Venkataraman, D. Fabrication Conditions for Efficient Organic Photovoltaic Cells from Aqueous Dispersions of Nanoparticles. *RSC Adv.* **2014**, *4*, 45325–45331.

(95) Li, Y.; Yu, T.; Pui, T.; Chen, P.; Zheng, L.; Liao, K. Fabrication of Transparent and Conductive Carbon Nanotube/polyvinyl Butyral Films by a Facile Solution Surface Dip Coating Method. *Nanoscale* **2011**, *3*, 2469–2471.

(96) Oh, J.; Yuan, H.-C.; Branz, H. M. An 18.2%-Efficient Black-Silicon Solar Cell Achieved through Control of Carrier Recombination in Nanostructures. *Nat. Nanotech.* **2012**, *7*, 743–748.

(97) Deinega, A.; John, S. Solar Power Conversion Efficiency in Modulated Silicon Nanowire Photonic Crystals. *J. Appl. Phys.* **2012**, *112*, 1–7.

(98) Verlinden, P. J.; Aleman, M.; Posthuma, N.; Fernandez, J.; Pawlak, B.; Robbelein, J.; Debucquoy, M.; Van Wichelen, K.; Poortmans, J. Simple Power-Loss Analysis Method for High-Efficiency Interdigitated Back Contact (IBC) Silicon Solar Cells. *Sol. Energy Mater. Sol. Cells* **2012**, *106*, 37–41.

(99) Battaglia, C.; Yin, X.; Zheng, M.; Sharp, I. D.; Chen, T.; Mcdonnell, S.; Azcatl, A.; Carraro, C.; Ma, B.; Maboudian, R.; et al. Hole Selective MoOx Contact for Silicon Solar Cells. *Nano Lett.* **2014**, *14*, 967–971.

(100) Jeong, S.; McGehee, M. D.; Cui, Y. All-Back-Contact Ultra-Thin Silicon Nanocone Solar Cells with 13.7% Power Conversion Efficiency. *Nat. Commun.* **2013**, *4*, 1–7.

(101) Li, G.; Zhu, R.; Yang, Y. Polymer Solar Cells. *Nat. Photon.* **2012**, *6*, 153–161.

(102) You, J.; Dou, L.; Yoshimura, K.; Kato, T.; Ohya, K.; Moriarty, T.; Emery, K.; Chen, C.-C.; Gao, J.; Li, G.; et al. A Polymer Tandem Solar Cell with 10.6% Power Conversion Efficiency. *Nat. Commun.* **2013**, *4*, 1–10.

(103) Chen, C.-C.; Chang, W.-H.; Yoshimura, K.; Ohya, K.; You, J.; Gao, J.; Hong, Z.; Yang, Y. An Efficient Triple-Junction Polymer Solar Cell Having a Power Conversion Efficiency Exceeding 11%. *Adv. Mater.* **2014**, *26*, 5670–5677.

(104) http://www.heliatek.com/newscenter/latest_news/neuer-weltrekord-fur-organische-solarzellen-heliatek-behauptet-sich-mit-12-zelleffizienz-als-technologiefuhrer/?lang=en#. Heliatek consolidates its technology leadership by establishing a new world record for organic solar technology with a cell efficiency of 12%.

(105) Green, M. A. Silicon Solar Cells: State of the Art. *Phil. Trans. R. Soc. A* **2013**, *371*, 20110413.

(106) Gratzel, M. Photoelectrochemical Cells. *Nature* **2001**, *414*, 338–344.

(107) Goetzberger, A.; Hebling, C.; Schock, H.-W. Photovoltaic Materials, History, Status and Outlook. *Mater. Sci. Eng. R.* **2003**, *40*, 1–46.

(108) Blakers, A.; Zin, N.; McIntosh, K. R.; Fong, K. High Efficiency Silicon Solar Cells. *Energy Procedia* **2013**, *33*, 1–10.

(109) Bringing Solar Cell Efficiencies into the Light. *Nat. Nanotech.* **2014**, *9*, 657.

(110) Escalante, J. M.; Martínez, A. Optical Gain by Simultaneous Photon and Phonon Confinement in Indirect Bandgap Semiconductor Acousto-Optical Cavities. *Opt. Quant. Electron.* **2013**, *45*, 1045–1056.

(111) Munguía, J.; Bluet, J.-M.; Marty, O.; Bremond, G.; Mermoux, M.; Rouchon, D. Temperature Dependence of the Indirect Bandgap in Ultrathin Strained Silicon on Insulator Layer. *Appl. Phys. Lett.* **2012**, *100*, 102107.

(112) Luo, J.; Franceschetti, A.; Zunger, A. Direct-Bandgap InAs Quantum Dots Have Long-Range Electron - Hole Exchange Whereas Indirect Gap Si Dots Have Short-Range Exchange. *Nano Lett.* **2009**, *9*, 2648–2653.

(113) Goetzberger, A.; Hebling, C. Photovoltaic Materials, Past, Present, Future. *Sol. Energy Mater. Sol. Cells* **2000**, *62*, 1–19.

(114) Green, M. A. Thin-Film Solar Cells: Review of Materials, Technologies and Commercial Status. *J. Mater. Sci. Mater. Electron.* **2007**, *18*, 15–19.

(115) Jung, I. H.; Lo, W.-Y.; Jang, J.; Chen, W.; Zhao, D.; Landry, E. S.; Lu, L.; Talapin, D. V; Yu, L. Synthesis and Search for Design Principles of New Electron Accepting Polymers for All-Polymer Solar Cells. *Chem. Mater.* **2014**, *26*, 3450–3459.

(116) Niklas, J.; Mardis, K. L.; Banks, B. P.; Grooms, G. M.; Sperlich, A.; Dyakonov, V.; Beaupré, S.; Leclerc, M.; Xu, T.; Yu, L.; et al. Highly-Efficient Charge Separation and Polaron Delocalization in Polymer-Fullerene Bulk-Heterojunctions: A Comparative Multi-Frequency EPR and DFT Study. *Phys. Chem. Chem. Phys.* **2013**, *15*, 9562–9574.

(117) Niv, A.; Abrams, Z. R.; Gharghi, M.; Gladden, C.; Zhang, X. Overcoming the Bandgap Limitation on Solar Cell Materials. *Appl. Phys. Lett.* **2012**, *100*, 083901.

(118) ASTM International. Standard Test Method for Electrical Performance of Photovoltaic Cells Using Reference Cells Under Simulated Sunlight. 1–6.

(119) Mori, D.; Benten, H.; Okada, I.; Ohkita, H.; Ito, S. Highly Efficient Charge-Carrier Generation and Collection in Polymer/polymer Blend Solar Cells with a Power Conversion Efficiency of 5.7%. *Energy Environ. Sci.* **2014**, *7*, 2939–2943.

(120) Mahmood, K.; Swain, B. S.; Amassian, A. Double-Layered ZnO Nanostructures for Efficient Perovskite Solar Cells. *Nanoscale* **2014**.

(121) Song, B.; Rolin, C.; Zimmerman, J. D.; Forrest, S. R. Effect of Mixed Layer Crystallinity on the Performance of Mixed Heterojunction Organic Photovoltaic Cells. *Adv. Mater.* **2014**, *26*, 2914–2918.

(122) Bolognesi, M.; Gedefaw, D.; Dang, D.; Henriksson, P.; Zhuang, W.; Tessarolo, M.; Wang, E.; Muccini, M.; Seri, M.; Andersson, M. R. 2D Π-Conjugated benzo[1,2-b:4,5-B′]dithiophene- and Quinoxaline-Based Copolymers for Photovoltaic Applications. *RSC Adv.* **2013**, *3*, 24543–24552.

(123) Cheng, W.; Wu, Z.; Wen, S.; Xu, B.; Li, H.; Zhu, F.; Tian, W. Donor–acceptor Copolymers Incorporating polybenzo[1,2-b:4,5-B′]dithiophene and Tetrazine for High Open Circuit Voltage Polymer Solar Cells. *Org. Electron.* **2013**, *14*, 2124–2131.

(124) Carsten, B.; Szarko, J. M.; Son, H. J.; Wang, W.; Lu, L.; He, F.; Rolczynski, B. S.; Lou, S. J.; Chen, L. X.; Yu, L. Examining the Effect of the Dipole Moment on Charge Separation in Donor-Acceptor Polymers for Organic Photovoltaic Applications. *J. Am. Chem. Soc.* **2011**, *133*, 20468–20475.

(125) Lu, Y.; Xiao, Z.; Yuan, Y.; Wu, H.; An, Z.; Hou, Y.; Gao, C.; Huang, J. Fluorine Substituted Thiophene–quinoxaline Copolymer to Reduce the HOMO Level and Increase the Dielectric Constant for High Open-Circuit Voltage Organic Solar Cells. *J. Mater. Chem. C* **2013**, *1*, 630–637.

(126) Liang, Y.; Feng, D.; Wu, Y.; Tsai, S.-T.; Li, G.; Ray, C.; Yu, L. Highly Efficient Solar Cell Polymers Developed via Fine-Tuning of Structural and Electronic Properties. *J. Am. Chem. Soc.* **2009**, *131*, 7792–7799.

(127) Qi, B.; Wang, J. Fill Factor in Organic Solar Cells. *Phys. Chem. Chem. Phys.* **2013**, *15*, 8972–8982.

(128) Guo, X.; Zhou, N.; Lou, S. J.; Smith, J.; Tice, D. B.; Hennek, J. W.; Ortiz, R. P.; Navarrete, J. T. L.; Li, S.; Strzalka, J.; et al. Polymer Solar Cells with Enhanced Fill Factors. *Nat. Photon.* **2013**, *7*, 825–833.

(129) Guliani, R.; Jain, A.; Kapoor, A. Exact Analytical Analysis of Dye-Sensitized Solar Cell : Improved Method and Comparative Study. *Open Renew. Energ. J.* **2012**, 49–60.

(130) Anand, T. J. S.; Zaidan, M. Electro Synthesised NiTe2 Thin Films with the Influence of Additives. *Adv. Mat. Res.* **2014**, *925*, 159–163.

(131) Srinivas, K. Nanoparticles Influence on Dye-Sensitized Solar Cells Based on TiO2. *J. Nanosci. Nanotechnol.* **2014**, *2*, 32–39.

(132) Mottishaw, J. D.; Kilin, D.; Cheng, H.-P.; Karasiev, V. V.; Fan, Q. H.; Sun, H. Elucidating the Role of Non-Radiative Processes in Charge Transfer of Core–shell Si–SiO 2 Nanoparticles. *Mol. Phys.* **2013**, *112*, 422–429.

(133) Scharber, M. C.; Sariciftci, N. S. Efficiency of Bulk-Heterojunction Organic Solar Cells. *Prog. Polym. Sci.* **2013**, *38*, 1929–1940.

(134) Su, Y.-W.; Lan, S.-C.; Wei, K.-H. Organic Photovoltaics. *Mater. Today* **2012**, *15*, 554–562.

(135) Tang, Z.; Tress, W.; Inganäs, O. Light Trapping in Thin Film Organic Solar Cells. *Mater. Today* **2014**, *17*, 389–396.

(136) Ohkita, H.; Ito, S. Transient Absorption Spectroscopy of Polymer-Based Thin-Film Solar Cells. *Polymer (Guildf).* **2011**, *52*, 4397–4417.

(137) Benanti, T. L.; Venkataraman, D. Organic Solar Cells: An Overview Focusing on Active Layer Morphology. *Photosynth. Res.* **2006**, *87*, 73–81.

(138) Kallmann, H.; Pope, M. Photovoltaic Effect in Organic Crystals. *J. Chem. Phys.* **1959**, *30*, 585–586.

(139) Tang, C. W. Two-Layer Organic Photovoltaic Cell. *Appl. Phys. Lett.* **1986**, *48*, 183–185.

(140) Gadisa, A.; Oosterbaan, W. D.; Vandewal, K.; Bolsée, J.-C.; Bertho, S.; D'Haen, J.; Lutsen, L.; Vanderzande, D.; Manca, J. V. Effect of Alkyl Side-Chain Length on Photovoltaic Properties of Poly(3-alkylthiophene)/PCBM Bulk Heterojunctions. *Adv. Funct. Mater.* **2009**, *19*, 3300–3306.

(141) Min, J.; Luponosov, Y. N.; Gerl, A.; Polinskaya, M. S.; Peregudova, S. M.; Dmitryakov, P. V.; Bakirov, A. V.; Shcherbina, M. A.; Chvalun, S. N.; Grigorian, S.; et al. Alkyl Chain Engineering of Solution-Processable Star-Shaped Molecules for High-Performance Organic Solar Cells. *Adv. Energy Mater.* **2014**, *4*, 1301234.

(142) Gevaerts, V. S.; Koster, L. J. A.; Wienk, M. M.; Janssen, R. A. J. Discriminating between Bilayer and Bulk Heterojunction Polymer: Fullerene Solar Cells Using the External Quantum Efficiency. *ACS Appl. Mater. Interfaces* **2011**, *3*, 3252–3255.

(143) Zhong, Z.; Liu, J.; Xie, Z. Y.; Wang, Z. Y. Significant Efficiency Enhancement of Bulk Heterojunction Organic Photovoltaics Using Solution-Processable Interfacial Bilayers. *ChemElectroChem* **2014**, *1*, 471–475.

(144) Deibel, C.; Dyakonov, V. Polymer–fullerene Bulk Heterojunction Solar Cells. *Rep. Prog. Phys.* **2010**, *73*, 096401.

(145) Yu, G.; Gao, J.; Hummelen, J. C.; Wudl, F.; Heeger, A. J. Polymer Photovoltaic Cells: Enhanced Efficiencies via a Network of Internal Heterojunctions. *Science (80-.).* **1195**, *270*, 1789–1791.

(146) Eftaiha, A. F.; Sun, J.-P.; Hill, I. G.; Welch, G. C. Recent Advances of Non-Fullerene, Small Molecular Acceptors for Solution Processed Bulk Heterojunction Solar Cells. *J. Mater. Chem. A* **2014**, *2*, 1201–1213.

(147) Bloking, J. T.; Han, X.; Higgs, A. T.; Kastrop, J. P.; Pandey, L.; Norton, J. E.; Risko, C.; Chen, C. E.; Bredas, J.-L.; McGehee, M. D.; et al. Solution-Processed Organic Solar Cells with Power Conversion Efficiencies of 2.5% Using Benzothiadiazole/Imide-Based Acceptors. *Chem. Mater.* **2011**, *23*, 5484–5490.

(148) Urien, M.; Bailly, L.; Vignau, L.; Cloutet, E.; Cuendias, A. De; Wantz, G.; Cramail, H.; Hirsch, L.; Parneix, J.-P. Effect of the Regioregularity of Poly (3-Hexylthiophene) on the Performances of Organic Photovoltaic Devices. *Polym. Int.* **2008**, *57*, 764–769.

(149) Kim, Y.; Cook, S.; Tuladhar, S. M.; Choulis, S. A.; Nelson, J.; Durrant, J. R.; Bradley, D. D. C.; Giles, M.; McCulloch, I.; Ha, C.-S.; et al. A Strong Regioregularity Effect in Self-Organizing Conjugated Polymer Films and High-Efficiency Polythiophene:fullerene Solar Cells. *Nat. Mater.* **2006**, *5*, 197–203.

(150) Kline, R. J.; McGehee, M. D.; Kadnikova, E. N.; Liu, J.; Fréchet, J. M. J. Controlling the Field-Effect Mobility of Regioregular Polythiophene by Changing the Molecular Weight. *Adv. Mater.* **2003**, *15*, 1519–1522.

(151) Ma, W.; Kim, J. Y.; Lee, K.; Heeger, A. J. Effect of the Molecular Weight of Poly(3-Hexylthiophene) on the Morphology and Performance of Polymer Bulk Heterojunction Solar Cells. *Macromol. Rapid Commun.* **2007**, *28*, 1776–1780.

(152) Goh, C.; Kline, R. J.; McGehee, M. D.; Kadnikova, E. N.; Fréchet, J. M. J. Molecular-Weight-Dependent Mobilities in Regioregular poly(3-Hexyl-Thiophene) Diodes. *Appl. Phys. Lett.* **2005**, *86*, 122110.

(153) Li, G.; Shrotriya, V.; Huang, J.; Yao, Y.; Moriarty, T.; Emery, K.; Yang, Y. High-Efficiency Solution Processable Polymer Photovoltaic Cells by Self-Organization of Polymer Blends. *Nat. Mater.* **2005**, *4*, 864–868.

(154) Ma, W.; Yang, C.; Gong, X.; Lee, K.; Heeger, A. J. Thermally Stable, Efficient Polymer Solar Cells with Nanoscale Control of the Interpenetrating Network Morphology. *Adv. Funct. Mater.* **2005**, *15*, 1617–1622.

(155) Irwin, M. D.; Buchholz, D. B.; Hains, A. W.; Chang, R. P. H.; Marks, T. J. P-Type Semiconducting Nickel Oxide as an Efficiency-Enhancing Anode Interfacial Layer in Polymer Bulk-Heterojunction Solar Cells. *PNAS* **2007**, *105*, 2783–2787.

(156) Liao, S.-H.; Li, Y.-L.; Jen, T.-H.; Cheng, Y.-S.; Chen, S.-A. Multiple Functionalities of Poly Fl Uorene Grafted with Metal Ion- Intercalated Crown Ether as an Electron Transport Layer for Bulk- Heterojunction Polymer Solar Cells: Optical Interference, Hole Blocking, Interfacial Dipole, and Electron Conduction. *J. Am. Chem. Soc.* **2012**, *134*, 14271–14274.

(157) He, D.; Zuo, C.; Chen, S.; Xiao, Z.; Ding, L. A Highly Efficient Fullerene Acceptor for Polymer Solar Cells. *Phys. Chem. Chem. Phys.* **2014**, *16*, 7205–7208.

(158) Dou, L.; You, J.; Hong, Z.; Xu, Z.; Li, G.; Street, R. A.; Yang, Y. 25th Anniversary Article: A Decade of Organic/Polymeric Photovoltaic Research. *Adv. Mater.* **2013**, *25*, 6642–6671.

(159) Lin, Y.-Y.; Chen, C.-W.; Chu, T.-H.; Su, W.-F.; Lin, C.-C.; Ku, C.-H.; Wu, J.-J.; Chen, C.-H. Nanostructured Metal Oxide/conjugated Polymer Hybrid Solar Cells by Low Temperature Solution Processes. *J. Mater. Chem.* **2007**, *17*, 4571–4576.

(160) Kiebooms, R.; Zojer, E.; Markart, P.; Resel, R.; Schepper, L. De; Vanderzande, D.; Gelan, J.; Stals, L.; Tasch, S.; Leising, G. Application of New PPV Precursor Polymers in Organic LEDs. *Synth. Met.* **1999**, *102*, 997.

(161) Hoppe, H.; Glatzel, T.; Niggemann, M.; Schwinger, W.; Schaeffler, F.; Hinsch, a.; Lux-Steiner, M. C.; Sariciftci, N. S. Efficiency Limiting Morphological Factors of MDMO-PPV:PCBM Plastic Solar Cells. *Thin Solid Films* **2006**, *511-512*, 587–592.

(162) Rispens, M. T.; Meetsma, A.; Rittberger, R.; Brabec, C. J.; Sariciftci, S. N.; Hummelen, J. C. Influence of the Solvent on the Crystal Structure of PCBM † and the Efficiency of MDMO-PPV : PCBM " Plastic " Solar Cells. *Chem. Commun.* **2003**, 2116–2118.

(163) Kroon, J. M.; Wienk, M. M.; Verhees, W. J. H.; Hummelen, J. C. Accurate Efficiency Determination and Stability Studies of Conjugated Polymer/fullerene Solar Cells. *Thin Solid Films* **2002**, *403-404*, 223–228.

(164) Shao, S.; Liu, F.; Xie, Z.; Wang, L. High-Efficiency Hybrid Polymer Solar Cells with Inorganic P- and N-Type Semiconductor Nanocrystals to Collect Photogenerated Charges. *J. Phys. Chem. C* **2010**, *114*, 9161–9166.

(165) Qian, L.; Zheng, Y.; Choudhury, K. R.; Bera, D.; So, F.; Xue, J.; Holloway, P. H. Electroluminescence from Light-Emitting polymer/ZnO Nanoparticle Heterojunctions at Sub-Bandgap Voltages. *Nano Today* **2010**, *5*, 384–389.

(166) Chambers, D. K.; Selmic, S. Advanced Characterization of the Electronic Structure of MEH-PPV. *Mater. Res. Soc. Symp. Proc.* **2005**, *871*.

(167) Umeyama, T.; Takamatsu, T.; Tezuka, N.; Matano, Y.; Araki, Y.; Wada, T.; Yoshikawa, O.; Sagawa, T.; Yoshikawa, S.; Imahori, H. Synthesis and Photophysical and Photovoltaic Properties of Porphyrin - Furan and - Thiophene Alternating Copolymers. *J. Phys. Chem. C* **2009**, *113*, 10798–10806.

(168) Martínez-Díaz, M. V.; de la Torre, G.; Torres, T. Lighting Porphyrins and Phthalocyanines for Molecular Photovoltaics. *Chem. Commun.* **2010**, *46*, 7090–7108.

(169) Gregg, B. A.; Fox, M. A.; Bard, A. J. Photovoltaic Effect In Symmetrical Cells of a Liquid Crystal Porphyrin. *J. Phys. Chem.* **1990**, *94*, 1586–1598.

(170) Sun, Q.; Dai, L.; Zhou, X.; Li, L.; Li, Q. Bilayer- and Bulk-Heterojunction Solar Cells Using Liquid Crystalline Porphyrins as Donors by Solution Processing. *Appl. Phys. Lett.* **2007**, *91*, 253505.

(171) Huijser, A.; Savenije, T. J.; Shalav, A.; Siebbeles, L. D. A. An Experimental Study on the Molecular Organization and Exciton Diffusion in a Bilayer of a Porphyrin and poly(3-Hexylthiophene). *J. Appl. Phys.* **2008**, *104*, 034505.

(172) Lawrence, M. F.; Huang, Z.; Langford, C. H.; Ordonez, I. Photocurrent Generation and Cbarge Transport in SnOz/Ion-Exchange Polymer-ZnTPP/Au Cells. *J. Phys. Chem.* **1993**, *97*, 944–951.

(173) Kerp, H. R.; Donker, H.; Koehorst, R. B. M.; Schaafsma, T. J.; van Faassen, E. E. Exciton Transport in Organic Dye Layers for Photovoltaic Applications. *Chem. Phys. Lett.* **1998**, *298*, 302–308.

(174) Kocherzhenko, A. A.; Patwardhan, S.; Grozema, F. C.; Anderson, H. L.; Siebbeles, L. D. A. Mechanism of Charge Transport along Zinc Porphyrin-Based Molecular Wires. *J. Am. Chem. Soc.* **2009**, *131*, 5522–5529.

(175) Itoh, E.; Higuchi, Y.; Furuhata, D.; Shirotori, T. Enhancement of the Open-Circuit Voltage and Hole Conduction of Tetraphenyl Porphyrin/C60 Multilayered Photovoltaic Device by the Insertion of Oxide Hole Collection Layers. *Jpn. J. Appl. Phys.* **2011**, *50*, 01BC14.

(176) Brennan, B. J.; Liddell, P. A.; Moore, T. A.; Moore, A. L.; Gust, D. Hole Mobility in Porphyrin- and Porphyrin-Fullerene Electropolymers. *J. Phys. Chem. B* **2013**, *117*, 426–432.

(177) Zhao, L.; Wagner, P.; Elliott, A. B. S.; Griffith, M. J.; Clarke, T. M.; Gordon, K. C.; Mori, S.; Mozer, A. J. Enhanced Performance of Dye-Sensitized Solar Cells Using Carbazole-Substituted Di-Chromophoric Porphyrin Dyes. *J. Mater. Chem. A* **2014**, *2*, 16963–16977.

(178) Senge, M. O.; Fazekas, M.; Notaras, E. G. A.; Blau, W. J.; Zawadzka, M.; Locos, O. B.; Ni Mhuircheartaigh, E. M. Nonlinear Optical Properties of Porphyrins. *Adv. Mater.* **2007**, *19*, 2737–2774.

(179) Fischer, M. K. R.; Lopez-Duarte, I.; Wienk, M. M.; Martinez-Diaz, M. V.; Janssen, R. A. J.; Bauerle, P.; Torres, T. Functionalized Dendritic Oligothiophenes: Ruthenium Phthalocyanine Complexes and Their Application in Bulk Heterojunction Solar Cells. *J. Am. Chem. Soc.* **2009**, *131*, 8669–8676.

(180) Kerp, H. R.; Donker, H.; Koehorst, R. B. M.; Schaafsma, T. J.; van Faassen, E. E. Exciton Transport in Organic Dye Layers for Photovoltaic Applications. *Chem. Phys. Lett.* **1998**, *298*, 302–308.

(181) Claessens, C. G.; Hahn, U.; Torres, T. Phthalocyanines: From Outstanding Electronic Properties to Emerging Applications. *Chem. Rec.* **2008**, *8*, 75–97.

(182) Vivo, P.; Ojala, M.; Chukharev, V.; Efimov, A.; Lemmetyinen, H. Role of a Phthalocyanine–fullerene Dyad in Multilayered Organic Solar Cells. *J. Photochem. Photobiol. A Chem.* **2009**, *203*, 125–130.

(183) Stübinger, T.; Brütting, W. Exciton Diffusion and Optical Interference in Organic Donor–acceptor Photovoltaic Cells. *J. Appl. Phys.* **2001**, *90*, 3632–3641.

(184) Yang, L.-G.; Chen, H.-Z.; Wang, M. Optimal Film Thickness for Exciton Diffusion Length Measurement by Photocurrent Response in Organic Heterostructures. *Thin Solid Films* **2008**, *516*, 7701–7707.

(185) Gao, J.; Xu, J. B.; Zhu, M.; Ke, N.; Ma, D. Thickness Dependence of Mobility in CuPc Thin Film on Amorphous SiO2 Substrate. *J. Phys. D Appl. Phys.* **2007**, *40*, 5666–5669.

(186) Kraus, M.; Haug, S.; Brütting, W.; Opitz, A. Achievement of Balanced Electron and Hole Mobility in Copper-Phthalocyanine Field-Effect Transistors by Using a Crystalline Aliphatic Passivation Layer. *Org. Electron.* **2011**, *12*, 731–735.

(187) Ofuji, M.; Ishikawa, K.; Takezoe, H.; Inaba, K.; Omote, K. Crystallite Size Effect on the Hole Mobility of Uniaxially Aligned Copper Phthalocyanine Thin-Film Field-Effect Transistors. *Appl. Phys. Lett.* **2005**, *86*, 062114.

(188) Peumans, P.; Forrest, S. R. Very-High-Efficiency Double-Heterostructure Copper phthalocyanine/C6 Photovoltaic Cells. *Appl. Phys. Lett.* **2001**, *79*, 126–128.

(189) Cheng, Y.-J.; Yang, S.-H.; Hsu, C.-S. Synthesis of Conjugated Polymers for Organic Solar Cell Applications. *Chem. Rev.* **2009**, *109*, 5868–5923.

(190) Liang, Y.; Luping, Y. A New Class of Semiconducting Polymers for Bulk Heterojunction Solar Cells with Exceptionally High Performance. *Acc. Chem. Res.* **2010**, *43*, 1227–1236.

(191) Son, H. J.; Wang, W.; Xu, T.; Liang, Y.; Wu, Y.; Li, G.; Yu, L. Synthesis of Fluorinated Polythienothiophene- Co -Benzodithiophenes and Effect of Fluorination on the Photovoltaic Properties. *J. Am. Chem. Soc.* **2011**, *133*, 1885–1894.

(192) Blouin, N.; Michaud, A.; Leclerc, M. A Low-Bandgap Poly(2,7-Carbazole) Derivative for Use in High-Performance Solar Cells. *Adv. Mater.* **2007**, *19*, 2295–2300.

(193) Beiley, Z. M.; Hoke, E. T.; Noriega, R.; Dacuña, J.; Burkhard, G. F.; Bartelt, J. A.; Salleo, A.; Toney, M. F.; McGehee, M. D. Morphology-Dependent Trap Formation in High Performance Polymer Bulk Heterojunction Solar Cells. *Adv. Energy Mater.* **2011**, 954–962.

(194) Park, S. H.; Roy, A.; Beaupré, S.; Cho, S.; Coates, N.; Moon, J. S.; Moses, D.; Leclerc, M.; Lee, K.; Heeger, A. J. Bulk Heterojunction Solar Cells with Internal Quantum Efficiency Approaching 100%. *Nat. Photon.* **2009**, *3*, 297–302.

(195) Zhu, Z.; Waller, D.; Gaudiana, R.; Morana, M.; Muhlbacher, D.; Scharber, M.; Brabec, C. Panchromatic Conjugated Polymers Containing Alternating Donor / Acceptor Units for Photovoltaic Applications. *Macromolecules* **2007**, *40*, 1981–1986.

(196) Hou, J.; Chen, H.-Y.; Zhang, S.; Li, G.; Yang, Y. Synthesis, Characterization, and Photovoltaic Properties of a Low Band Gap Polymer Based on Silole-Containing Polythiophenes and 2,1,3-Benzothiadiazole. *J. Am. Chem. Soc.* **2008**, *130*, 16144–16145.

(197) Liang, Y.; Wu, Y.; Feng, D.; Tsai, S.-T.; Son, H.-J.; Li, G.; Yu, L. Development of New Semiconducting Polymers for High Performance Solar Cells. *J. Am. Chem. Soc.* **2009**, *131*, 56–57.

(198) Liang, Y.; Xu, Z.; Xia, J.; Tsai, S.-T.; Wu, Y.; Li, G.; Ray, C.; Yu, L. For the Bright Future-Bulk Heterojunction Polymer Solar Cells with Power Conversion Efficiency of 7.4%. *Adv. Mater.* **2010**, *22*, E135–E138.

(199) Huo, L.; Zhang, S.; Guo, X.; Xu, F.; Li, Y.; Hou, J. Replacing Alkoxy Groups with Alkylthienyl Groups: A Feasible Approach to Improve the Properties of Photovoltaic Polymers. *Angew. Chem. Int. Ed.* **2011**, *50*, 9697–9702.

(200) Huang, Y.; Guo, X.; Liu, F.; Huo, L.; Chen, Y.; Russell, T. P.; Han, C. C.; Li, Y.; Hou, J. Improving the Ordering and Photovoltaic Properties by Extending Π-Conjugated Area of Electron-Donating Units in Polymers with D-A Structure. *Adv. Mater.* **2012**, *24*, 3383–3389.

(201) Adhikary, P.; Venkatesan, S.; Adhikari, N.; Maharjan, P. P.; Adebanjo, O.; Chen, J.; Qiao, Q. Enhanced Charge Transport and Photovoltaic Performance of PBDTTT-C-T/PC70BM Solar Cells via UV-Ozone Treatment. *Nanoscale* **2013**, *5*, 10007–10013.

(202) Wienk, M. M.; Kroon, J. M.; Verhees, W. J. H.; Knol, J.; Hummelen, J. C.; van Hal, P. A.; Janssen, R. A. J. Efficient methano[70]fullerene/MDMO-PPV Bulk Heterojunction Photovoltaic Cells. *Angew. Chem. Int. Ed.* **2003**, *42*, 3371–3375.

(203) Ross, R. B.; Cardona, C. M.; Guldi, D. M.; Sankaranarayanan, S. G.; Reese, M. O.; Kopidakis, N.; Peet, J.; Walker, B.; Bazan, G. C.; Van Keuren, E.; et al. Endohedral Fullerenes for Organic Photovoltaic Devices. *Nat. Mater.* **2009**, *8*, 208–212.

(204) Sharma, G. D.; Roy, M. S.; Mikroyannidis, J. A.; Justin Thomas, K. R. Synthesis and Characterization of a New Perylene Bisimide (PBI) Derivative and Its Application as Electron Acceptor for Bulk Heterojunction Polymer Solar Cells. *Org. Electron.* **2012**, *13*, 3118–3129.

(205) Sharma, G. D.; Suresh, P.; Mikroyannidis, J. A.; Stylianakis, M. M. Efficient Bulk Heterojunction Devices Based on Phenylenevinylene Small Molecule and Perylene–pyrene Bisimide. *J. Mater. Chem.* **2010**, *20*, 561–567.

(206) Rajaram, S.; Armstrong, P. B.; Kim, B. J.; Frechet, J. M. J. Morphology and Performance of. *Chem. Mater.* **2009**, *21*, 2008–2010.

Chapter 2

Experimental Techniques

2.1 Overview

The experimental techniques used in these studies are described in this section. These experimental techniques are used in the publications that were reproduced in the latter chapters. The theoretical background of the various techniques and the various instrumentations are presented. The details are described such that the reader does not need to consult other sources for explanation of the techniques used.

2.2 Steady-state Spectroscopy

Steady-state spectroscopy includes two spectroscopic techniques used for initial investigation of organic materials and chromophores. These techniques are UV-visible absorption spectroscopy and fluorescence spectroscopy. These techniques were used throughout these studies for the initial investigation of organic compounds. The compounds are investigated over a range of frequencies in each of the techniques.

The UV-visible absorption spectroscopy involves the measurement of the absorption of light radiation, as a function of frequency or wavelength, due to the interaction of light with the sample in solution phase. As the sample interacts and absorbs energy in the form of packets of light known as photons, there is a transition from the ground state to the excited state. This

transition of state is what is reflected in the absorption spectrum which is a measure of absorbed intensity of light as a function of wavelengths. The absorption process is based on the principle of Beer-Lambert law in which the absorbance of light of a sample at a given wavelength is directly proportional to the concentration of the sample for a given path length. The constant of proportionality is the molar extinction coefficient usually represented by ε and measured in $M^{-1}cm^{-1}$. The molar extinction coefficient only varies with the wavelength of the input light. The Beer-Lambert law is represented mathematically by:[1]

$$A = \log\left(\frac{I_o}{I}\right) = \varepsilon \cdot l \cdot c \qquad \textbf{Equation 2.1}$$

In Equation 2.1, A is the absorbance or optical density of the sample of concentration c (*mol/l*) placed in a cuvette with path length of *l* (cm) in the direction of travel of light which had an initial intensity, I_o before passing through the sample and a final attenuated intensity *I* after passing through the sample (see Figure 2.1). Another important parameter that can be determined from the molar extinction coefficient is the one-photon absorption cross section. The one-photon absorption cross section, σ (in cm^2) is a measure for the one-photon absorption process and it is related to the molar extinction coefficient by:

$$\sigma = \frac{2.303 \cdot \varepsilon \cdot c}{n} \qquad \textbf{Equation 2.2}$$

In Equation 2.2, n is the number of absorbing molecules per cubic centimeter, ε is the molar extinction coefficient obtained from Equation 2.1 in $M^{-1}cm^{-1}$ and c is the concentration in *mol/l*. The strength of light absorption is mostly reported in the form of molar extinction coefficient in the literature and for organic molecules, it varies between 10^3 and 10^6 $M^{-1}cm^{-1}$.[2] The molar extinction coefficient increases with the increasing strength of the organic molecules to absorb photons. Figure 2.1 shows the schematics of the parameters involved in

the absorption process.

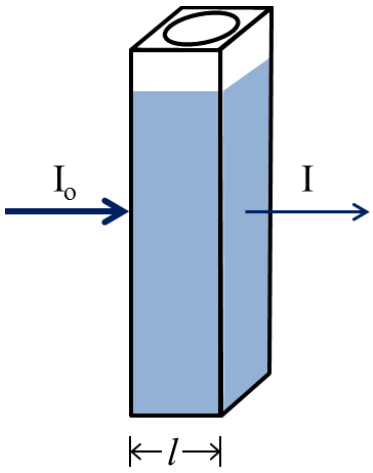

Figure 2.1 Light absorption in a sample

In the studies highlighted in this dissertation, absorbance was measured with an Agilent 8453 UV-visible spectroscopy system and the absorption data was collected with a user interface implemented by a general purpose Agilent Chemstation software that was linked to the spectroscopy system with a network cable. The radiation source for the spectroscopy system is the combination of deuterium-discharge lamp and tungsten lamp. The use of the combined lamps ensures that the spectroscopy system covers the electromagnetic spectrum from the ultraviolet wavelength range to the short wave near-infrared wavelength range (190 nm - 1100 nm). The light from the lamps is received and collimated by the source lens. The collimated light passes through the shutter or stray light filter into the sample in the sample compartment. Quartz cuvettes manufactured by Starna were used to hold the samples and these cuvettes typically have optical path of 0.4 cm or 1 cm depending on the face of the cuvette placed in the direction of the collimated light. Before reading the absorption data, the spectrum of the blank solvent is taken and this is used by the Agilent Chemstation software to correct for the background. The light from the sample is passed through the spectrograph lens which refocuses the collimated light beam before passing it through a slit located at the focus of the

spectrograph lens. The light is then sent to a grating which disperses the light onto a diode array which measures the intensity of the light beam.

The other aspect of steady state measurement is the fluorescence emission spectra measurement. The timescale of fluorescence decay of most organic molecules is in picosecond or nanosecond, therefore when organic molecules are exposed to light, steady state is reached almost immediately. The steady state measurement can be obtained from the integral of the decay kinetics over all time intervals. The relationship between the steady state intensity and the decay profile is shown in Equation 2.3.[1]

$$I_{SS} = \int_0^\infty I_o e^{-\frac{t}{\tau}} dt = I_o \tau$$ **Equation 2.3**

I_o in Equation 2.3 depends on the concentration of the organic molecule and τ is the lifetime of excited state decay. The steady state intensity is proportional to the lifetime. An important parameter that is used as a measure of the ability of an organic molecule to undergo fluorescence is known as the quantum yield, ϕ. Quantum yield is the number of emitted photons relative to the number of absorbed photons. Quantum yield could be as high as unity and this is exhibited by fluorophores which have very bright emission like rhodamine. The quantum yield was measured by fluorescence comparative method, which involves the use of well characterized standard samples with known quantum yield value.[3] Standard samples were chosen to ensure that they absorb at the same excitation wavelength for the organic molecule and also emit in similar region as the organic molecule. In order to minimize re-absorption effects, the optical densities of the organic molecules and the standard did not exceed 0.1. Some of the standards used for these studies were zinc phthalocyanine[4] and 5,10,15,20-tetraphenylporphin[5]. The fluorescence quantum yield is calculated using Equation 2.4.

$$\phi_{sample} = \phi_{std} \cdot \left(\frac{Grad_{sample}}{Grad_{std}} \right) \cdot \left(\frac{\eta_{sample}}{\eta_{std}} \right)^2 \qquad \textbf{Equation 2.4}$$

In Equation 2.4, *std* denotes the standard, *Grad* is the gradient from the plot of integrated fluorescence intensity against the absorbance and η is the refractive index of the solvent used to prepare each solution in order to correct for the solvent effect.

The fluorescence spectrum measurement was done by Spex FluoroMax-2 spectrophotometer. The light source in the spectrophotometer is a xenon lamp that is mounted vertically. The light beam from the xenon lamp is focused on the entrance slit of an excitation monochromator with an elliptical mirror. The slit width is adjustable in units of bandpass which can range from 0 to 30 nm depending on the signal strength. For highly fluorescent organic compounds, the bandpass needs to be narrow to avoid exposing the detector to too high signal levels which can damage it. Diffraction gratings in the excitation monochromator enabled single wavelength excitation of samples placed in the sample chamber. The fluorescence was measured by a detector placed at right angle to the excitation beam to eliminate background signal and minimize noise due to stray light. Gratings in the emission monochromator placed in front of the detector ensure efficient collection of each emission wavelength. The FluoroMax-2 spectrophotometer is controlled by a computer through a serial link. Standard quartz cuvettes with path length of 0.4 cm were used for the fluorescence measurement and the FluoroMax-2 spectrophotometer is capable of emission and excitation spectra measurements in the wavelength region from 300 nm to 900 nm.

2.3 Two-photon Absorption Spectroscopy

Two-photon absorption (TPA) is the simultaneous absorption of two photons which can be of the same or different frequencies in order to excite an organic molecule from the ground

state to the excited state. The difference between the energy of the ground and excited states is the sum of the energy of the two photons that are absorbed. TPA is different from sequential absorption in which there is a well-defined intermediate state. For an organic macromolecule with a bandgap equivalent to the energy of 450 nm wavelength, excitation to the excited state could be achieved by the simultaneous absorption of two photons having wavelengths of 900 nm if the organic compounds is two-photon absorption active. The energy of a photon is inversely related to the wavelength of the photon as illustrated. Therefore, it will take two 900 nm photons to excite an organic molecule with a band gap equivalent to the energy of 450 nm. The Jablonski diagram for TPA process is shown in Figure 2.2.[1] The phenomenon of TPA was originally predicted by Maria Goeppert-Mayer in 1931[6] but the experimental verification of TPA did not happen until the invention of lasers thirty years later.[7,8] This was the motivation behind the unit of two-photon absorption cross-section which is the combination of leading letters of Goeppert-Mayer (1 GM = 10^{-50} cm^4 s $photon^{-1}$). The two photon absorption cross section is a measure of an organic molecule to absorb two photons simultaneously.

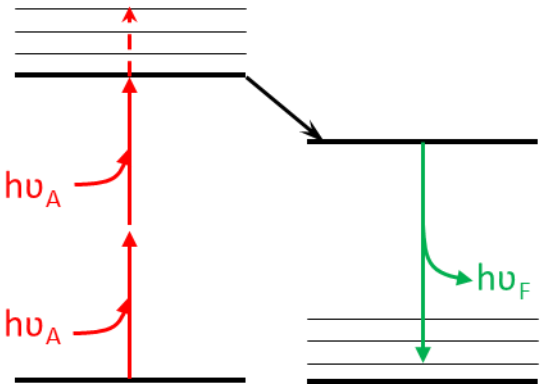

Figure 2.2 Jablonski diagram for two-photon absorption and fluorescence processes[1]

Two-photon absorption has a quadratic dependence on the intensity of the incident photon unlike the one-photon absorption which has a linear dependence. Consequently, the two-photon absorption is not constant across the cuvette but absorption is at its peak at the

focus of the beam where the incident intensity is highest. This effect can lead the localized excitation. This effect has contributed to the application of two-photon absorption in optical data storage, photodynamic therapy, optical power limiting, imaging, micro-fabrication and lithography.[9] The localized effect of two-photon absorption and the transparency and two-photon activity of some materials at the far-infrared region have been explored in these applications.

Two-photon excited fluorescence (TPEF) and nonlinear transmission (NLT) methods were methods explored in this research work to determine two-photon absorption cross-section of organic samples. The TPEF is the more accurate of the two methods. The TPEF set-up consists of Spectra Physics diode-pumped Mai Tai mode-locked Ti:sapphire oscillator which is capable of producing sub 100 fs pulse in the wavelength range of 700 – 980 nm. The laser is able to deliver pulses at average power up to 2 W at repetition rate of 80 MHz, noise less than 0.15%, stability less than $\pm$1%, polarization greater than 500:1 horizontal, beam divergence less than 1.2 mrad and beam diameter less than 1.2 mm. The wavelength output from the Mai-Tai can be extended by pumping a synchronously pumped parametric oscillator (OPAL) with the output beam from Mai-Tai. The OPAL is capable of delivering tunable femtosecond pulses from 1100 to 2500 nm. Other wavelengths can also be obtained through the frequency doubling of the output from OPAL using first and second harmonic BBO crystals. The OPAL produces laser pulses with repetition rate of 82 MHz with pulse duration less than 130 fs, average power between 150 mW and 250 mW, bandwidth greater than 15 nm, beam divergence less than 1 mrad, beam diameter less than 2 mm and polarization greater than 100:1 horizontal. The quality of mode-lock and the wavelength selection of the laser beam are monitored by directing the beam through a fiber optic cable to an Ocean Optics spectrometer.

The wavelength and quality of the beam can be adjusted by changing the prism positions in the laser through the external knobs of the laser. After obtaining the right wavelength and beam quality, the beam is directed to a variable neutral density wheel by using set of mirrors in the set-up. The variable neutral density wheel ensures the control of the power of the excitation beam. An optical glass is used to direct a small option of the incident beam into a high-speed silicon photodiode connected to a multimeter which gives feedback to the computer interface. The signal received from the multimeter ensures that the beam power of the excitation beam is monitored. The fluorescence beam is collected at right angle to the excitation beam to avoid the excitation beam finding its way into the photomultiplier tube (PMT). The monochromator, placed in front of the PMT, is used to select the fluorescence wavelength of interest which is then detected by a photomultiplier tube (R152P, Hamamatsu, Hamamatsu City, Japan) connected to a computer via a photo-counting unit.

The two-photon absorption cross-sections by fluorescence method were calculated by using a reference solution of Styryl 9M[10] with known two-photon absorption cross-section. From the fundamental standpoint,[11] the collected fluorescence from two-photon excitation is related to solution and laser parameters as shown in Equation 2.5:

$$F(t) = \frac{1}{2}\eta\delta[c]n \cdot \frac{g_p}{\pi\lambda f\tau}\phi\left\langle P(t)\right\rangle^2 \qquad \textbf{Equation 2.5}$$

In Equation 2.5 above, F(t) is the intensity of the fluorescence photons collected, η is the fluorescence quantum yield, δ is the two-photon absorption cross-section in GM, [c] is the concentration of the sample in molarity, n is the refractive index of the sample solvent, g_p is the shape factor of the laser pulse which can be taken as 0.664 for a Gaussian shape, λ is the wavelength of excitation beam in nm, f is the frequency of pulses from the laser source, τ is the pulse duration, ϕ is the collection efficiency of the laser system and <P(t)> is the input

intensity. Some of the parameters in Equation 2.5 are associated with the laser and can be assumed to be the same for samples excited at the same wavelength. Consequently, it is possible to calculate the two-photon absorption cross-section by running the two-photon absorption experiment on a standard with known concentration, refractive index and quantum yield; and then relating the two-photon absorption cross-section of an organic macromolecule to the properties of the standard through the constant laser parameters. By taking the logarithm of Equation 2.5, it is possible to express the equation in the form of the slope-intercept form of equation of a line (y = mx + b) as given in Equation 2.6:

$$\log(\ F(t)) = 2\log\ < P(t) > + \log(\ \frac{1}{2}\eta\delta[c]n \cdot \frac{g_p}{\pi\lambda f\tau}\phi) \qquad \textbf{Equation 2.6}$$

As it can be attested from Equation 2.6, the logarithmic plot of the data sets of the fluorescence intensity and the input power will have a slope of 2 for a two-photon absorbing organic material. For logarithmic plots of fluorescence intensity versus the input power for both the sample and the standard having slopes of 2, Equation 2.7 will hold for the same input power for both the sample and the standard:

$$\log[\ F(t)_{sample}\ ] - b_{sample} = \log[\ F(t)_{std}\ ] - b_{std} \qquad \textbf{Equation 2.7}$$

In Equation 2.7, b is the intercept on the vertical axis with functional relationship given by

$$b = \log\left[\frac{1}{2}\eta\delta[c]n \cdot \frac{g_p}{\pi\lambda f\tau}\phi\right] \qquad \textbf{Equation 2.8}$$

Further manipulation of Equation 2.7 will result in an exponential relationship between the fluorescence intensity and b given by:

$$\frac{F(t)_{sample}}{F(t)_{std}} = 10^{(b_{sample} - b_{std})} \qquad \textbf{Equation 2.9}$$

If the logarithms of input power for both the sample and the standard are zero, Equation 2.6

simplifies to

$$F(t) = \frac{1}{2}\eta\delta[c]n \cdot \frac{g_p}{\pi\lambda f\tau}\phi \quad \text{at } \log\left[P\langle t\rangle\right] = 0 \qquad \textbf{Equation 2.10}$$

Substitution of the expression in Equation 2.10 in place of the fluorescence intensity in Equation 2.9 results in

$$\frac{\frac{1}{2}\eta_{sample}\delta_{sample}[c]_{sample}n_{sample} \cdot \frac{g_p}{\pi\lambda f\tau}\phi}{\frac{1}{2}\eta_{std}\delta_{std}[c]_{std}n_{std} \cdot \frac{g_p}{\pi\lambda f\tau}\phi} = 10^{(b_{sample} - b_{std})} \qquad \textbf{Equation 2.11}$$

The laser parameters are independent of the sample and therefore cancel out in Equation 2.11. After solving the two-photon absorption cross-section of the sample in terms of the sample and standard properties, we are left with the final expression given by

$$\delta_{sample} = \frac{10^{(b_{sample} - b_{std})} \cdot \eta_{std}\delta_{std}[c]_{std}n_{std}}{\eta_{sample}[c]_{sample}n_{sample}} \qquad \textbf{Equation 2.12}$$

The concentrations of the sample and the standard can be obtained through direct measurement of known mass in a given volume of solvent while the quantum yield can be calculated using the standard method described in Section 2.3. For dilute samples, the refractive index of the samples can be taken as that of the solvent used in preparing the sample, while b can be read directly from the logarithmic plot of fluorescence intensity versus the input power as the y-intercept.

The other method that was explored in this research work is the nonlinear transmission method. This method is based on the measurement of the two-photon absorption cross-section by measuring the changes in the nonlinear transmittance of the organic material as a function of the intensity of the excitation laser beam. The nonlinear optical set-up used for this study is shown in Figure 2.3.

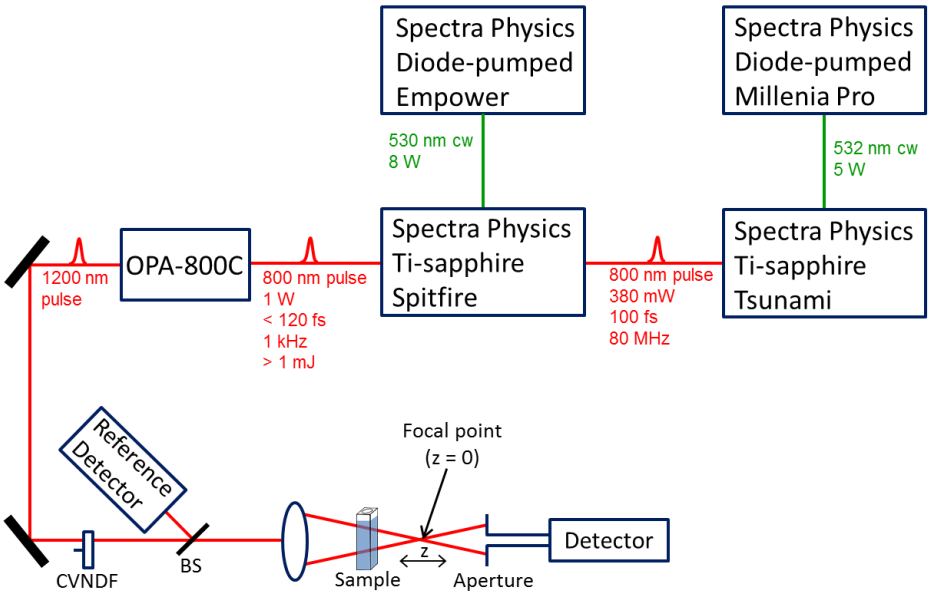

Figure 2.3 Nonlinear optical set-up for two-photon absorption cross-section measurement

The nonlinear optical set-up is used to generate a 1200 nm incident beam used in the two-photon absorption cross-section measurement. Spectra Physics diode-pumped Millenia Pro was used to generate 5W, 523 nm continuous wave beam which pumped a Ti-sapphire regenerative oscillator (Tsunami, Spectra Physics). Seed pulses from the regenerative oscillator were sent to Ti-sapphire regenerative amplifier (Spitfire, Spectra Physics) with pump beam of 8W, 530 nm from Nd:YLF laser (Spectra Physics, Empower). The 100 fs, 1 mJ output laser pulse at 800 nm wavelength with an average power of 1 W from the Ti-sapphire regenerative amplifier was used to pump an optical parametric amplifier (OPA-800C), which has the capability of producing laser pulse in a wavelength range of 300 – 1200 nm, to produce the incident wavelength. The incident wavelength was generated using the second harmonic of the idler and the output beam was set at 1200 nm. The intensity of the incident beam was controlled by a circular variable neutral density filter (CVNDF) before the beam was split into two for calibration of the incident beam by a beam splitter. A focusing lens with a focal length of 25 cm was used to focus the incident beam on the samples. The transmitted beam through

the samples was measured using an open-aperture detector. The two-photon absorption cross-section is related to the transmission through the correlation given in Equation 2.13 and Equation 2.14.[12]

$$T(z) = 1 - \frac{\beta I_o L}{2^{3/2}\left(1 + \frac{z^2}{z_o^2}\right)}$$ **Equation 2.13**

$$\delta = \frac{10^3 \times \beta h \nu}{Nc}$$ **Equation 2.14**

In Equation 2.13 and Equation 2.14, β is the two-photon absorption coefficient, I_o is the intensity of the incident beam at the focus, L is the length of the sample in the direction of propagation of the beam, z is the position of the sample in the direction of the beam, h is the Planck's constant, ν is the frequency of light, N is the number of molecules of the organic sample in a concentration given by c and δ is the two-photon absorption cross-section.

2.4 Time-Domain Lifetime Measurements

The fluorescence lifetime is a measure of the time a fluorophore spends in the excited state before returning to the ground state by emitting a photon. The photons are emitted at random times, resulting in an exponentially decay curve. For an exponentially-fitted decay profile, the time it takes for 63% of the population of the excited electrons to return to the ground state is the fluorescence lifetime. Fluorescence lifetimes can be of the order of femtosecond to nanosecond time scale depending on the material and its environment. Time-domain lifetime measurements provide more information than the steady-state data. Analysis of the lifetime measurements can give better insights into the energy and electron transfer processes from the donor to the acceptor of organic molecules. Collisional quenching, fluorescence anisotropy and rotational diffusion which depend largely on the environment of

the organic molecule can also be studied from the lifetime measurement data.[1]

Depending on the desired time resolution for the lifetime measurement, two different techniques were used during this research study: femtosecond fluorescence upconversion and time-correlated single photon counting (TCSPC). Femtosecond fluorescence upconversion is suitable for lifetime measurements in the femtosecond or picosecond time-scales while TCSPC is generally used for measurements in the nanosecond time scales. For any lifetime measurement to be significant, it has to be outside the instrument response function (IRF) of the laser. The IRF is the response of the laser instrument to scattered excitation pulse. The IRF was measured by using a dilute scattering sample such as water and adjusting emission monochromator to the excitation wavelength. The instrument response can be used to increase the accuracy of analyzed data by subtracting the effect of the IRF from the experimental data. This is done through a process known as deconvolution. If the measured instrument response function is I(t) and the sample response to a pulse excitation is f(t), then the experimentally measured signal is given by the convolution integral:

$$N(t) = \int_0^t I(\tau) f(t-\tau) d\tau \qquad \textbf{Equation 2.15}$$

A MATLAB-based deconvolution program developed in Professor Goodson's laboratory was used to find the sample response that corresponds to experimentally measured signal based on Equation 2.15.

Anisotropy measurements can be used to provide information on the orientation of the transition dipole moment of organic molecules and the rigidity of the various molecular environments. Anisotropy measurement is based on the photoselective excitation of the organic molecules by polarized light having the same orientation as the the transition dipole moment of the excited organic molecules. In isotropic solution, organic molecules are randomly oriented

and upon excitation, only molecules with absorption transition dipole parallel to the electric vector of the excitation light are selectively excited. Consequently, partially oriented excited molecules result. During the lifetime of excited states, polarization can change from the initial maximum value as a result of rotational diffusion. If the emission intensities measured through excitation by parallel and perpendicular oriented excitation beam are given by $I_{\parallel}$ and $I_{\perp}$, the fluorescence anisotropy is given by the following relationship:[1]

$$r = \frac{I_{\parallel} - G \cdot I_{\perp}}{I_{\parallel} + 2G \cdot I_{\perp}} \qquad \textbf{Equation 2.16}$$

In Equation 2.16, r is the fluorescence anisotropy and G is the g factor which is used to correct for the different sensitivities of the detectors for vertically and horizontally polarized light.

For a single-photon absorption process, the maximum anisotropy is 0.4 and this occurs when the absorption and emission dipoles are collinear which corresponds to a case where the angle between the absorption and the emission dipoles is 0^{o}. The anisotropy value is less than 0.4 for most organic molecules and the anisotropy value depends largely on the excitation wavelength. For an organic molecule having angle θ between the absorption and emission dipoles, the fluorescence anisotropy is given by the relationship:

$$r = \frac{2}{5}\left(\frac{3\cos^{2}\theta - 1}{2}\right) \qquad \textbf{Equation 2.17}$$

Anisotropy is dependent on the excitation wavelength but independent of sample concentration. The factor of 2/5 in Equation 2.17 is as a result of probability of light absorption. It must be noted that dilute scattering solution can have anisotropy exceeding 0.4. Therefore, the presence of scattering light in a fluorescence process can cause the anisotropy to exceed 0.4. In addition, for multiphoton absorption process, the anisotropy value exceeds the value of 0.4 observed for one-photon process. When the absorption and emission dipoles are

perfectly aligned in two-photon absorption process, the maximum anisotropy value is 0.57 while the value increases to 0.66 in three-photon absorption process.[1] At the magic angle of 54.7^{o} between the absorption and emission dipoles, the anisotropy in all types of absorption process is zero.

One other phenomenon that was studied through time-domain lifetime measurement is the fluorescence resonance energy transfer (FRET). FRET involves the transfer of energy from an excited donor group to an acceptor group in the ground state without the appearance of photon. It is essential that the fluorescence spectrum of the donor group must overlap with the absorption spectrum of the acceptor group for FRET to occur. This phenomenon has found its usefulness in solar cell materials because the spectral gap of a solar material could be widened by careful integration of another material with complementary absorption band. The rate and efficiency of energy transfer between the donor and acceptor group depends on a number of factors such as the extent of spectral overlap of the emission spectrum of the donor with the absorption spectrum of the acceptor, the relative orientation of the donor and acceptor transition dipoles, and the distance between the donor and acceptor molecules.

The rate of energy transfer from a donor to an acceptor in an organic material is given by[13]

$$k_T(r) = \frac{1}{\tau_D}\left(\frac{R_0}{r}\right)^6 \qquad \textbf{Equation 2.18}$$

where τ_D is the florescence decay lifetime of the donor molecule in the absence of the acceptor molecule, R_0 is the Förster radius which is the distance between the donor and the acceptor when the transfer efficiency is 50%; r is the distance between the donor and the acceptor molecules in the organic system. Therefore, the rate of energy transfer is inversely related to

the sixth power of the center to center distance between the donor and acceptor molecules. For energy transfer to be efficient, it is important that the transfer rate must be faster than the fluorescence decay rate. The efficiency of energy transfer is the fraction of the absorbed energy by the donor that is transferred to the acceptor. The transfer efficiency can be expressed in terms of the measurable parameters of the fluorescence time of the donor without the acceptor (τ_D) and the fluorescence time of the donor with the acceptor (τ_{DA}). The transfer efficiency (E) is given by:

$$E = 1 - \frac{\tau_{DA}}{\tau_D}$$ **Equation 2.19**

Having given some background about time-resolved fluorescence measurement, the two methods of measuring the fluorescence lifetimes will be discussed.

2.4.1 Time-resolved fluorescence upconversion

The time-resolved fluorescence experiments were performed using a fluorescence set-up with the schematics shown in Figure 2.4. The time-resolved fluorescence upconversion set-up comprises two lasers – Spectra Physics Millennia and Spectra Physics Tsunami lasers. The Spectra Physics Millennia laser is powered by a laser diode which is capable of delivering up to 5 W of power. This laser has a gain medium of neodymium-doped yttrium vanadate ($Nd:YVO_4$). When electrical signal or light of certain wavelength interacts with gain medium in the laser, another beam of different characteristic wavelength of the gain medium material is produced. For the Millennia laser, a green continuous beam with a wavelength of 532 nm is generated through frequency doubling by the nonlinear optics in the Millennia laser. This beam serves as input to the second laser (Spectra Physics Tsunami) which has Ti-sapphire as gain medium. The Tsunami laser is capable of generating < 80 fs pulses at wavelengths between

780 and 820 nm at a repetition rate of 82 MHz. The output of this laser has an average power of 700 mW. Ultrafast-pulsed output of the Ti-sapphire Tsunami laser is generated through a process called mode-locking. Mode-locking is a technique in optics used to generate pulses of extremely short durations in the order of femtosecond or picosecond. The pulsed output from the Ti-sapphire laser is generated through self-starting passive mode-locking which involves the incorporation of saturable absorber with suitable properties in the laser resonator. The saturable absorber preferentially allows light which has somewhat high intensities to pass through it because they have enough intensity to saturate absorption more than the light of lower intensities for each round trip in the resonator. After many round trips, a single pulse will remain with all the weaker intensity beams already absorbed by the saturable absorber. This process is repeated to produce series of fast energetic pulses of light. The optimal operating wavelength of the Tsunami laser is 800 nm; this wavelength was used for this study. The 800 nm beam is passed through a series of focusing elements on to a β–barium borate (BBO) crystal to generate 400 nm beam from second harmonic generation. The residual fundamental 800 nm beam is passed through a dichroic mirror into an optical delay line while the generated 400 nm beam is reflected by the dichroic mirror towards the sample. A berek compensator is used to control the polarization of the beam so that the beam entering the sample is plane-polarized. The sample is placed in a 1 mm rotating cell to eliminate the effect of localized excitation of the sample which can result photo-degradation and damage of the sample. The fluorescence from the sample is collected by an achromat and directed through a number of focusing elements and mirrors into a nonlinear sum frequency β–barium borate crystal where it is recombined with the gate pulse. The gate pulse and the fluorescence must be spatially and temporally overlapped for efficient measurement of the fluorescence. The overlapping

arrangement of the fluorescence beam and the gate pulse is ensured by efficient alignment of the focusing elements and mirrors in the upconversion set up to ensure that the light beams pass through the right path in space. The sum frequency beam generated from the combination of the fluorescence beam and the gate pulse is usually in the wavelength range of 300 – 400 nm. The gate pulse has a step size of 6.25 fs and it is capable of ensuring that lifetimes up to 1 ns can be measured using the fluorescence upconversion technique. The sum frequency beam is passed through focusing lens into the monochromator which picks out the desired wavelength from the upconverted beam and then send the wavelength into the photomultiplier tube (R152P, Hamamatsu, Hamamatsu City, Japan) for detection. The excitation beam used for the study varied between 17 mW and 20 mW. Standard dyes of Coumarin 30[14], Coumarin 153 and Cresyl violet[15] were used in the process of alignment of the laser systems. The choice of the dye depends on the operating fluorescence wavelength. The absorption spectrum of the sample is measured at the start and end of the experiments to confirm that there is no photo-degradation in the course of the fluorescence measurement especially for long experimental scans. In cases where photo-stability is a concern, fresh samples are used for each experimental run. The fluorescence lifetimes of the samples are obtained by fitting the experimentally determined fluorescence decay curve to exponential function using the fitting function in Origin 8. More rigorous deconvolution fitting procedure in an in-house developed program on the platform of MATLAB is used for extremely small fluorescence lifetimes in the order of femtosecond.

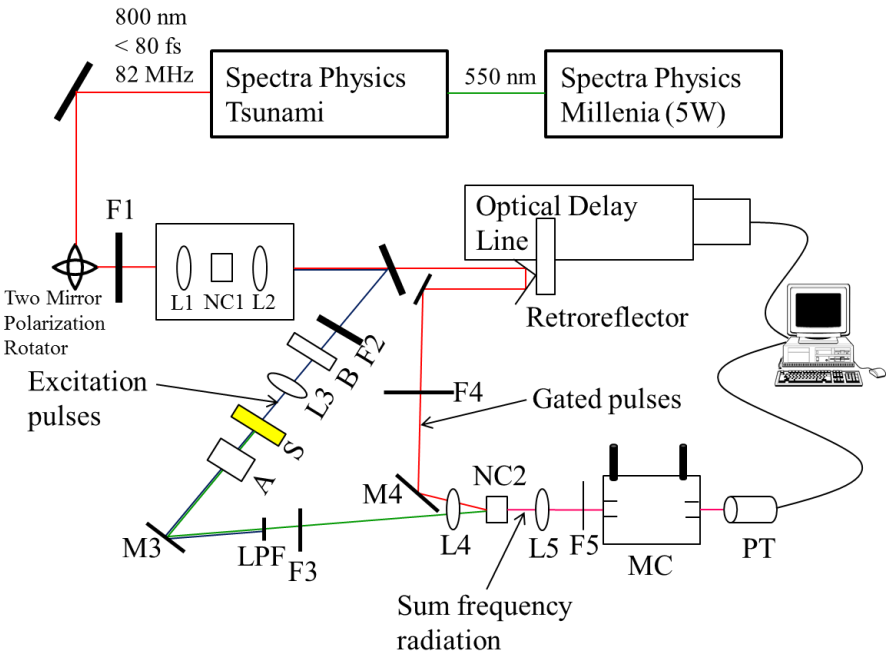

Figure 2.4 Time-resolved fluorescence upconversion set-up. Lenses are indicated with 'L'; nonlinear crystals, 'NC'; focusing elements, 'F'; mirrors, 'M'; sample, 'S'; berek compensator, 'B'; achromat, 'A'; low pass filter, 'LPF'; monochromator, 'MC', photomultiplier, 'PT'.

2.4.2 Time-correlated single photon counting (TCSPC)

The time-correlated single photon counting (TCSPC) is another method commonly used for time-domain lifetime measurements. TCSPC is similar to the fluorescence upconversion technique in terms of how the laser beam used to excite the organic samples is generated. The resolution of the two techniques and the approach in which the fluorescence is collected are the two striking differences between the two frequently used fluorescence measurement methods. The femtosecond fluorescence upconversion is capable of measuring the fluorescence lifetimes in femtosecond to picosecond time ranges while TCSPC is capable of measuring fluorescence lifetimes in the range of picosecond to nanosecond.

The TCSPC set-up consists of a Kapteyn Murnane (KM) Laboratories mode-locked Ti-sapphire femtosecond laser pumped by a Millenia V Nd:YVO_4 (Spectra Physics). The pump

beam is a 5W continuous green light at 532 nm. The output from the KM laser is capable of being tuned between 780 to 830 nm. For the experiment conducted in this study, the output from the KM laser was set at 800 nm wavelength with pulse duration of ~ 30 fs and a repetition rate of 90 MHz. The output beam from the KM laser was frequency-doubled through the second harmonic generation by using a β-barium borate crystal to obtain a 400 nm pulsed beam. For polarization studies, the beam is passed through a polarizer in order to set the polarization of excitation beam hitting the sample. In studies where the polarization effect is not desired, the polarizer can be set at the magic angle of 54.7^{o}. At this angle, the total fluorescence is measured without reference to the polarization. The sample is contained in a 0.4 cm path length rectangular quartz cell.

The fluorescence measurement using the TCSPC set-up is unique because of the method of collection of the fluorescence beams. The dynamics of fluorescence decay is so fast that the detector cannot accurately measure it. Therefore, the detector is set to measure 1 photon per 100 excitation pulses. Once the excitation pulse excites the sample, a signal is produced and passed through constant function discriminator (CFD) which accurately measures the arrival time of the beam. The signal is then passed to a time-to-amplitude converter (TAC) which converts the signal to a voltage ramp. The voltage ramp continues to increase until the emission pulse arrives at the detector and stops the ramp-up process. The voltage ramp is linearly related to the difference between the time the excitation pulse excites the sample and the time the emission beam reaches the detector. The voltage signal is amplified by a programmable gain amplifier (PGA) and converted to a numerical value by an analog-to-digital converter (ADC). The numerical value is stored as a single event in the appropriate bin which depends on the time delay between the excitation beam and the emission

beam. The process is repeated numerous times by repeatedly exciting the sample to generate a histogram of the decay process. The measurement of 1 photon per 100 excitation pulses is essential because the detector has a dead time of about tens of microseconds to hundreds of nanoseconds between detection of photons. These times are greater than the fluorescence lifetimes of organic samples. If the detector is allowed to measure all the emission photons, the fluorescence lifetime will be skewed towards short time because of the inability to measure late arriving photons due to the dead time of the detector between measurements.

The fluorescence emission of the sample is collected at a direction perpendicular to the excitation beam through a monochromator which is used to spectrally resolve the fluorescence beam. The photomultiplier tube detects the fluorescence and the result is transmitted to the computer through an interface card (Time-Harp). The computer displays the histogram of the different time bins using specialized software, PicoQuant. The PicoQuant Fluofit software is used to analyze the result and fit the lifetime distribution models into exponential decay function. The IRF, which is measured via the Rayleigh scattering of a scattering medium, is overlaid on the decay function in order to verify the significance of the decay process. The IRF has a full width at half maximum (FWHM) of 330 ps. To ensure that the sample is stable in the course of the fluorescence measurements, the absorbance of the sample is measured before and after each measurement. The TCSPC set-up is shown in Figure 2.5.

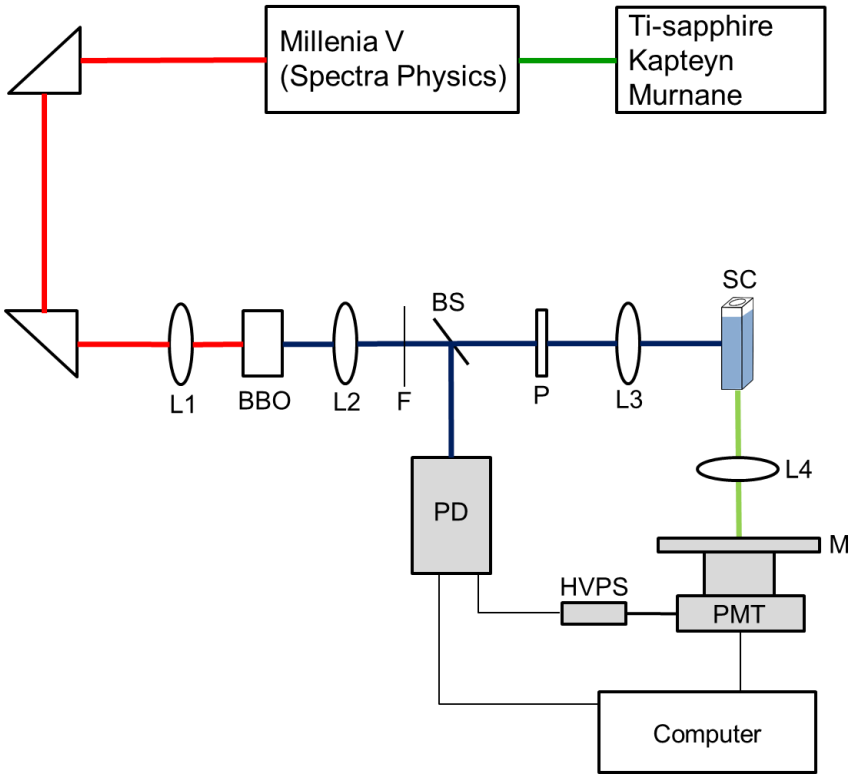

Figure 2.5 Time-correlated single photon counting (TCSPC) set-up. Lenses are indicated with 'L'; nonlinear crystal, 'BBO'; focusing elements, 'F'; beam splitter, 'BS'; sample cell, 'SC'; photodiode, 'PD'; photomultiplier tube, 'PMT'; polarizer, 'P'; monochromator, 'M'.

References

(1) Lacowitz, J. R. *Principles of Fluorescence Spectroscopy*; 3rd ed.; Springer: New York, 2010.

(2) Mahmood, K.; Hussain, M.; M., A. A Study of the Molar Absorptivity and Structure of Vitamin B2 Relationship. *Jour. Chem. Soc. Pak.* **2001**, *23*, 205–209.

(3) Maciejewski, A.; Steer, R. P. Spectral and Photophysical Properties of 9,10-Diphenylanthracene in Perfluoro-N-Hexane: The Influence of Solute-Solvent Interactions. *J. Photochem.* **1986**, *35*, 59–69.

(4) Vincett, P. S.; Voigt, E. M.; Rieckhoff, K. E. Phosphorescence and Fluorescence of Phthalocyanines. *J. Chem. Phys.* **1971**, *55*, 4131.

(5) Seybold, P. G.; Gouterman, M. Porphyrins XIII: Fluorescence Spectra and Quantum Yields. *J. Mol. Spectros.* **1969**, *31*, 1–13.

(6) Goppert-Mayer, von M. Uber Elementarakte Mit Xwei Quantensprungen, 1931, Vol. 114.

(7) Kaiser, W.; Garrett, C. G. B. Two-Photon Excitation in CaF2:Eu2+. *Phys. Rev. Lett.* **1961**, *7*, 229–232.

(8) D., A. I. Optical Double-Quantum Absorption in Cesium Vapar. *Phys. Rev. Lett.* **1962**, *9*, 453.

(9) Ajami, A.; Husinsky, W.; Liska, R.; Pucher, N. Two-Photon Absorption Cross Section Measurements of Various Two-Photon Initiators for Ultrashort Laser Radiation Applying the Z-Scan Technique. *J. Opt. Soc. Am. B* **2010**, *27*, 2290–2297.

(10) Makarov, N. S.; Drobizhev, M.; Rebane, A. Two-Photon Absorption Standards in the 550-1600 Nm Excitation Wavelength Range. *Opt. Express* **2008**, *16*, 4029.

(11) Xu, C.; Webb, W. W. Measurement of Two-Photon Excitation Cross Sections of Molecular Fluorophores with Data from 690 to 1050 Nm. *J. Opt. Soc. Am. B* **1996**, *13*, 481–491.

(12) Nag, A.; De, A. K.; Goswami, D. Two-Photon Cross-Section Measurements Using an Optical Chopper: Z -Scan and Two-Photon Fluorescence Schemes. *J. Phys. B At. Mol. Opt. Phys.* **2009**, *42*, 065103–065109.

(13) Scholes, G. D. Long-Range Resonance Energy Transfer in Molecular Systems. *Annu. Rev. Phys. Chem.* **2003**, *54*, 57–87.

(14) Jones II, G.; Jackson, W. R.; Choi, C.; Bergmark, W. R. Solvent Effects on Emission Yield and Lifetime for Coumarin Laser Dyes. Requirements for a Rotary Decay Mechanism. *J. Phys. Chem.* **1985**, *89*, 294–300.

(15) Magde, D.; Brannon, J. H.; Cremers, T. L.; Olmsted, J. Absolute Luminescence Yield of Cresyl Violet. A Standard for the Red. *J. Phys. Chem.* **1979**, *83*, 696–699.

Chapter 3

Synthesis and Ultrafast Time Resolved Spectroscopy of Peripherally Functionalized Zinc Phthalocyanine Bearing Oligothienylene-ethynylene Subunits

3.1 Original Publication Information

The text in this chapter was originally published as:

"Synthesis and Ultrafast Time Resolved Spectroscopy of Peripherally Functionalized Zinc Phthalocyanine Bearing Oligothienylene-ethynylene Subunits" Oluwasegun O. Adegoke, Mine Ince, Amaresh Mishra, Ashley Green, Oleg Varnavski, M. Victoria Martínez-Díaz, Peter Bäuerle, Tomás Torres and Theodore Goodson, III. *Journal of Physical Chemistry C* **2013**, *117*, 20912-20918

Modifications were made to the original publication to adapt it to the style of the content of this dissertation. References and supporting information of the original manuscript are included in this chapter.

3.2 Abstract

Two new soluble tri-tert-butyl zinc(II) phthalocyanines, **1** and **2**, bearing dendritic oligothienylene-ethynylene (DOT) groups as one of the peripheral substituents, have been prepared. The conjugated DOT moieties were introduced to cover the spectral window between 380 and 550 nm, where the ZnPc does not exhibit a strong absorption, in order to improve light harvesting. For their preparation, a convergent approach has been used starting from the

corresponding iodoPc as precursor. Further transformation of the iodo groups by a Pd-catalyzed Sonogashira reaction with the appropriate DOT-functionalized terminal alkyne allowed the easy preparation of extended π-conjugated compounds **1** and **2**. The compounds have been characterized by standard spectroscopic methods, and their photophysical behaviors have been established by using ultrafast time-resolved techniques. Femtosecond upconversion measurements showed an ultrafast energy transfer from the DOT to zinc phthalocyanine in a time scale of 300 fs. As the number of thiophene groups increases in the dyads, the extent of ultrafast energy transfer was found to increase. Compounds **1** and **2** have been tested as donor components in bulk heterojunction (BHJ) solar cells. Their efficiencies are compared with RuPc analogues previously reported by us.

3.3 Introduction

Phthalocyanines (Pc's) have been used frequently as active components in organic (OPVs) and hybrid (DSSCs) solar cells.[1–4] Apart from their unique electronic properties and chemical structure, they show an extended photo response in the region between 600 and 800 nm, where the maximum solar flux occurs. That means that only extremely thin films are necessary to absorb a substantial fraction of solar light. Pc-based OPVs can be prepared either by vacuum evaporation or by solution processing techniques. Unsubstituted Pc's are practically insoluble in common organic solvents due to aggregation phenomena. Therefore, devices cannot be easily prepared by solution processing. However, they have been successfully used as the active layer in vacuum-deposited small molecule solar cells. Conversely, solution-processing techniques are frequently used with chemically modified Pc's. The introduction of suitable substituents either in peripheral or in the axial position of the macrocycle, besides allowing modulation of its electronic properties, increases the solubility of these compounds in

organic solvents.

In the case of solution processed bulk heterojunction solar cells, there are only a few examples of soluble Pc derivatives blended with soluble acceptor materials to form a bulk heterojunction (BHJ) active layer.[5–7] The example reported by Palomares et al.[8] consists of a small molecule organic solar cell based on a soluble tetra-tert-butyl zinc phthalocyanine (ZnTBPc)/PCBM blend, which produces a short current density (J_{SC}) around 3.57 mA cm^{-2}, and open circuit voltage (V_{OC}) around 0.53 V. This corresponds to power conversion efficiency of approximately 0.77%. On the other hand, efficiencies up to 1.6% in solution-processed bulk heterojunction solar cells have been reported by us.[9] The cells comprised of highly soluble ruthenium phthalocyanines (RuPc's) that were axially functionalized with pyridyl-(DOT)s up to the third generation, and blended with fullerene derivatives (either PCBM or $PC_{71}BM$). A high short current density of 8.3 $mAcm^{-2}$ resulted from the introduction of DOTs moieties, which allowed the improvement of light harvesting ability between 380 and 550 nm, where the RuPc does not exhibit a strong absorption. The results pointed out that the design of new Pc macrocycles for BHJ solar cells still needs some improvements. One of the reasons for the low performance of Pc's is the low V_{OC} values. Modifications on the molecular structure of Pc by the introduction of different groups at distinct positions aimed at extending the absorption spectra and at tuning the electronic configuration of the excited states are expected to be efficient ways to improve the conversion efficiency of solution processed phthalocyanine-based BHJ solar cells.

In this work, we have particularly chosen oligothiophenes to be incorporated at distinct positions of Pc because of oligothiophenes' versatile chemistry and availability of many synthetic routes. As previously reported by Mishra *et al.*,[10] ethynylene-functionalized

oligothiophenes have promising optoelectronic properties that need to be explored in light-harvesting applications. The large, conjugated π-systems suitable for efficient electron transfer processes, high thermal stability and relative longer exciton-diffusion length of zinc phthalocyanine make the investigation of the performance of zinc phthalocyanine bearing oligothienylene-ethynylene subunits appealing.[9,11]

In this context, the current work focuses on the synthesis and ultrafast time-resolved spectroscopy studies of new peripherally functionalized zinc phthalocyanines bearing dendritic oligothienylene-ethynylene subunits. The evaluation of optical, kinetic, and structural data will provide important incentives for optimizing the performance of these kinds of systems in solar cells. Zinc phthalocyanine has frequently been used as either donor or acceptor material in solar cell devices,[12−14] while dendritic oligothiophenes have mostly been explored as donor materials in donor-acceptor solar cell systems.[9,13−18] In dye-sensitized nanowire array solar cells involving zinc phthalocyanine donor and ruthenium polypyrine complex, resonance energy transfer from the zinc phthalocyanine resulted in a 4-fold increase in quantum yields in the solar cell.[13] KC *et al.*[14] reported an energy transfer from a free-base porphyrin to zinc phthalocyanine within 0.2 ps in a supramolecular solar cell. Quaterthiophene has been explored as donor material in a light harvesting system involving mono- and bis-Bodipy as acceptors, and an efficient energy transfer was observed.[15] The combined effect of the photon harvesting ability of oligothiophenes between 380 and 550 nm, and the high absorption of zinc phthalocyanine between 650 and 720 nm has not been investigated in any solar cell material. We report herein two different ZnPc-oligothiophene dendron dyads, **1** and **2** matching key requirements for OPV, such as a relatively low-lying HOMO energy level and a narrow band gap. Furthermore, tetra-tert-butyl zinc phthalocyanine [$Zn(t\text{-}Bu)_4Pc$][8] was used as a reference

compound for the purpose of comparison. We used ultrafast time-resolved techniques to show the kinetics of excited state decay and energy transfer from DOT to zinc phthalocyanine in the dyads.

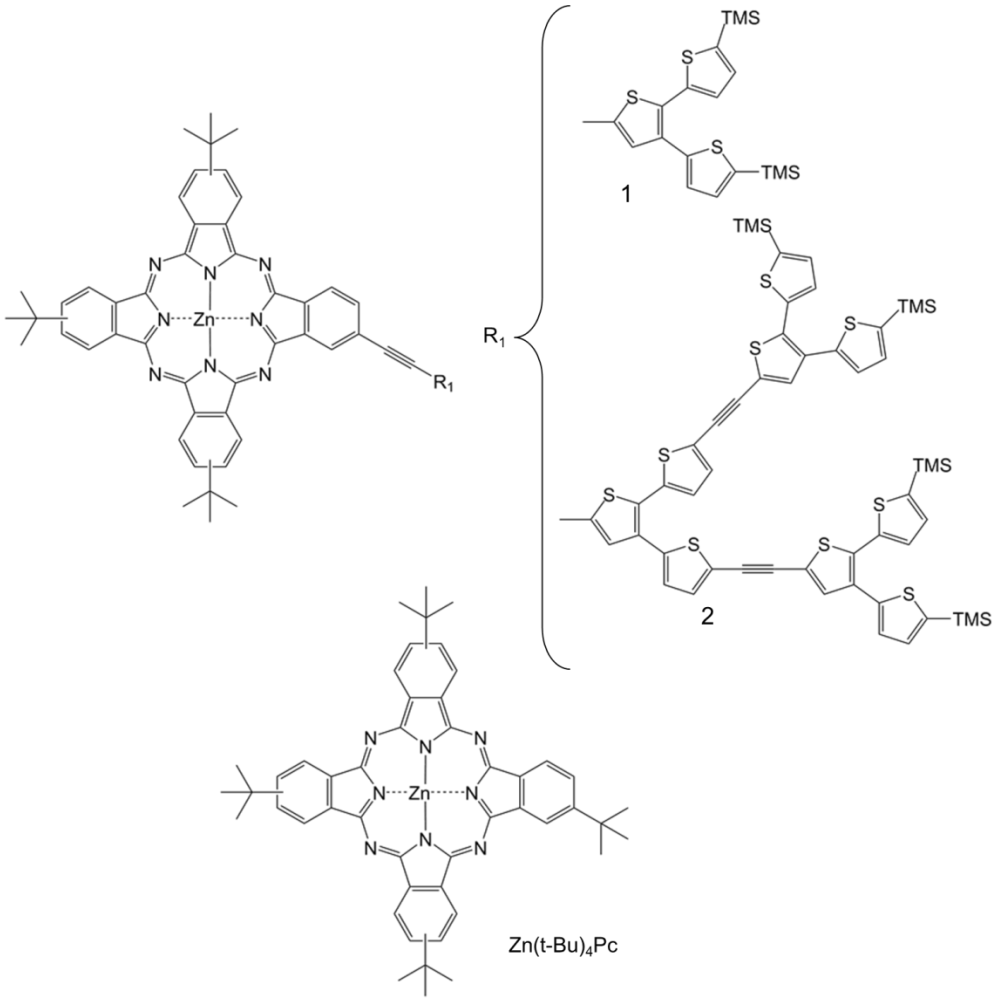

Figure 3.1 Molecular structures of ZnPc-DOT dyads **1** and **2** and reference compound **Zn(t-Bu)$_4$Pc**.

3.4 Experimental Section

3.4.1 Sample preparation

The reference compound Zn(t-Bu)$_4$Pc and the two ZnPc-DOT derivatives **1** and **2** were dissolved in spectroscopic grade of toluene. The concentrations of the prepared solutions were such that the optical densities were always below 0.5.

3.4.2 Steady state measurements

The steady state measurements on the samples were performed at room temperature. Equal concentrations of 5.0×10^{-6} M were used for all samples. The samples were placed in 4 mm quartz cuvettes. Steady state absorbance spectra were measured with an Agilent 8432 UV-visible absorption spectrometer. The absorption spectra were measured before and after experiments to ensure that there was no appreciable photodegradation during experiments. The emission and excitation spectrum measurements were performed with Fluoromax-2 spectrophotometer. The quantum yields of the samples were measured using a known procedure.[19] Coumarin 30, dissolved in ethanol,[20] cresyl violet, dissolved in methanol,[21] and zinc phthalocyanine, dissolved in 1% pyridine in toluene,[22] were used as standards. Quantum yields were measured at excitation wavelengths of 400 and 605 nm.

3.4.3 Femtosecond time-resolved fluorescence measurements

The time-resolved fluorescence experiments were carried out using a fluorescence setup that had previously been described.[23–25] The system contains 80-fs pulses at 800 nm wavelength with a repetition rate of 82 MHz. These pulses were produced by a mode-locked Ti-sapphire femtosecond laser (Spectra Physics Tsunami), pumped by a 532 nm continuous light output from another laser (Spectra Physics Millennia), which has a gain medium of Nd:YVO_4. The pulsed output laser beam was split to generate the fundamental and excitation beam pulses by a second harmonic crystal. The fundamental beam was at a wavelength of 800 nm while the excitation beam was at a wavelength of 400 nm. The polarization of the excitation beam was controlled by a berek compensator. The fluorescence emitted by the sample was up-converted in a nonlinear crystal of β-barium borate by using the fundamental beam which was delayed with a computer-controlled optical delay line. This procedure enables

the fluorescence to be resolved temporally. The up-converted signal from the barium borate crystal is directly proportional to the fluorescence from the sample. The up-converted light was resolved spectrally by passing it through a monochromator and detecting it using a photomultiplier tube (R1527P, Hamamatsu, Hamamatsu City, Japan). The power of the excitation beam was ~12 mW. Standard dyes were used for calibrating the system. The instrument response function (IRF) has duration of ~220 fs. Lifetimes of fluorescence decay and rise times were obtained by fitting the experimental profile with multi-exponential decay functions convoluted with IRF. The lifetimes in the nanosecond time scale were measured using time-correlated single photon counting (TCSPC) technique.

3.5 Results and Discussion

3.5.1 Synthesis

Two Zn (II) phthalocyanines, **1** and **2** (Figure 3.1), covalently linked to oligothienylene-ethynylene dendrons have been prepared. Compounds **1** and **2** bear three donor tert-butyl groups at the peripheral positions, and first- and second-generation of DOTs were attached through an alkynyl connector to the fourth isoindole Pc unit. The synthesis and electrochemical properties of the first- and second-generation of trimethylsilylethynyl-functionalized oligothiophene dendrons has previously been reported by Bäuerle and co-workers.[10] Dyads **1** and **2** were obtained in 67% and 51% yield, respectively, by means of Pd-catalyzed Sonogashira reaction between the tri(tert-butyl)iodoZnPc[26] and the corresponding alkynylDOT **3a,b**. Both reactions were carried out in dry tetrahydrofuran (THF) in the presence of $[PdCl_2(PPh_3)_2]$ as a catalyst, triethylamine (TEA) as the base, and a catalytic amount of copper (I) iodide (Scheme 3.1). For details, please see the Supporting Information.

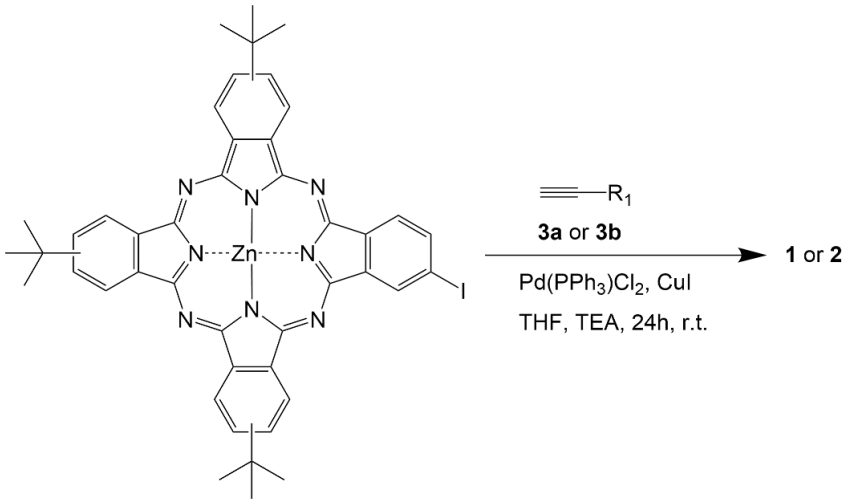

Scheme 3.1 Synthetic Route to ZnPc-DOT Dyads 1 and 2 (For R_1 values, see Figure 3.1).

The structures of dyads **1** and **2** were confirmed by IR and UV-vis spectroscopy, and matrix-assisted laser desorption/ionization time-of-flight (MALDI-TOF) spectrometry. The ^{1}H NMR spectra of tri(tert-butyl)ZnPc-DOTs **1** and **2** in d_8-THF show several multiplets corresponding to the aromatic Pc protons, between 9.5 and 8.0 ppm. The DOT protons can be easily distinguished in the region between 7.7 and 7.2 ppm (Figure S3.1 and Figure S3.3 in Supporting Information).

3.5.2 Steady state measurements

The steady state UV−vis absorption spectra of reference ZnPc and ZnPc-DOT dyads **1** and **2** in toluene are shown in Figure 3.2, and the data are presented in Table 3.1. The obtained absorption spectrum for the reference zinc phthalocyanine is similar to the reported spectrum in the literature.[27] The absorption spectra of dyads **1** and **2** are dominated by two intense Q bands at 677 and 695 nm and Soret-bands at around 355 nm, whereas only a single Q-band at 677 nm was observed for the parent ZnPc. The disruption of the symmetry in the phthalocyanine molecule due to the presence of the dendrons in dyads **1** and **2** resulted in a split in the Q-band.[28] It can be observed that the presence of the dendritic oligothienylene-ethynylene in the

dyads **1** and **2** provided a slight red-shift (5−8 nm) of the Soret bands relative to the reference ZnPc. The molar absorption coefficients of the dyads' Soret bands increase with increasing generation from **1** to **2**. This trend is evident in the higher molar absorption coefficient in dyad **2** compared to dyad **1** between 300 and 500 nm.

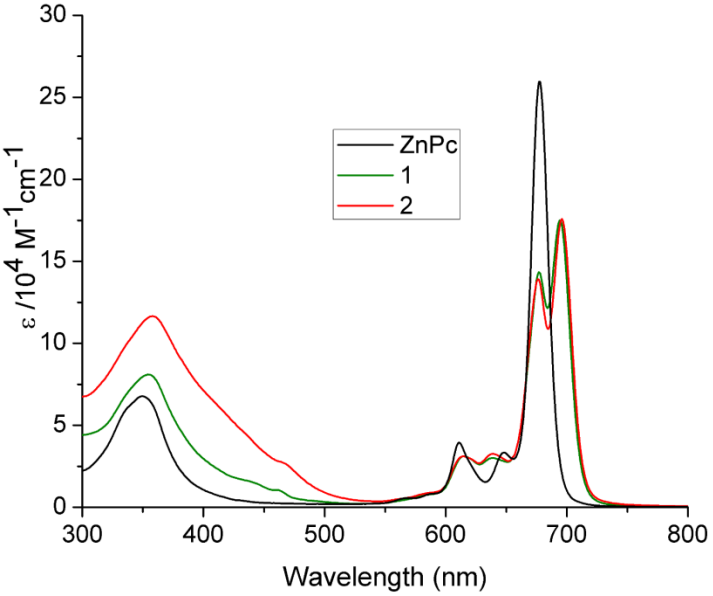

Figure 3.2 Absorption spectra of reference ZnPc, dyads 1 and 2 in toluene (~ 5×10^{-6} M).

Table 3.1 Steady state optical properties of reference ZnPc and ZnPc-DOTs **1** and **2**

Compound	λ_{abs} (nm) [ε ($M^{-1}cm^{-1}$)]	λ_{em} (nm)	λ_{exc} (nm)	ϕ_f
ZnPc	350 [67645], 677 [259548]	457, 683	348, 607, 664, 684	0.0014[a], 0.071[b], 0.30[c]
dyad 1	355 [80839], 677 [143169], 694 [174946]	459, 699	358, 611, 670	0.0018[a], 0.18[b], 0.20[c]
dyad 2	358 [116771], 676 [138961], 696 [175529]	524, 700	366, 610, 670	0.0044[a], 0.32[b], 0.18[c]

Quantum yields (ϕ_f) were measured at excitation wavelength of 400 nm[a,b] and 605 nm[c], with fluorescence spectra centered at 530 nm[a] and 700 nm[b,c]. λ_{abs}, λ_{em} and λ_{exc} represent the wavelengths for the peak absorbance, emission and excitation respectively.

The reference ZnPc and the substituted dyads were excited at 400 nm to obtain the

steady state emission spectra shown in Figure 3.3. The emission spectra were normalized by the maximum intensity of ZnPc dyad **2**. The fluorescence spectrum of ZnPc showed a broad peak at 450 nm. A similar peak at 450 nm was obtained for dyad **1**. However, the fluorescence peak of dyad **2** was red-shifted to 525 nm. The red-shift of the emission spectrum of dyad **2** may be as a result of apparent increase in conjugation due to the presence of more thiophene oligomers in dyad **2** than dyad **1**. Emission from phthalocyanine can be observed between 650 and 750 nm for all the samples with the reference ZnPc having an emission peak around 683 nm. The phthalocyanine emission peaks in dyads **1** and **2** were red-shifted to ~700 nm. The phthalocyanine emission peak of dyad **2** was more than twice that of the reference ZnPc at same concentration suggesting an efficient energy transfer from oligothienylene-ethynylene dendrons to phthalocyanine. The increase of phthalocyanine fluorescence intensity from dyad **1** to dyad **2** may be a result of an increase in the efficiency of energy transfer from thiophene groups to phthalocyanine as the number of thiophene groups increases or a result of increased energy absorption by thiophenes for transfer to phthalocyanine (see Figure 3.2).

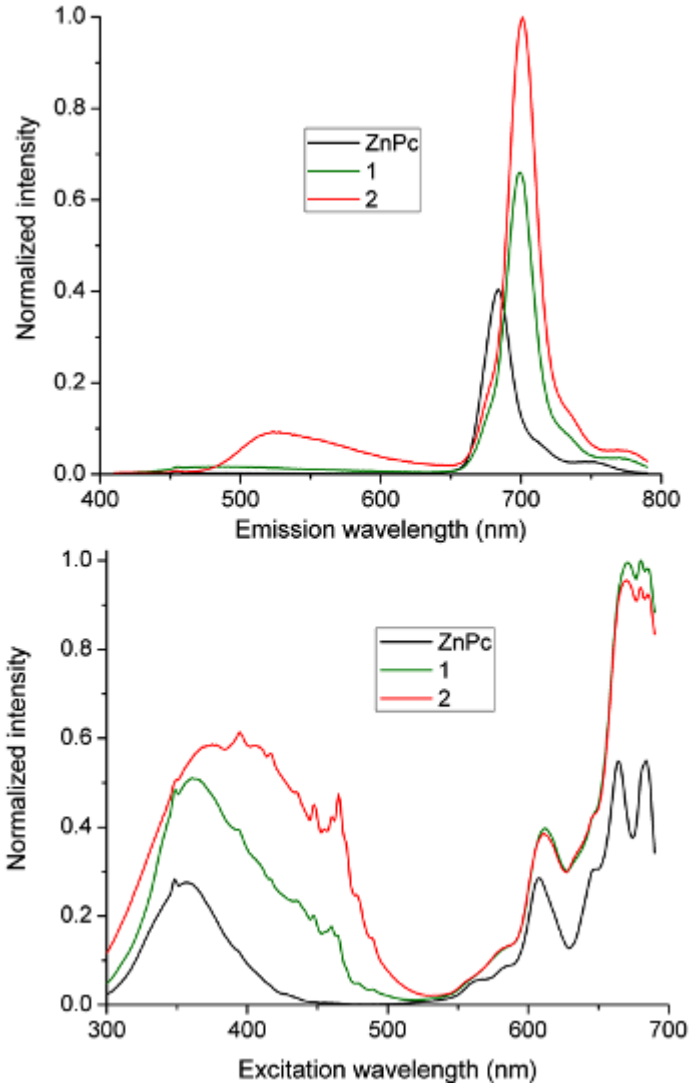

Figure 3.3 Emission (excitation wavelength: 400 nm) and excitation (emission wavelength: 700 nm) spectra of reference ZnPc, dyads **1** and **2**, in toluene (~ 5.0×10^{-6} M). Emission intensities are normalized.

The excitation spectrum similarly depicted an energy transfer from oligothienylene-ethynylene to phthalocyanine. The excitation spectrum, shown in the lower panel of Figure 3.3, is for emission at 700 nm which comes from phthalocyanine. As observed in the figure, the emission intensities from the dyads were higher than the emission intensity from reference ZnPc, especially at lower wavelengths where the excitation of the dendrons is most intense. Consequently, the increased emission from the dyads must have been as a result of energy

transfer from the dendrons. As the excitation wavelength increases, the fluorescence from dyads **1** and **2** were similar because of the exclusive excitation of the phthalocyanine in the samples at longer wavelengths. For the emission of 550 nm, which was also used in this study, the peaks of the excitation spectra (see Figure S3.5 in Supporting Information) were observed at 400 nm for all the samples.

The fluorescence centered at 530 nm, which comes mainly from the dendrons, was quenched as a result of the transfer of energy to phthalocyanine. The energy transfer is evident in the low quantum yield values of 0.0014 and 0.0018 obtained at the low wavelength peak for dyads **1** and **2**, respectively. Quantum yield values of 0.09 and 0.15 had previously been reported for the dendrons attached to the dyads.[10] The quantum yields of the emission from the phthalocyanine ends of the dyads (fluorescence centered at 700 nm) were enhanced from 0.071 in reference ZnPc to 0.18 and 0.32 in dyads **1** and **2** respectively, when the samples were excited at 400 nm wavelength (see Table 3.1) because of the presence of the dendrons. This implies that the quenching of fluorescence at shorter wavelengths, as shown by the low quantum yields at the low wavelength region, was a result of energy transfer to the longer wavelengths. This energy transfer contributed to the higher quantum yields in the dyads (0.18 in dyad **1** and 0.32 in dyad **2**) than in the reference ZnPc (0.071) at the longer wavelength region when excitation was carried out at 400 nm wavelength. To demonstrate that the difference in the quantum yields of the dyads, when excited at 400 nm, was due to the energy transfer from the different dendrons attached to ZnPc, we found the quantum yields at excitation wavelength of 605nm. As shown in Table 3.1, quantum yields of 0.30, 0.20, and 0.18 were obtained for reference ZnPc, dyads **1** and **2**, respectively. The quantum yields obtained for the dyads were quite similar because of the exclusive excitation of phthalocyanine

ends at 605 nm. The difference in the quantum yield of ZnPc compared to the dyads may have been as a result of better symmetry in the reference compound than in the dyads. The similar quantum yields in the dyads at excitation wavelength of 605 nm confirm the earlier conclusion that there must have been an energy transfer from the dendrons when the samples were excited at 400 nm.

3.5.3 Femtosecond time-resolved fluorescence

Emission wavelengths of 480, 550, and 700 nm were considered for the study. Of particular interest are the short components of decay kinetics and the time it takes for excitation energy to transfer from the dendrons to phthalocyanine in the dyads. For the reference ZnPc, there were short components of 300 and 220 fs, and intermediate components of 61 ps and 445 ps for emission wavelengths of 480 and 550 nm, respectively. The excited states were observed to have fully relaxed after 3.49 and 3.45 ns for emission of 480 and 550 nm, respectively (Table 3.2). However, the decay at emission wavelength of 700 nm was delayed with the short component being around 5 ps, and the excited state relaxed after 4.08 ns. There was no excitation energy transfer from higher energy state to lower energy state in the reference compound. Figure 3.4 shows the fluorescence kinetics of reference ZnPc.

Table 3.2 Fluorescence lifetimes at different emission wavelengths

Compound	λ_{em} (nm)	τ_1 (ps)	τ_2 (ns)	τ_R (ps)
ZnPc	480	0.3	3.49	
	550	0.22	3.45	
	700	5	4.08	
dyad 1	480	0.3	9.87	
	700		2.51	0.3
dyad 2	550	0.3	4.25	
	700		2.40	0.3

τ_1, τ_2 and τ_R are the short and long component decay times and rise time, respectively.

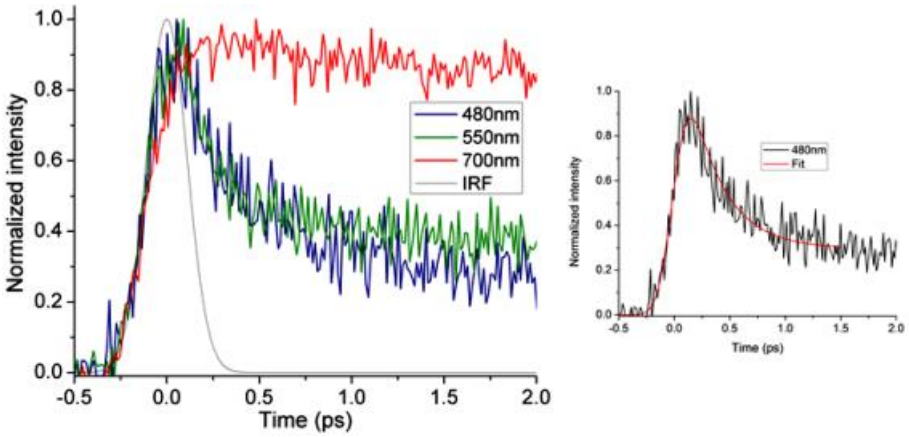

Figure 3.4 Short-time-scale fluorescence kinetics of reference ZnPc after excitation with 400 nm beam at emission wavelengths of 480, 550, and 700 nm. On the right is the fit for the emission wavelength of 480 nm.

A fast decay component of 300 fs was observed in the decay kinetics of ZnPc dyad **1** at emission wavelength of 480 nm, with an intermediate time component of 157 ps, and the excited state was fully relaxed after 9.87 ns (Table 3.2). At emission wavelength of 700 nm, a rise time was observed with a time constant of 300 fs, an identical time scale to the short component decay time of 480 nm emission. It can therefore be inferred that there is an excitation energy transfer from the higher energy state at 480 nm at a time scale of 300 fs. Similarly, for the dyad **2**, an energy transfer was observed from the emission wavelength of 550 to 700 nm at a time scale of 300 fs (see Table 3.2). The long decay components of 700 nm emission of dyads **1** and **2** were found to be 2.51 and 2.40 ns. The closeness of the decay times of the dyads suggests that the 700 nm emission was coming from the phthalocyanine moiety, which was present in the two dyads. Figure 3.5 illustrates the fluorescence kinetics of ZnPc dyads **1** and **2**.

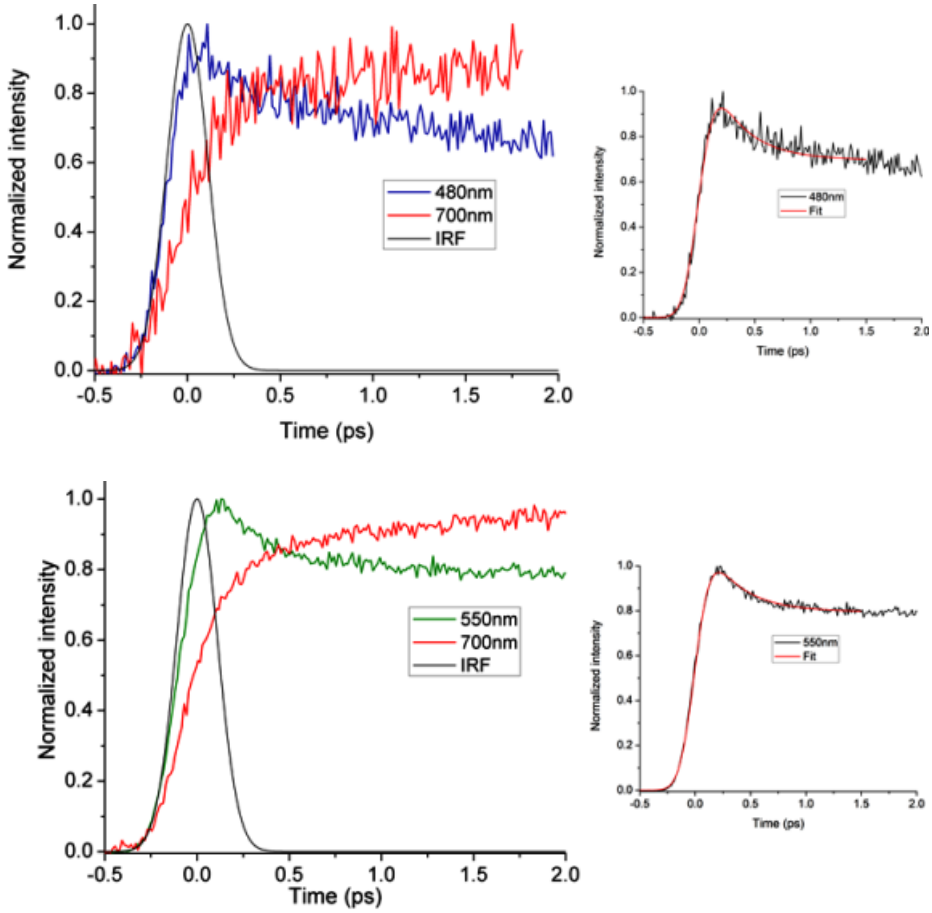

Figure 3.5 Short-time-scale fluorescence kinetics of ZnPc dyads **1** (top panel) and **2** (bottom panel) after excitation with 400 nm beam at emission wavelengths of 480 and 700 nm, and 550 and 700 nm, respectively. To the right are the 480 and 550 nm emission fits for ZnPc dyads **1** and **2**.

In order to add more credence to energy transfer from oligothienylene-ethynylene moiety to zinc phthalocyanine in the dyads, equal concentrations (1.9×10^{-5} M) of reference ZnPc, and dyads **1** and **2** in toluene were prepared for fluorescence upconversion experiment at emission wavelength of 700 nm under similar experimental conditions. As observed in Figure 3.6 (normalized by maximum photon counts from dyad **2**), the photon counts (35000) from dyad **2** were significantly more than those of dyad **1** (24000) and reference ZnPc (4000). Because the emission at 700 nm occurs only from the phthalocyanine moiety of the dyads, the additional photons from dyads **1** and **2** relative to zinc phthalocyanine could only be a result of

energy transfer from DOT.

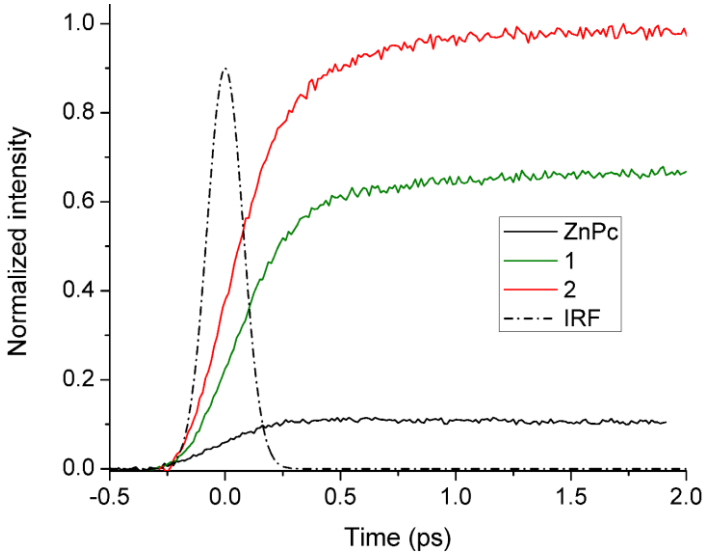

Figure 3.6 Short-time scale fluorescence kinetics of reference ZnPc, ZnPc dyads **1** and **2** in toluene (~ 1.9×10^{-5} M) after excitation with 400 nm beam at emission wavelength of 700 nm.

3.5.4 Photovoltaic studies

BHJ solar cells using dyads **1** and **2** as electron donors and PCBM as an electron acceptor in the active layer were fabricated and characterized. The device structure was ITO/PEDOD:PS/Pc-DOT (**1** or **2**):PCBM (1:2 w/w)/LiF/Al. The ratio of donor to acceptor materials was optimized at 1:2, and the thickness of the active layer was optimized for each donor/acceptor blend, and was typically 60-70 nm. According to preliminary photovoltaic results, the device having dyad **1** exhibits a J_{SC} value of 3.05 mA cm^{-2}, a V_{OC} value of 0.62 V and a FF value of 0.29, resulting in a solar energy conversion efficiency (η) of 0.56%. On the other hand, the cell consisting of dyad **2** in an active layer produced a V_{OC} around 0.63 V, a FF value of 0.26 and a very low short-circuit photocurrent density (J_{SC}) around 0.81 mA cm^{-2}. This corresponds to power conversion efficiency approximately 0.13%. In order to improve the performance of the cell based on dyad **1**, an additional device was fabricated with dyad **1**-

$PC_{71}BM$ in a ratio of 1:2. The device allowed for increased performances of J_{SC} = 4.28 mA cm^{-2} leading to a PCE of 0.71%. Compared to the $PC_{61}BM$ device, the improved performance for $PC_{71}BM$ device is mainly due to the large increment of the short circuit current, which could be attributed to the better absorption properties of $PC_{71}BM$ in the range of 450-700 nm. These PCE values are lower than the ones obtained with related ruthenium phthalocyanines (RuPc's), axially functionalized with pyridyl-(DOT)s and blended with fullerene derivatives (either $PC_{61}BM$ or $PC_{71}BM$).[9] Although V_{OC} and FF values for ZnPc's **1** and **2** are comparable to those of their RuPc analogues, lower short current densities are obtained in the second case. This is most probably due to the lower absorption of compounds **1** and **2** in the range from 450 to 650 nm, which is not compensated by the shifting to the red of the Q-band on going from RuPc's to ZnPc's. The J_{SC} values obtained for devices prepared from dyads **1** and **2** (3.05 and 0.81 mA cm^{-2}, respectively) are also lower than that of the model compound tetra-t-butyl phthalocyanine (3.57 mA cm^{-2}). Unfortunately, we have no clear explanation for this observation. The reduced J_{SC} values in dyads **1** and **2** cannot be attributed to absorption properties of dyads, which are similar to that of tetra-t-butyl zinc phthalocyanine in the range from 650 to 700 nm. It could be due to recombination of photogenerated charge carriers in the BHJ device.

3.6 Conclusions

Two highly soluble zinc phthalocyanines bearing one dendritic oligothienylene-ethynylene as a peripheral substituent were designed and synthesized for studying their photophysical and photovoltaic properties. The conjugated peripheral groups enhance the absorption between 380 and 550 nm, where ZnPc's do not exhibit a strong absorption, thus improving the light harvesting performance of the dyads. Femtosecond upconversion

measurements have shown ultrafast energy transfer from oligothienylene-ethynylene to zinc phthalocyanine, which enables light in the region between 380 and 550 nm to be captured and transferred to the phthalocyanine moiety in a time scale of 300 fs. We were able to show that the extent of energy transfer increased from dyad **1** to dyad **2** due to increased absorption of light with increasing generation of the substituent oligothienylene-ethynylene groups from dyad **1** to dyad **2**. BHJ solar cells constructed using dyads **1** and **2** as electron donor and $PC_{61}BM$ and $PC_{71}BM$ as electron acceptors in the active layer showed lower efficiencies than the corresponding RuPc analogues previously studied by us, due to their lower absorption in the visible range. We are presently preparing new ZnPc's with different conjugated substituents at peripheral positions in order to study their mechanism of recombination, fundamentally important for increasing the power conversion efficiency of these systems.

3.7 Supporting Information: Synthesis of Zn(II)Pc-DOTs 1 and 2 and Characterization

Experiment Section

General procedure: To a freshly distilled and deaerated THF/ TEA (8:1) solution (9 ml) containing tri(*tert*-butyl)iodophthalocyanine (64 mg, 0.07 mmol), $[Pd(PPh_3)Cl_2]$ (5 mg, 0.007 mmol) and CuI (1.5 mg, 0.007 mmol), the corresponding DOT-functionalized terminal alkyne **3a** or **3b** (0.22 mmol) was added and the mixture was stirred for 24 h at room temperature. The solvent was then removed under reduced pressure, and the green solid was extracted with $CHCl_3$, washed with water and dried over Na_2SO_4. The crude product was purified by column chromatography on silica gel (Hexane/dioxane, 3:1).

Dyad **1** was obtained as a mixture of regioisomers (55 mg, 0.047 mmol) as a green solid. Yield: 67%. ^{1}HNMR (d_8-THF, 300 MHz): δ (ppm) = 9.5-8.9 (m, 9H, Ar-H), 8.3-8.2 (m, 3H, Ar-H), 7.7 (d, *J*=9 Hz, 1H, Ar-H), 7.3-7.2 (m, 4H, Ar-H), 1.8 (s, 27H, $C(CH_3)_3$), 0.3 (s,

18H, TMS). IR (film): ν (cm^{-1}) = 2955, 2928, 1620, 1491, 1400, 1325, 1094, 997, 839, 762, 748. UV/Vis (THF): λ_{max} (log ε) = 695 (5.2), 678 (5.1), 642 (4.4), 617 (4.4), 352 (4.9). MS (MALDI, ditranol), m/z: 1158.3 [M^+]. HRMS (MALDI-TOF, DCTB): calc. for $C_{64}H_{62}N_8S_3Si_2Zn$: [M^+]: m/z: 1158.3084, found 1158.3051.

Dyad **2** was obtained as a mixture of regioisomers (65 mg, 0.035 mmol) as green solid. Yield: 51%. ^{1}HNMR (d_8-THF, 300 MHz): δ (ppm) = 9.5-8.9 (m, 9H, Ar-H), 8.4-8.2 (m, 3H, Ar-H), 7.7 (d, *J* =12 Hz, 1H, Ar-H), 7.6 (s, 2H, Ar-H), 7.4 (t, *J* =3 Hz 2H, Ar-H), 7.3-7.2 (m, 2H, Ar-H), 7.2-7.1 (m, 8H, Ar-H), 1.8 (s, 27H, $C(CH_3)_3$), 0.3 (s, 36H, TMS). IR (film): ν (cm^{-1}) = 2957, 2920, 1728, 1624, 1497, 1254, 1101, 993, 839, 758. UV/Vis (THF): λ_{max} (log ε) = 696 (5.2), 678 (5.1), 640 (4.5), 617 (4.4), 345 (5.0). MS (MALDI, DCTB), m/z: 1842.3 [M^+]. HRMS (MALDI-TOF, dithranol): calc. for $C_{98}H_{90}N_8S_9Si_4Zn$: [M^+]: m/z: 1842.3138, found 1842.3148.

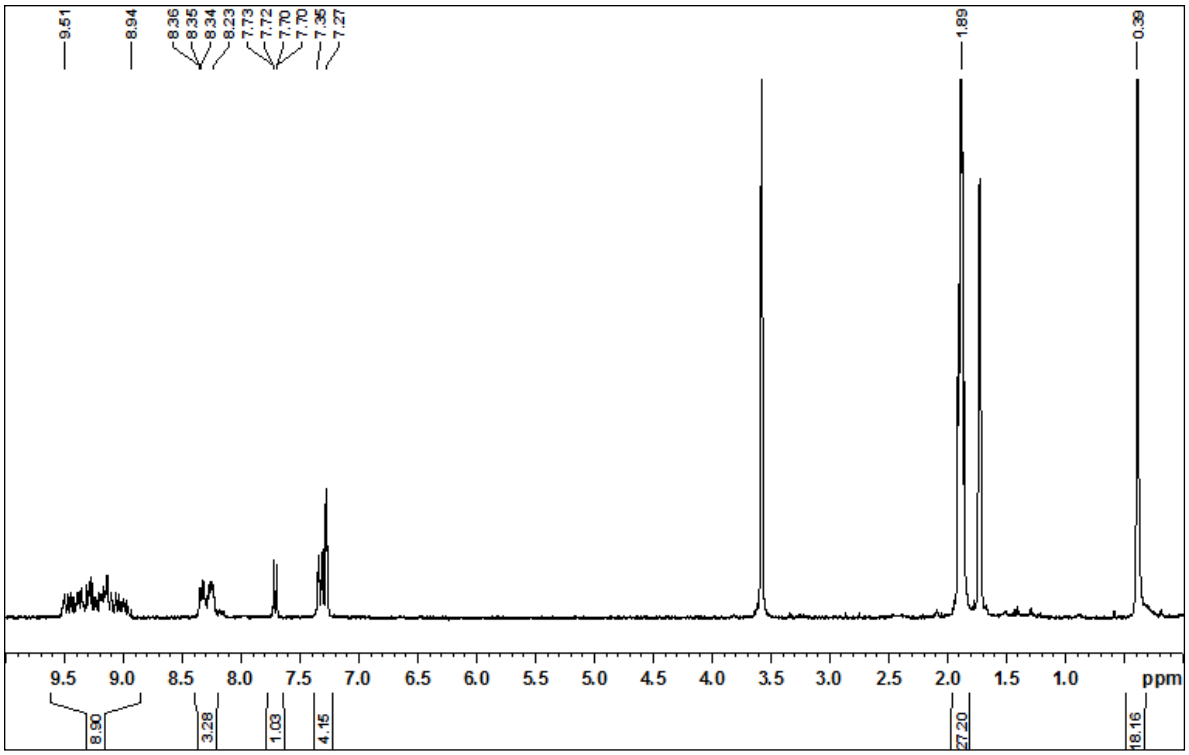

Figure S3.1 ^{1}H-NMR (d_8-THF) spectrum for ZnPc-DOT **1**.

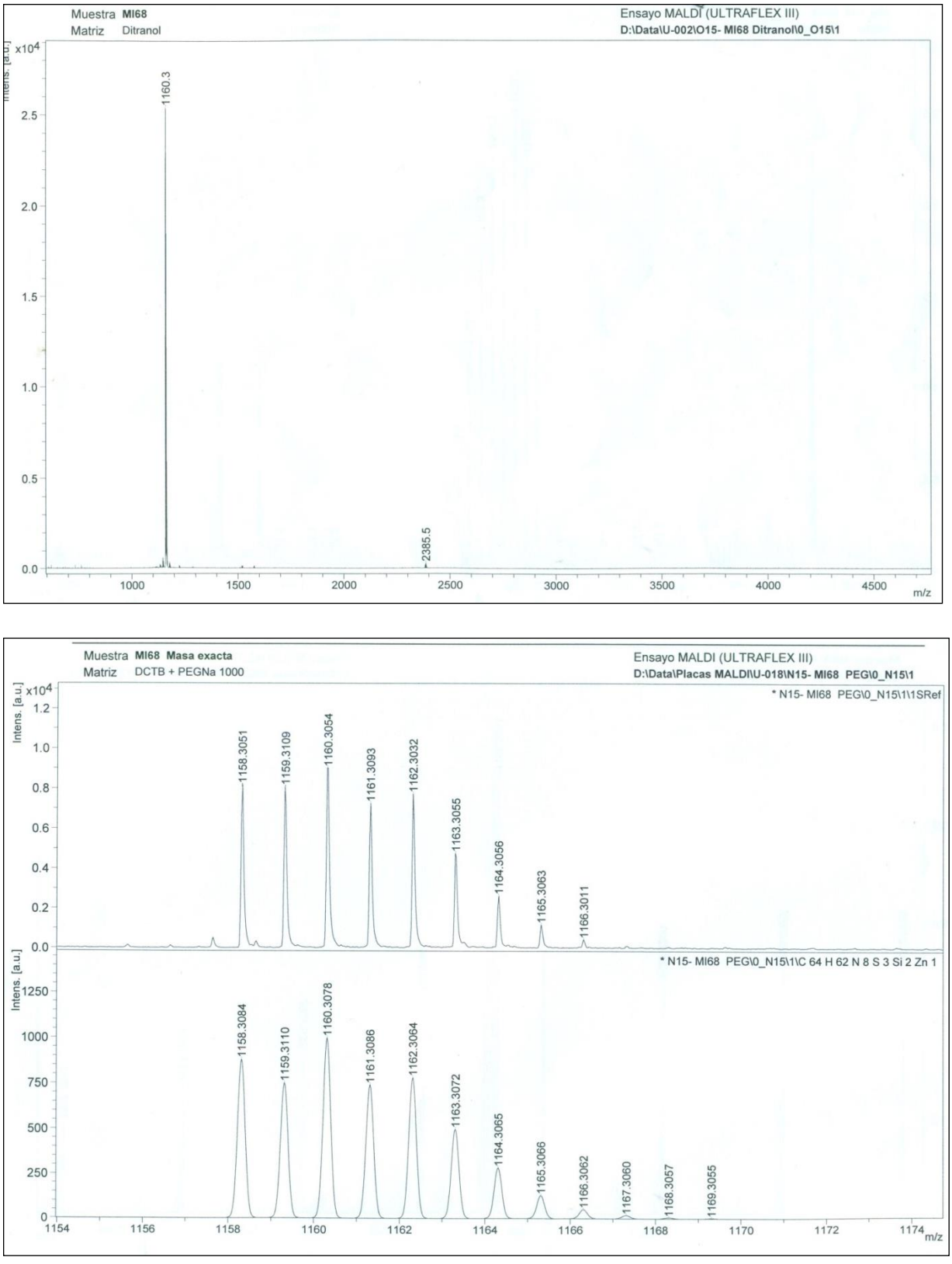

Figure S3.2 MS and HRMS spectra of ZnPc-DOT **1**.

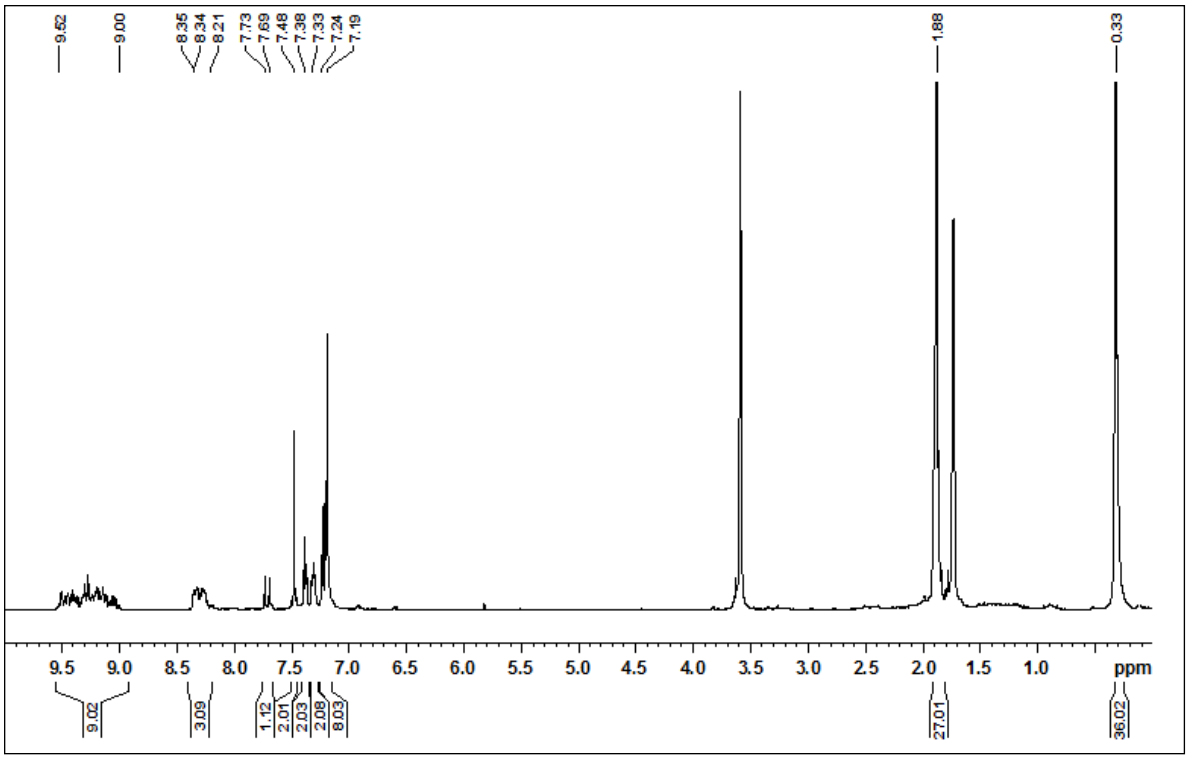

Figure S3.3 ^{1}H NMR (d_8-THF) of ZnPc-DOT **2**.

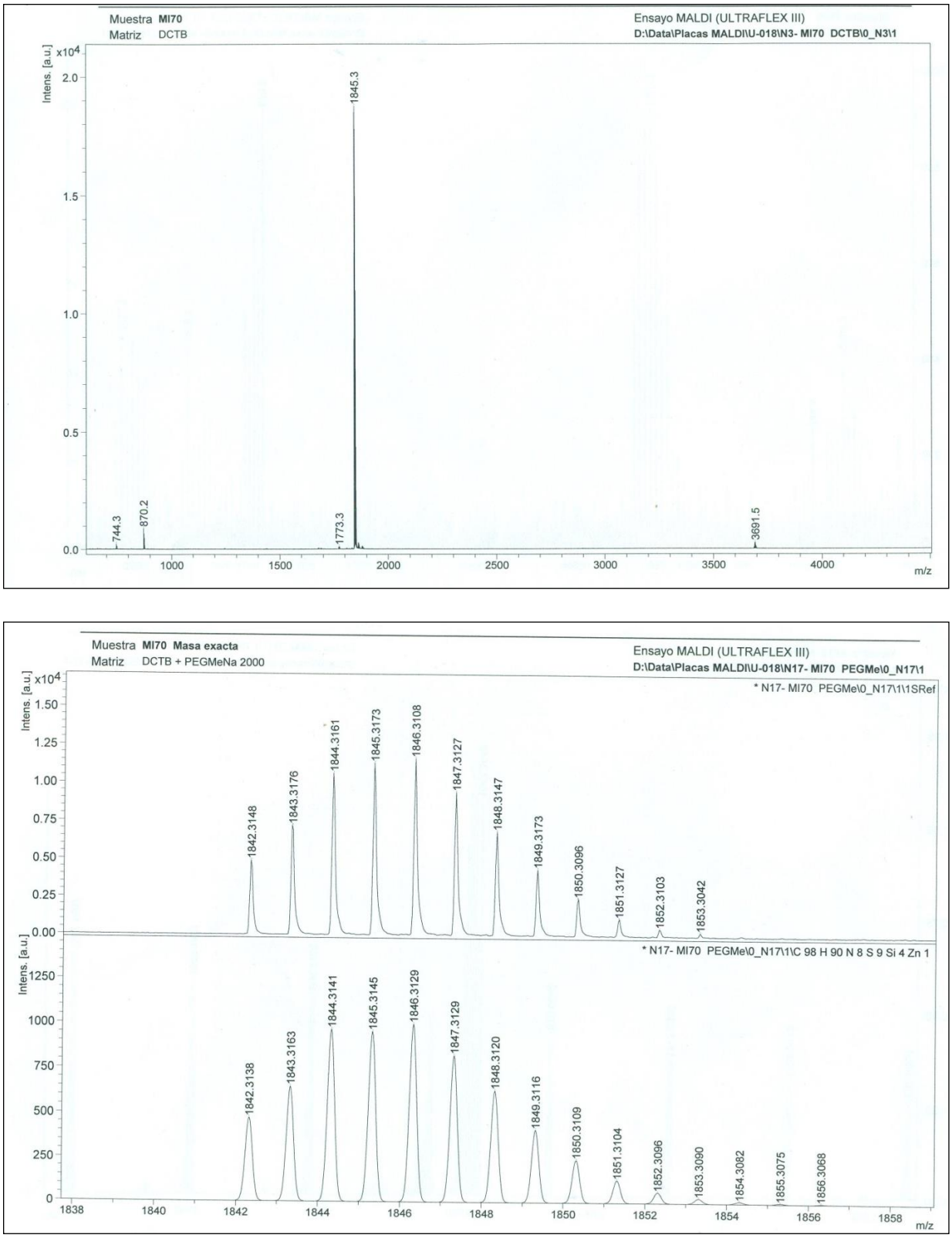

Figure S3.4 MS and HRMS spectra of ZnPc-DOT **2**.

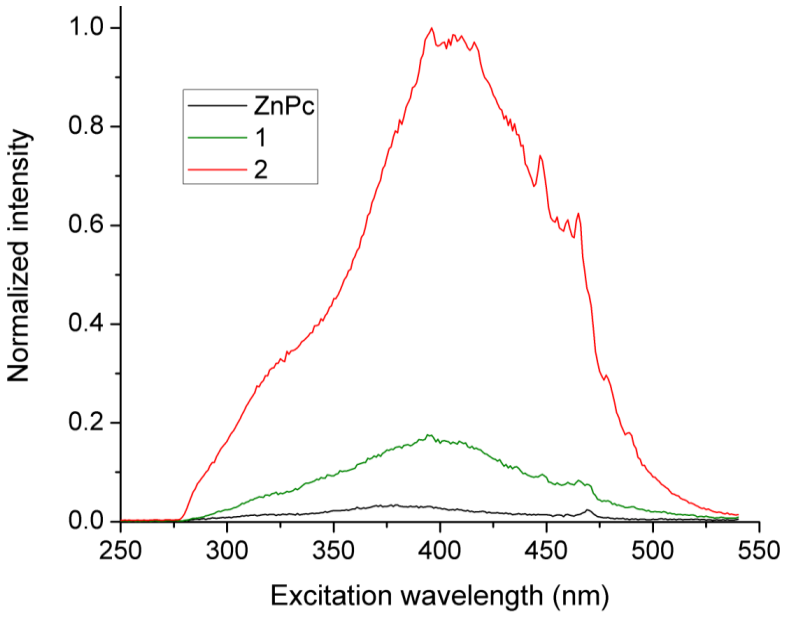

Figure S3.5 Excitation spectra of reference ZnPc, Zn(II)Pc-DOTs **1** and **2**.

References

1. Martínez-Díaz, M. V.; Torres, T. In *Handbook of Porphyrin Science*; Kadish, K., Smith, K. M., Guilard, R., Eds.; World Scientific Press: Singapore, **2010**; pp 141−181.

2. Martínez-Díaz, M. V.; de la Torre, G.; Torres, T. *Chem. Commun.* **2010**, *46*, 7090−108.

3. Walter, M. G.; Rudine, A. B.; Wamser, C. C. *J. Porphyrins Phthalocyanines* **2010**, *14*, 759−792.

4. Imahori, H.; Umeyama, T.; Kurotobi, K.; Takano, Y. *Chem. Commun.* **2012**, *48*, 4032−45.

5. Wang, Q.; Li, Y.; Yan, X.; Rathi, M.; Ropp, M.; Galipeau, D.; Jiang, *J. Appl. Phys. Lett.* **2008**, *93*, 1−4.

6. Silvestri, F.; Lopez-Duarte, I.; Seitz, W.; Beverina, L.; Martínez-Díaz, M. V.; Marks, T. J.; Guldi, D. M.; Pagani, G. A.; Torres, T. *Chem. Commun.* **2009**, 4500−4502.

7. Varotto, A.; Nam, C.-Y.; Radivojevic, I.; Tomé, J. P. C.; Cavaleiro, J. A. S.; Black, C. T.; Drain, C. M. *J. Am. Chem. Soc.* **2010**, *132*, 2552−4.

8. Sánchez-Díaz, A.; Pacios, R.; Muñecas, U.; Torres, T.; Palomares, E. *Org. Electron.* **2011**, *12*, 329−335.

9. Fischer, M. K. R.; Lopez-Duarte, I.; Wienk, M. M.; Martínez-Díaz, M. V.; Janssen, R. A. J.; Bäuerle, P.; Torres, T. *J. Am. Chem. Soc.* **2009**, *131*, 8669−8676.

10. Mishra, A.; Ma, C.; Janssen, R. A. J.; Bäuerle, P. *Chem.-Eur. J.* **2009**, *15*, 13521−13534.

11. Kerp, H. R.; Donker, H.; Koehorst, R. B. M.; Schaafsma, T. J.; van Faassen, E. E. *Chem. Phys. Lett.* **1998**, *298*, 302−308.

12. Koeppe, R.; Fuchsbauer, A.; Lu, S.; Sariciftci, N. S. *Prog. Colloid Polym. Sci.* **2008**, *135*, 16−20.

13. Shankar, K.; Feng, X.; Grimes, C. A. *ACS Nano* **2009**, *3*, 788−94.

14. KC, C. B.; Stranius, K.; D'Souza, P.; Subbaiyan, N. K.; Lemmetyinen, H.; Tkachenko, N. V.; D'Souza, F. *J. Phys. Chem. C* **2013**, *117*, 763−773.

15. Zrig, S.; Rémy, P.; Andrioletti, B.; Rose, E.; Asselberghs, I.; Clays, K. *J. Org. Chem.* **2008**, *73*, 1563−1566.

16. Bongiovanni, G.; Botta, C.; Di Silvestro, G.; Loi, M. A.; Mura, A.; Tubino, R. *Chem. Phys. Lett.* **2001**, *345*, 386−394.

17. Nakamura, T.; Araki, Y.; Ito, O.; Takimiya, K.; Otsubo, T. *J. Phys. Chem. A* **2008**, *112*, 1125−32.

18. Zhang, J.; Fischer, M. K. R.; Bäuerle, P.; Goodson, T. *J. Phys. Chem. B* **2013**, *117*, 4204−4215.

19. Maciejewski, A.; Steer, R. P. J. *Photochem.* **1986**, *35*, 59−69.

20. Jones, G., II; Jackson, W. R.; Choi, C.; Bergmark, W. R. *J. Phys. Chem.* **1985**, *89*, 294−300.

21. Magde, D.; Brannon, J. H.; Cremers, T. L.; Olmsted, J. *J. Phys. Chem.* **1979**, *83*, 696−699.

22. Vincett, P. S.; Voigt, E. M.; Rieckhoff, K. E. *J. Chem. Phys.* **1971**, *55*, 4131.

23. Varnavski, O.; Yan, X.; Mongin, O.; Blanchard-Desce, M.; Goodson, T. *J. Phys. Chem. C* **2007**, *111*, 149−162.

24. Varnavski, O.; Samuel, I. D. W.; Pålsson, L.-O.; Beavington, R.; Burn, P. L.; Goodson, T. *J. Chem. Phys.* **2002**, *116*, 8893.

25. Varnavski, O.; Leanov, A.; Liu, L.; Takacs, J.; Goodson, T., III. *J. Phys. Chem. B* **2000**, *104*, 179−188.

26. Maya, E. M.; Vazquez, P.; Torres, T. *Chem.-Eur. J.* **1999**, *5*, 2004−2013.

27. Savolainen, J.; van der Linden, D.; Dijkhuizen, N.; Herek, J. L. *J. Photochem. Photobiol. A* **2008**, *196*, 99−105.

28. Claessens, C. G.; Hahn, U.; Torres, T. *Chem. Rec.* **2008**, *8*, 75−97.

Chapter 4

Investigations of the Effect of the Acceptor Strength on the Optical and Electronic Properties in Conjugated Polymers for Solar Applications

The work in this chapter has been submitted to *Journal of American Chemical Society (JACS)* with the title:

"Investigations of the Effect of the Acceptor Strength on the Optical and Electronic Properties in Conjugated Polymers for Solar Applications" Oluwasegun O. Adegoke, In Hwan Jung, Luping Yu and Theodore Goodson III.

Modifications were made to the manuscript to adapt it to the style of the content of this dissertation. References and supporting information of the manuscript are included in this chapter.

4.1 Abstract

New low band gap electron-accepting polymers PNSW, PNTPD, PNPDI and PECN[1] containing thieno[2′,3′:5′,6′]pyrido[3,4-g]thieno[3,2-c]isoquinoline-5,11(4H,10H)-dione (**TPTI**) and fluorenedicyclopentathiophene dimalononitrile (**FDCPT-CN**) were investigated. Also investigated was poly[[4,8-bis[(2-ethylhexyl)oxy]benzo[1,2-b:4,5-b′]dithiophene-2,6-diyl][3-fluoro-2-[(2-ethylhexyl)carbonyl]thieno[3,4-b]thiophenediyl]] (PTB7) which is based on repeating units of thienothiophene (**TT**) and benzodithiophene (**BDT**), and one of the most efficient solar cell materials. The steady state, ultrafast dynamics and nonlinear optical properties of these organic polymers were probed. All the polymers showed broad absorption

in the visible region. PNPDI and PECN showed extended absorption into the near-IR region. The polymers had HOMO levels of -5.73 to -5.15 eV and low bandgaps of 1.47 to 2.45 eV. Fluorescence upconversion studies on the polymers showed longer lifetimes of 1.6 and 2.4 ns for PNSW and PNTPD respectively while PNPDI and PECN showed very fast decays within 353 fs and 110 fs. Two-photon absorption investigation of the polymers showed that the absorption cross sections may be in the region of 1.0-6.4×10^4 GM per monomer. The electronic structure calculations of the polymers indicated that the LUMO is localized on the more electron-withdrawing co-monomers while the HOMO was localized on the more-electron-donating co-monomers. As the difference between the electron affinities of the co-monomers in the polymers decrease, the HOMO and LUMO become distributed throughout the monomers. All of the measurements suggest that high difference in the electron affinities of the co-monomers of the polymers contribute to improvement of the photophysical properties (absorption, nonlinear properties) necessary for good solar cell performance.

4.2 Introduction

The search for a clean, renewable source of energy to replace fossil fuels has existed for many decades.[1,2] The vast amount of energy reaching the earth from the sun has necessitated research into ways in which humans can tap into this resource. Consequently, there had been advances into development and synthesis of organic photovoltaic (OPV) materials in the last two decades.[3–9] OPV materials show great promise to replace relatively expensive inorganic counterparts because of their flexibility, ease of production and variety of emerging promising organic compounds for solar cell applications.[9–14] There has been recent progress in the field of OPV, with power conversion efficiency (PCE) reaching over 10% with a polymer tandem solar

cell.[15] However, in order for solar energy conversion into electricity to be commercially viable, it is necessary to be able to fabricate solar cell device with a PCE over 15%.[16,17]

One of the most studied solar-harvesting polymers is poly(3-hexylthiophene) (P3HT).[18–23] Devices based on P3HT were optimized to produce PCEs up to 5%.[24–27] Significant improvements in the design of light harvesting materials have led to advancements in solar cell efficiencies, most recently reaching as high as 10%.[28,29] One strategy that has been adopted to improve the PCE is the inducement of intramolecular charge transfer in organic polymers by designing conjugated donor-acceptor copolymers.[30–37] Organic polymers which have been developed using this approach, and have been reported to have PCEs close to 8% in photovoltaic devices, are the poly(thienothiophene-benzodithiophene) (PTB) polymer series containing repeating units of alternating thieno[3,4-b]thiophene (TT) and benzodithiophene (BDT).[16,38–41] The HOMO and LUMO levels of the polymers were optimized by introducing different substituents into the backbone of the polymer series. The common substituents that were explored are the electron-donating alkyl and alkoxyl groups on the BDT unit and electron-withdrawing esters and fluorine atom on the TT unit. The best polymer in the PTB series with the highest PCE is poly[[4,8-bis[(2-ethylhexyl)oxy]benzo[1,2-b:4,5-b′]dithiophene-2,6-diyl][3-fluoro-2-[(2-ethylhexyl)carbonyl]thieno[3,4-b]thiophenediyl]] (PTB7).[16] The excellent performance of PTB7 has generated intense research to understand how the structures of polymers correlate to their performance. PTB7 possesses low-lying HOMO and LUMO levels, a small bandgap, good film morphology with phenyl butyric acid methyl ester (PCBM), and good absorption over the entire visible and near-infrared regions (NIR).[39,42–45] Another reason that has been attributed to its excellent performance is the strong electron-withdrawing effect of the TT unit on the electron-rich BDT unit.[16] There is a bias in the π-electron density

distribution towards the TT unit which results in induced negative and positive charges on the TT and BDT units respectively. The induced charges on the TT and BDT units cause enhancement of the dipole moment in PTB7.[16] The presence of electronegative fluorine and electron-withdrawing ester group on the TT unit enhances the electron-withdrawing ability of the TT unit. Consequently, there is a good charge transfer in PTB7.

Emerging organic photovoltaic materials depend on the "push-pull" concept or donor-acceptor mechanism. Carsten *et al.*[16] worked on different polymers with alternating TT having different electron-withdrawing substituents and BDT units to investigate the "push-pull" concept. In the study, poly[(4,8-bis(octyloxy)benzo(1,2-b:4,5-b′)dithiophene-2,6-diyl)(2-((2-ethylhexyl)carbonyl)thieno(3,4-b)thiophenediyl)] (PTB2) did not have a fluorine atom and PTB7 did have a fluorine atom attached to the TT unit. Poly[(4,8-bis((2-ethylhexyl)oxy)-3,7-difluorobenzo(1,2-b:4,5-b′)dithiophene-2,6-diyl)(2-((2-ethylhexyl)carbonyl)thieno(3,4-b)thiophenediyl)] (PTBF2) had two opposing fluorine atoms attached to the BDT unit while poly[(4,8-bis((2-butyloctyl)oxy)benzo(1,2-b:4,5-b')dithiophene-2,6-diyl)(2,2'-bis(((2-butyloctyl)oxy)carbonyl)-6,6'-bithieno(3,4-b)thiophenediyl)] (PBB3) had two adjacent TT units in a trans-conformation. These substituents were able to reduce the energy levels of the polymers because of their electron-withdrawing effect. Deep-lying HOMO level ensures oxidative stability of organic polymer materials.[46,47] PBB3 was found to have the best absorption in the NIR region due to the increased conjugation in its polymer chain as a result of the additional thiophene ring. It however showed the smallest ground and excited state dipole moments.[16] The ground and excited state dipole moments were lower than those of PTB7 by factors of 6 and 9 respectively. PTB2 and PTB7 were found to have the best dipole moments. The result shows that the presence of electronegative substituents in the organic polymer chain

affects the magnitude of the dipole moment. The position and configuration of the attached substituents play a huge role in the magnitude of the dipole moment. The reduced dipole moments observed in PTBF2 and PBB3 were due to the cancellation of the opposing electron-pulling effects of the electron-withdrawing groups attached to each of the polymers.[16] On the other hand, the fluorine and ester group in PTB7 complemented each other to draw a significant electron density to the TT unit. Consequently, there was a greater induced dipole moment in PTB7 monomer than PTBF2 and PBB3 which resulted in better charge transfer from the electron-donating BDT to the electron-withdrawing TT. The high induced dipole moment and good charge transfer in PTB7 contributed immensely to its excellent performance in solar cell device.

Until recently, there has been more focus on only the energetics of the donor polymers in bulk heterojunction (BHJ) systems because of the need to ensure a good offset between the LUMO of the donor polymer and the LUMO of the fullerene in polymer-fullerene blends. For effective charge carrier generation by exciton dissociation at the interface between the donor polymer and fullerene, the offset between the LUMO of the donor polymer and LUMO of fullerene acceptor must be at least 0.30 V.[48–50] However, it has been found recently that good charge separation in the donor polymer reduces the importance of the offset between the LUMO of the donor organic polymer and the LUMO of the fullerene acceptor needed for effective charge transfer.[16,51,52] In a study by Carsten *et al.*[16], the transient absorption results of blended films of PTB7 with fullerenes showed a fast excitonic state decay of less than 120 fs while blends of PTBF2 and PBB3 showed longer excitonic decay times of 19 ps and 190 ps respectively. On the other hand, the first component of the charge-separated state of PTB7, PTBF2 and PBB3 were found to be 87 ps, 1.6 ps and 6 ps respectively. The excitonic decay

time is related to the time it takes for the generated exciton in the active layer to be transferred to the fullerene acceptor in BHJ systems. Fast transfer of excitons from the active polymer layer to the fullerene acceptor occurs when the excitonic decay time is short. The charge separated state is linked to the time that the electrons and the holes are able to stay separated: when this time is short, the rate of charge recombination is fast. Therefore, it is necessary for a polymer blend with the fullerene acceptor to have a short excitonic decay time and a long charge-separated state. PTB7 had the shortest excitonic decay time and the longest charge-separated state. Based on the excitonic decay time and charge separated state obtained in the transient absorption experiment on the polymer/fullerene blend, PTB7 showed the most efficient charge transfer and the lowest charge recombination rate. This is in spite of the fact that the energetics of the three polymers was identical, and PTB2 even had better crystallinity than PTB7. The excellent performance of PTB7 could be attributed to enhanced transition dipole moment which increases the driving force for charge transfer from PTB7 to the fullerene acceptor and reduces the rate at which electrons and holes recombine.[16] It is important to understand the effect of induced dipole moment on exciton generation and recombination; and to characterize the structure-property relationships to further develop conjugated polymers for solar cell applications

In this paper, we present the results of a spectroscopic study of PTB7 in order to elucidate why the PTB7-based device offers excellent efficiency. The results of the spectroscopic studies of new polymers will be compared to those of PTB7. These polymers were originally designed to serve as possible replacements of fullerene derivatives in solar cell devices.[53] Fullerenes are efficient electron acceptors because of their high electron affinity and mobility. However, they are rather expensive and also suffer from low absorption at longer

wavelengths of the solar spectrum. The polymers were designed based on electron-accepting moieties, thieno[2′,3′:5′,6′]pyrido[3,4-g]thieno[3,2-c]isoquinoline-5,11(4H,10H)-dione (**TPTI**) and fluorenedicyclopentathiophene dimalononitrile (**FDCPT-CN**). The polymers investigated are the low band gap polymers PNSW, PNTPD, PNPDI which have TPTI within their structures and PECN which contains FDCPT-CN in its structure. In this work, in order to understand the efficiency of charge transfer in the polymers, the two-photon absorption cross-section, fluorescence upconversion and excited state dynamics have been investigated. The results suggest that the efficiency of the charge transfer processes increases as the difference in the electron affinities of the co-monomers in the polymers increases. As a result, PECN and PTB7, which have alternating electron-donating and electron-withdrawing co-monomers, were found to have the best charge transfer abilities among the investigated polymers.

4.3 Experimental Section

4.3.1 Materials

The synthesis of PTB7 and the polymers were carried out by Stille polycondensation method and purification was done by column chromatography.[40,53] The polymers were characterized by using ^{1}H-NMR, ^{13}C-NMR and mass spectroscopy (MALDI-TOF). The molecular weights of the polymers are shown in Table 4.1. The samples were dissolved in spectroscopic grade chloroform (Sigma-Aldrich, spectrophotometric grade). The optical densities of the samples were below 0.5 in order to avoid re-absorption during ultrafast measurements.

4.3.2 Steady state measurements

The steady state measurements of the samples were performed at room temperature.

Concentrations ranging from 1.7×10^{-7} M to 5.1×10^{-7} M were used for the samples. The samples were placed in 4 mm quartz cuvettes. Steady state absorbance spectra were measured using an Agilent 8432 UV-visible absorption spectrophotometer. The emission spectrum measurements were performed with Fluoromax-2 spectrophotometer. To ensure that there was no appreciable photo-degradation during the fluorescence lifetime measurements, absorption spectra measurements were taken before and after each measurement. There was no difference between the absorption spectra taken before and after the fluorescence lifetime measurements. The quantum yields of the samples were calculated using a known procedure[54,55] with 5,10,15,20-tetraphenyl-21H,23H-porphine (TPP) dissolved in toluene (ϕ_f = 0.11) used as standards.[56] The quantum yields were measured at excitation wavelength of 514 nm.

4.3.3 Fluorescence lifetime measurements

The time-resolved fluorescence experiments were performed using a fluorescence set-up that had previously been described.[57–60] Mode-locked Ti-sapphire femtosecond laser (Spectra Physics Tsunami) was used to generate 80-fs pulses at 800 nm wavelength with a repetition rate of 82 MHz. This mode-locked laser was pumped by a 532 nm continuous light output from another laser (Spectra Physics Millennia), which has a gain medium of neodymium-doped yttrium vanadate (Nd:YVO_4). An excitation pulse of 400 nm was generated by a second harmonic β-barium borate crystal and the residual 800 nm beam was made to pass through a computer-controlled motorized optical delay line. The polarization of the excitation beam was controlled by a berek compensator. The power of the excitation beam varied between 17 mW and 20 mW. The fluorescence emitted by the sample was up-converted by a non-linear crystal of β-barium borate by using the residual 800 nm beam which had been

delayed by the optical delay line with a gate step of 6.25 fs. This procedure enabled the fluorescence to be measured temporally. The monochromator is used to select the wavelength of the up-converted beam of interest and the selected beam is detected by a photomultiplier tube (R152P, Hamamatsu, Hamamatsu City, Japan). The photomultiplier tube converts the detected beam into photon counts which can be read from a computer. Coumarin 153 and Cresyl violet dyes were used for calibrating the laser. The instrument response function (IRF) has been determined from the Raman signal of water to have a pulse width of 110 fs.[61] Lifetimes of fluorescence decay were obtained by fitting the fluorescence decay profile with multi-exponential decay functions convoluted with IRF in MATLAB and Origin 8.

For polymer samples having lifetimes in the nanosecond range, fluorescence lifetimes were measured using time-correlated single photon counting (TCSPC) technique which has been described previously.[62] The laser used for the TCSPC measurement was a Kapteyn Murnane (KM) mode-locked Ti-sapphire laser. The output beam from the KM laser was at 800 nm wavelength, with pulse duration of ~ 30 fs. The output beam was frequency-doubled using a nonlinear barium borate crystal to obtain a 400 nm beam. A polarizer was used to vary the power of the 400 nm beam that excites the sample. Focus on the sample cell (quartz cuvette, 0.4 cm path length) was ensured using a lens of focal length 11.5 cm. Collection of fluorescence was done in a direction perpendicular to the incident beam into a monochromator and the output from the monochromator was coupled to a photomultiplier tube which converted the photons into counts.

4.3.4 Two-photon absorption measurements

The two-photon excitation fluorescence method was not used in the determination of the two-photon absorption cross-sections of the polymer samples because of the low quantum yields of some of the polymers. The two-photon absorption cross-sections of the polymer samples were measured by an open-aperture z-scan method. The nonlinear optical set-up used in our study is shown in Figure 4.1. The generation of the 1200 nm incident beam used in the experiment has been described previously.[62,63]

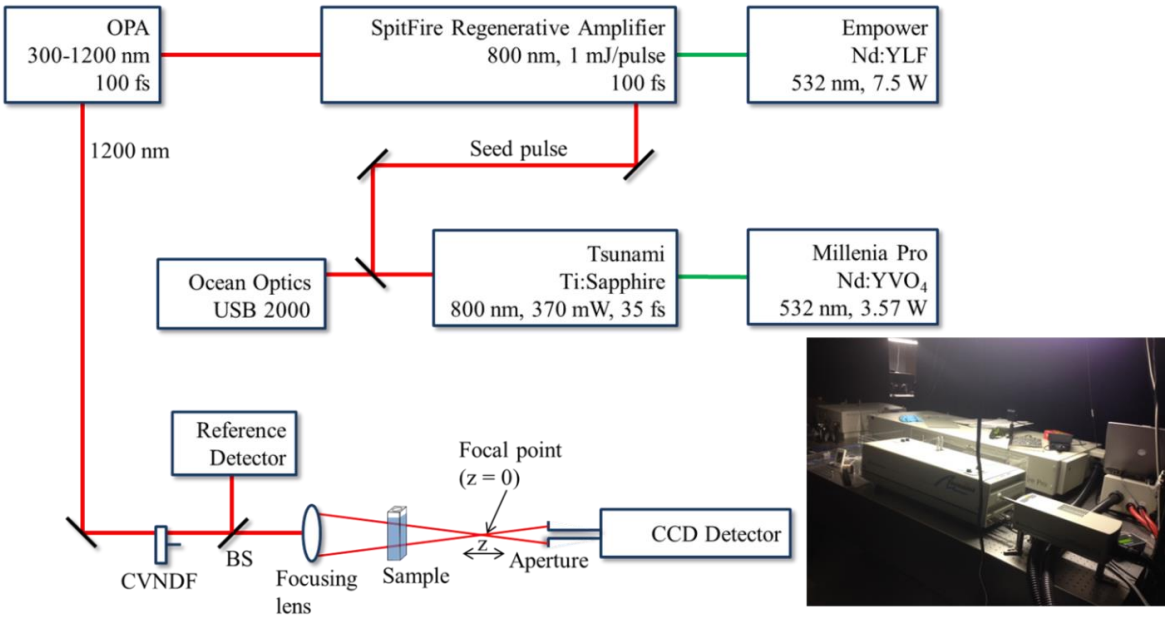

Figure 4.1 Schematics of the nonlinear optical set-up used for two-photon cross-section measurements. Inset: the nonlinear optical set-up

The Spectra Physics diode-pumped Millenia Pro generated 3.57 W, 532 nm continuous wave beam which was used as a pump beam for Ti:sapphire regenerative oscillator (Tsunami, Spectra Physics). Ti-sapphire regenerative amplifier (Spitfire, Spectra Physics) generated 100 fs, 1 mJ pulses at 800 nm with an average power of 1 W with seed pulses from the Ti-sapphire

regenerative oscillator (Tsunami, Spectra Physics) and a pump beam of 7.5 W, 532 nm from Nd:YLF laser (Spectra Physics, Empower). The incident beam was produced using an optical parametric amplifier (OPA-800C), with a wavelength range of 300 – 1200 nm. The incident beam was generated by the nonlinear crystal BBO in the OPA-800C using the second harmonic of the idler that was set at 1200 nm. The intensity of the incident beam was controlled by a circular variable neutral density filter (CVNDF). A beam splitter (BS) was used in splitting the incident beam into two for calibration purpose. A focusing lens, with a focal length of 25 cm, is placed before the sample to focus the incident beam. The transmitted beam through the sample is measured using an open-aperture detector and the result is processed using known correlations (Equation 4.1 and Equation 4.2)[64] in the literature to obtain the two-photon absorption cross-sections of the samples.

$$T(z) = 1 - \frac{\beta I_o \left(1 - e^{-\alpha L}\right)}{2^{\frac{3}{2}} \alpha \left(1 + \frac{z^2}{z_o^2}\right)} \qquad \textbf{Equation 4.1}$$

$$T(z) = 1 - \frac{\beta I_o L}{2^{\frac{3}{2}} \left(1 + \frac{z^2}{z_o^2}\right)} \quad \text{if} \quad \alpha << 1 \qquad \textbf{Equation 4.2}$$

In the equation above, I_o is the intensity of the incident beam at the focus, β is the two-photon absorption coefficient, L is the length of sample in the direction of the beam, z is the position of the sample in the direction of the beam. The two-photon absorption cross-section in the unit of GM (cm^4·s/photon·molecule) is evaluated by using Equation 4.3.

$$\sigma_2 = \frac{\beta h \nu \times 10^3}{Nc}$$ **Equation 4.3**

4.3.5 Molecular orbital calculations

The electronic structure calculation was implemented in the electronic structure code GAMESS (General Atomic and Molecular Electronic Structure System).[65,66] The configuration interaction singles (CIS) approach was employed in this work. CIS approach uses the restricted Hartree Fock (RHF) theory which generates all singly excited determinants of configuration interaction expansions. The CIS approach has the advantage of simultaneous calculation of a large number of excited states and the optimization of a desired selected state. In this study, the calculation was done for 11 excited states and the calculation was optimized for the first excited state. The basis set used was 6-31G and the initial molecular orbital guess was Hückel. The electronic structure calculation was carried out on the repeating monomers of the polymers. Electronic structure calculations of the monomers were preferred to the electronic structure calculations of the polymers in order to reduce computation times and also obtain the contribution of the monomers to the overall performance of the polymers. The structures of the monomers were drawn using ChemDraw. Methyl was used to represent the alkyl ends of the monomer in order to reduce the complexity of computation and reduce computation times. The repeating monomers were modeled using Avogadro software.[67] The GAMESS extension plug-in of Avogadro was used to prepare the input files for GAMESS-US[65,66] which was used for the molecular orbital calculations. The complexity of the building block of the monomer determines the convergence criterion used for the calculation and it varied from 10^{-7} to 10^{-5}. Gabedit[68] was used to visualize the molecular orbital results.

4.4 Results

4.4.1 Synthesis

The molecular structure of PTB7 and the synthetic route of the polymers, PNSW, PNTPD, PNPDI and PECN are provided below.[40,53] PNSW, PNTPD and PNPDI were synthesized by combining electron-accepting co-monomers with stannylated TPTI. The electron-accepting co-monomers used in the synthesis of PNSW, PNTPD and PNPDI are brominated thieno[3,4-d]isothiazol-3(2H)-one-1,1-dioxide (SW), thieno[3,4-c]pyrrole-4,6(5H)-dione (TPD), and 3,4,9,10-perylene diimide (PDI) respectively. PECN was synthesized through a similar process by combining brominated FDCPT-CN and stannylated 2,3-dihydrothieno[3,4-b][1,4]dioxine (EDOT). The detailed synthetic routes of the final polymers are shown in Scheme 4.1.

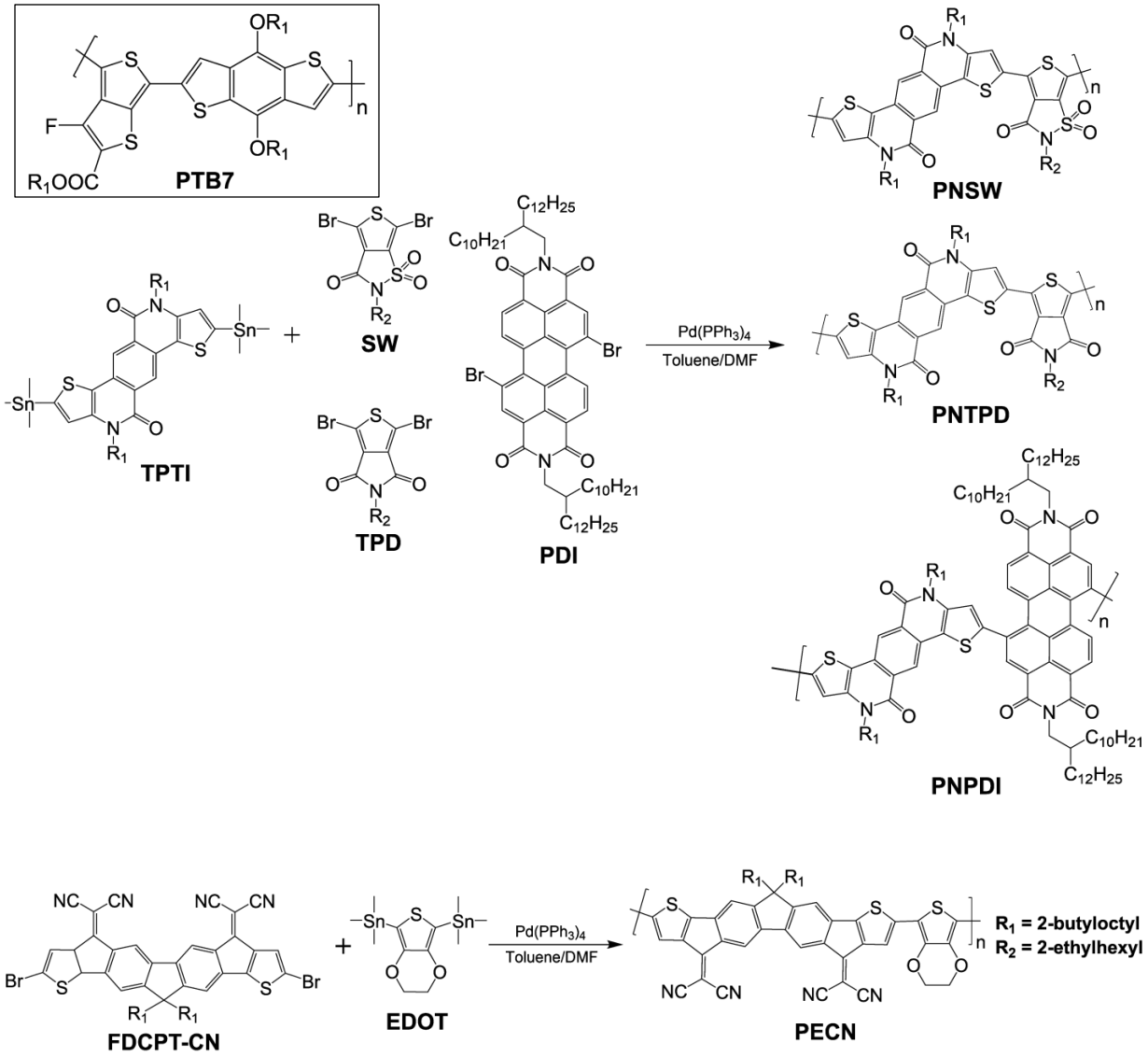

Scheme 4.1 Structure of PTB7 and schematic scheme for PNSW, PNTPD, PNPDI and PECN

PNSW, PNTPD and PNPDI have the TPTI unit in their polymer chains, but they contain different electron accepting moieties in SW, TPD and PDI respectively. The TPD unit has an electron-withdrawing imide group, while SW has a stronger electron-withdrawing sulfonamide unit. PDI is a well-known electron accepting unit containing diimide functionality. Due to the electron withdrawing ability of perylene-based compounds, Zhang *et al.* were able

to demonstrate effective electron and charge transfer from dendritic oligothiophene (DOT) to perylene bisimide (PBI).[69] PECN has donor-acceptor design configuration of strong electron-donating EDOT and strong electron-withdrawing FDCPT-CN moiety.

4.4.2 Steady state measurements

The steady state absorption spectra of the investigated polymers are shown in Figure 4.2. A summary of the steady state properties of the polymers is provided in Table 4.1. The absorbance of the polymer samples spans the entire visible spectrum. PTB7 had the highest molar absorptivity of 3.40×10^{6} $M^{-1} \cdot cm^{-1}$. The excellent absorptivity of PTB7 in the near-infrared region, where the solar flux peaks, may be critical to the observed excellent efficiency of its photovoltaic device.[39] The absorption spectrum of PTB7 was red-shifted relative to the TPTI-based polymers. The small bandgap of PTB7 and the red shift in the absorption spectrum of PTB7 can be attributed to the promotion of the quinoid population by the TT unit of the polymer which leads to concomitant decrease in bond length alternations. In addition, the presence of a strong electronegative fluorine atom and an electron-withdrawing ester in the TT co-monomer of PTB7 modulates the energy levels, consequently resulting in a small bandgap and contributing to the absorption of PTB7 at longer wavelengths. Only PECN has an absorption peak at a longer wavelength than PTB7. Coincidentally, PECN consists of alternating repeating units of strong electron-withdrawing FDCPT-CN and strong electron-donating EDOT, similar to the design motif of PTB7. PTB7 has a weak electron-donating BDT unit and a strong electron-withdrawing substituted TT. Therefore, the absorption in the infrared region of PECN can be attributed to the improved conjugation in the PECN unit and strong intermolecular interaction between the electron-donating and electron-withdrawing units of

PECN. The alternating donor-acceptor structure of the polymers enhances electron delocalization which results in the significant red shift relative to the other polymers. The absorption spectra of PTB7 and PECN extended to wavelengths of 800 nm and 900 nm respectively.

The primary absorption peak in PTB7 was obtained at 680 nm and this can be attributed to the π-π* interaction between the TT and BDT units. A small peak at 396 nm found in the spectrum of PTB7 can be attributed to a $S_0 \rightarrow S_1$ transition in the TT unit. PECN had the widest spectra coverage up to 900 nm and it had its most intense peak around 518 nm. The PECN peak around 486 nm can be attributed to the $S_0 - S_1$ transition in the EDOT unit while the intense peak at 518 nm is due to electron transition in FDCPT-CN. The broad absorption peak noticed at 753 nm can be attributed to π-π* interaction between FDCPT-CN and EDOT. The higher energy level of the HOMO in the electron-donor, EDOT and lower energy level in the electron-acceptor, FDCPT-CN gave rise to a low bandgap (see Figure 4.3) and the intra-chain charge transfer from the donor to the acceptor resulted in the absorption peak at 753 nm.

The onset of absorption in PNPDI was 766 nm. The proximity of the onset to the infrared region is due to the presence of a strong electron-withdrawing PDI moiety in PNPDI which extended its conjugation. There was a characteristic perylene C=C stretching mode associated with a π-π* transition.[70–73] Relative to the parent PDI, PNPDI had an extended absorption beyond 600 nm.[74,75] The interaction between the TPTI co-monomer and PDI gave rise to an absorption peak at 626 nm. The absorption spectrum of PNPDI also appeared to mirror the PDI spectrum. There was a hypsochromic shift of the absorption peaks of PNPDI relative to the parent compound PDI with the 504 nm absorption peak experiencing up to a

blue-shift of 20 nm. Relative to PNTPD, the absorption spectrum of PNSW was red-shifted because of the extra lone pair of electrons in the sulphonyl bond in SW in the structure of PNSW. There were noticeable vibronic states in the absorption spectrum of PNSW which were absent in the absorption spectrum of PNTPD.

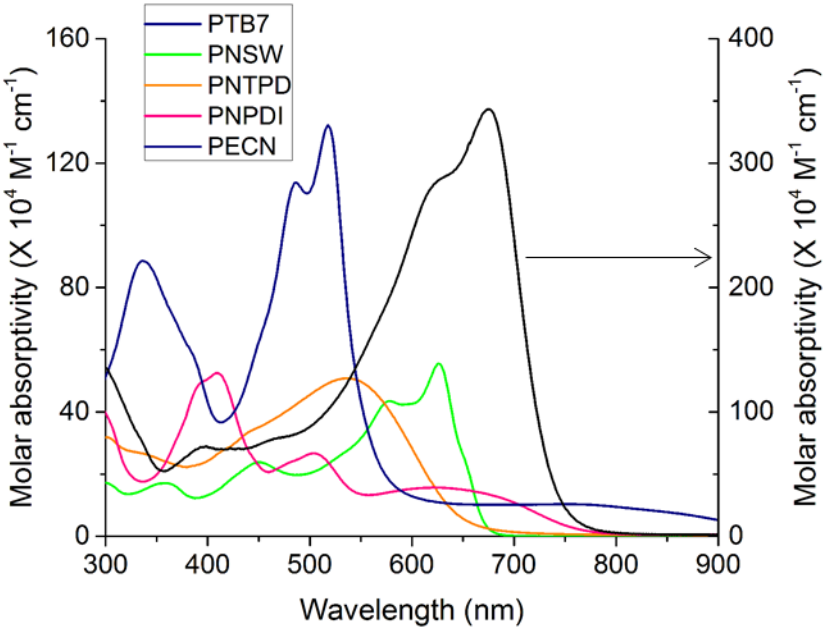

Figure 4.2 Absorption spectra of polymer samples. The molar absorptivity of PTB7 is denoted by the right scale

Table 4.1 Molecular Weight and Steady State Properties of Polymers

Polymers	**M_w (kDa)**	**PDI**	**$N_{monomer}$**	**λ_{abs} (nm)**	**λ_{em} (nm)**	**λ_{onset} (nm)**	**ϕ**
PTB7	146.0	2.4	92	628, 671	736	789	0.00857
PNSW	18.5	1.61	12	359, 450, 578, 626	591, 657	679	0.286
PNTPD	18.0	1.65	12	537	576, 646	673	0.455
PNPDI	39.2	2.17	11	409, 504, 626	589,656,778	766	0.0310
PECN	52.9	2.43	23	336, 486, 518, 753	660	946	0.00154

M_w is the molecular weight of the polymers, PDI is the polydispersity index, $N_{monomer}$ is the number of monomer in one molecule of the polymer, λ_{abs} is the absorption peak wavelength, λ_{em} is the emission peak wavelength, λ_{onset} is the onset of absorption and ϕ is the quantum yield of the polymer samples, with TPP as standard and at excitation wavelength of 514 nm.

As shown in Table 4.1 above, PTB7 had the highest molecular weight. There were 92 monomers in one molecule of the polymer. PECN had the second highest molecular weight and number of monomers in one molecule. PNSW and PNTPD had identical molecular weights and number of monomers in one molecule. The ability to form films with good morphology in solar cell device has been found to increase as the molecular weight of polymers increases.[76–78] The results of the electrochemical properties, investigated by cyclic voltammetry, are summarized in Figure 4.3. The TPTI-based polymers have similar HOMO values which indicate that the electron density in the HOMO may be residing in the TPTI moiety of the polymers. PNPDI which has the strongest electron-withdrawing co-monomer of PDI has the lowest LUMO out of the three polymers having TPTI. PECN has the smallest bandgap of all the polymers investigated. This is as a result of the coupled effects of the strong

electron-withdrawing FDCPT-CN and strong electron-donating EDOT.

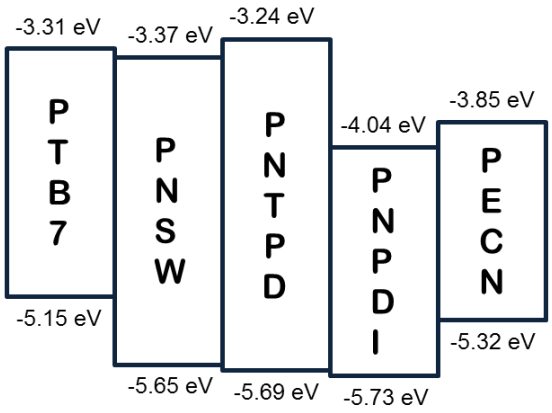

Figure 4.3 HOMO-LUMO energy levels of PTB7[16] and polymer samples[53]

The emission spectra of the polymers are shown in Figure 4.4. The primary emission peaks of PNSW and PNTPD are 659 nm and 646 nm respectively. These represent Stokes shifts of 33 nm and 109 nm for PNSW and PNTPD respectively. The relatively bulky sulphonyl group may have reduced the energy loss due to vibration from PNSW, hence the reason for its smaller Stokes shift relative to PNTPD which contains the less bulky imide functionality. The emission peaks at 659 nm and 646 nm in PNSW and PNTPD respectively may be attributed to the electronic coupling between the donor and acceptor units in the polymers. There were secondary fluorescence peaks in the emission spectra of PNSW and PNTPD at 591 nm and 576 nm which can be attributed to the emission from the TPTI units. The fluorescence from PTB7 occurred at 736 nm. Relative to PNSW and PNTPD, the emission from PTB7 is red-shifted and this red-shift can be related to the strong interaction between the weak electron-donating BDT and the strong electron-withdrawing TT. PNPDI has clearly defined emission peaks at 589 nm, 656 nm and 778 nm. Compared to the parent compound of PDI, the fluorescence spectrum is red-shifted and the florescence between 700 and 850 nm is

broader.

The quantum yields were measured by exciting the samples at 514 nm using 5,10,15,20-tetraphenyl-21H,23H-porphin (TPP) dissolved in toluene (ϕ = 0.11) as a standard. The quantum yield of PTB7 was found to be 8.6×10^{-3} and this relatively low value of quantum yield ensures that PTB7 does not lose most of its absorbed energy through a radiative pathway and therefore ensures that absorbed photons are converted into useful energy for solar cell devices. The TPTI-based polymers PNSW and PNTPD have relatively high quantum yields of 0.286 and 0.455. PNPDI, another polymer with TPTI co-monomer, however had a lower quantum yield of 0.0310. The fluorescence quantum yields of PDI derivatives have been reported to be close to unity.[79,80] The fluorescence quantum yield of PNPDI is much lower than the quantum yield of reported PDI derivatives. This might be as a result of twisting of the PDI core when attached to the TPTI co-monomer. This conclusion is in agreement with the result reported by Jung *et al.*[53] that PNPDI exhibited a distortion in its backbone structure by 48^{o}. A similar observation was also reported by Zhang *et al.*[81] in a compound containing dendritic oligothiophene and perylene bisimide in which the distortion of the PBI core caused self-quenching of emission, thereby resulting in the reduction of the quantum yield. PECN had the lowest quantum yield of 0.00154. The extremely low quantum yield of PECN indicates that it may be experiencing a fluorescence self-quenching mechanism.

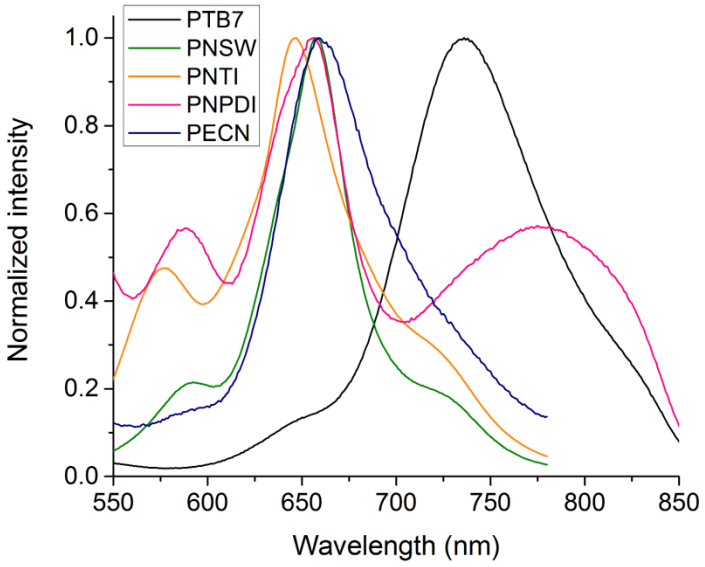

Figure 4.4 Emission spectra of polymer samples

4.4.3 Time-resolved fluorescence measurements

The polymer samples were excited at 400 nm and the fluorescence dynamics were investigated at emission wavelengths of 650 and 700 nm. The dynamics of excited state decay was fitted to a multi-exponential decay function. The lifetimes of PNSW and PNTPD were measured using time-correlated single photon counting (TCSPC) because the lifetimes of excited state decay for these polymers were on the order of many nanoseconds. As shown in Figure 4.5 and Table 4.2, PNPDI showed a short-lived lifetime of ~350 fs. PNPDI was excited in the $S_0 \rightarrow S_2$ electronic transition of perylene where the dipole moment is perpendicular to the long perylene axis. As reported in the literature, the lifetime of the parent PDI compound is 4 ns.[70,82,83] The measured lifetime of 350 fs observed in PNPDI is much shorter than typical fluorescence lifetime of PDI. The short fluorescence time may be connected to the quenching effect of TPTI which is geometrically arranged in a parallel orientation to PDI after excitation. The spatial arrangement allows for easy delocalization of excitation energy and a quick

pathway for fluorescence decay. The singlet relaxation time at fluorescence wavelength of 700 nm was also measured and the relaxation time was found to be 6.57 ps. No rise time was observed in the decay kinetics at 700 nm indicating that there was no energy transfer at this wavelength. It is noteworthy that attempts to measure long-lived state of PNPDI did not yield appreciable fluorescence counts for analysis which indicate that there is virtually no long-lived excited states in PNPDI. The lifetime of PECN was within the instrument response function (IRF) which has a full width at half maximum (FWHM) of 110 fs. The excitation was quickly delocalized throughout the PECN structure. The fast delocalization of excitation energy in PECN resulted in the fast dynamics that was measured in the fluorescence lifetime measurement. The dynamics of PTB7 singlet state decay at fluorescence wavelength of 700 nm was fitted to a bi-exponential decay function. The short decay component has a lifetime of 540 fs and there was a long-lived component of 11 ps (see Figure 4.5). The short component of the decay contributed about 78% of the depopulation of the excited states. The short component of 540 fs can be ascribed to internal conversion.

Shown in Figure 4.6 are the decay dynamics of PNSW and PNTPD, as measured by the TCSPC set-up. The decays were fitted to bi-exponential decay function. The lifetime of PNSW was found to have fully relaxed after 1.57 ns while the lifetime of PNTPD does not relax until after 2.40 ns. Both PNSW and PNTPD consist of electron-withdrawing co-monomers and the long-lived state may have been as a result of absence of a pathway for fast delocalization and relaxation of the excitation energy. PTB7 and PECN had donor-acceptor building block which ensures a fast energy delocalization and TPTI may have acted as a quenching unit for the fluorescence of PDI in PNPDI. These features were absent in PNPDI. These results appear to

be consistent with the quantum yields obtained for the samples in which more fluorescent polymers have longer relaxation times. A summary of the fluorescence lifetimes of the polymers is given in Table 4.2.

The fluorescence lifetime measurements of the polymers indicate that the fluorescence lifetime is inversely proportional to the difference in the electron affinities of the co-monomers in the polymers. PECN, which had the fast fluorescence dynamics, comprises of very good electron-donating EDOT and very strong electron-withdrawing FDCPT-CN. Therefore, there is a great difference in the electron affinities of the co-monomers making up PECN. PTB7 also has a similar backbone as PECN except that the electron-donating unit, BDT in PTB7 is not as strong as EDOT. PNSW and PNTPD both have electron-withdrawing units of varying degrees coupled together. The difference in the electron affinities of the co-monomers in PNSW is however higher than in PNTPD because of the presence of the sulphonyl unit. PNPDI is the only exception to the observation and this may be as a result of the parallel spatial arrangement of the TPTI and PDI co-monomers in PNPDI. The close parallel spatial arrangement of the TPTI and PDI co-monomers allows TPTI to quench the fluorescence of PDI resulting in the fast dynamics shown in Figure 4.5.

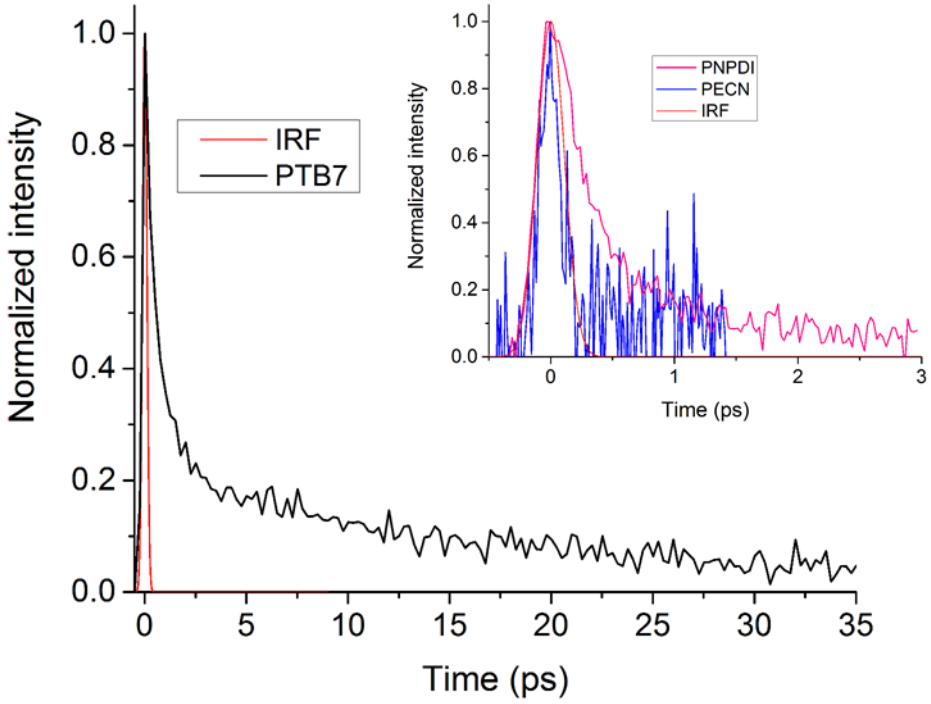

Figure 4.5 Decay dynamics of excited states of PTB7 at fluorescence wavelength of 700 nm Inset: Decay dynamics of excited states of polymers of PNPDI and PECN at fluorescence wavelength of 650 nm

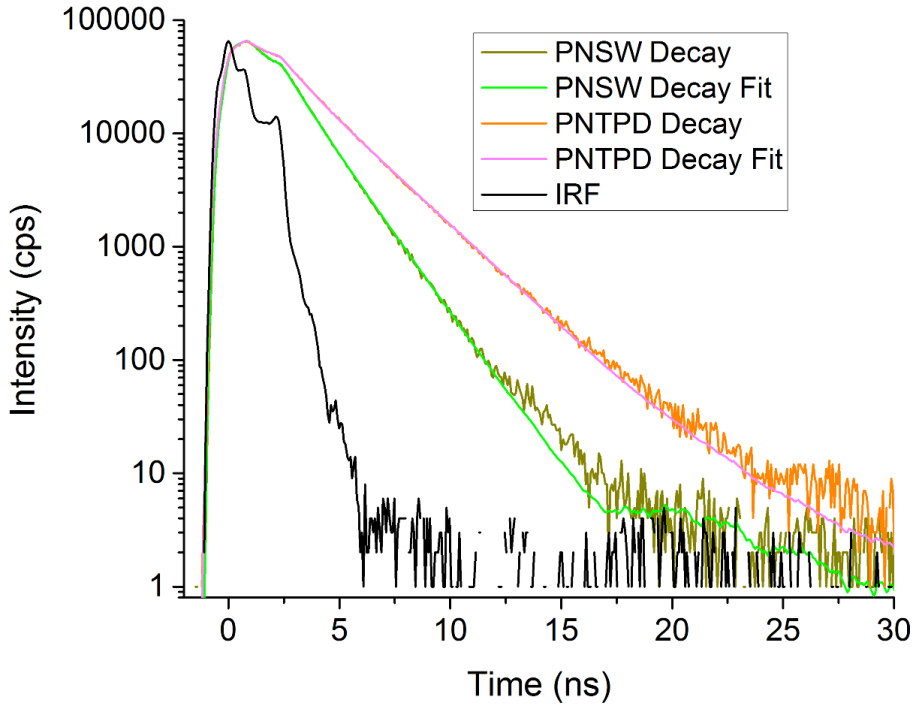

Figure 4.6 Decay dynamics of excited states of PNSW and PNTPD at fluorescence wavelength of 650 nm

Table 4.2 Fluorescence lifetimes of polymer samples

Polymer sample	τ_1 (ps)	τ_2 (ps)
PTB7	0.54	11.0
PNSW	690	1570
PNTPD	900	2400
PNPDI	0.353	
PECN	< 0.110	

4.4.4 Two-photon absorption

The two-photon absorption cross-sections of the investigated polymers were measured using the open-aperture z-scan method. This technique involves the measurement of the transmission through the samples as a function of the z-position with respect to the focal point at z = 0 (see Figure 4.1). The TPA cross-section measurement is based on the correlation between the transmittance and TPA cross-section as described in previous section of this article.[64] Styryl 9M was used as a standard in the determination of two photon absorption cross sections of the polymers. The two-photon absorption cross-sections of PNSW, PNTPD, PNPDI, PECN and PTB7 were measured as 3.30×10^4 GM, 2.92×10^4 GM, 4.84×10^4 GM, 19.04×10^4 GM and 9.60×10^4 GM respectively. All investigated polymers were studied at incident wavelength of 1200 nm except PTB7 which was studied at 1250 nm. PECN and PTB7 have the highest two photon absorption cross sections because of the presence of repeating donor-acceptor units in their structures which introduce nonlinearity and increase potential for charge transfer. PECN has a strong electron-donating EDOT co-monomer and a strong

electron-withdrawing FDCPT-CN co-monomer while PTB7 has a weak electron-donating BDT co-monomer and a strong electron-withdrawing TT co-monomer. This donor-acceptor backbone ensures that electron transfer from the donor group to the acceptor group takes place efficiently. The two-photon absorption cross-section increases as the transition dipole moment increases and charge transfer becomes more efficient. Therefore, the high two-photon absorption cross-section of PTB7 and PECN can be directly linked to the design motif of the two polymers. Unlike PTB7 and PECN, the other polymers have combinations of monomers with different strengths of electron-withdrawing ability and therefore could not take advantage of the push-pull concept that enhances two-photon absorption. The two-photon absorption cross section of PECN may have been additionally enhanced by the presence of the dicyanoyinyl group in its polymer chain. Dicyanoyinyl groups have been found to enhance two-photon cross-section due to the presence of delocalized electrons in the dicyanoyinyl bond.[84–86]

We are interested in finding the contribution of each conjugation unit in each of the polymer chain to the two-photon absorption cross-section. Bhatta *et al.*[43] found the number of monomers in the conjugating unit of PTB7 using the density functional theory calculation to be around 12 with a conjugation length of 147 Å. However, Niklas *et al.*[87] reported a shorter conjugation length of 40 Å and a conjugating unit of 3 to 4 monomers. Here, we use a conservative estimate of 6 monomers in the conjugating unit of PTB7 and 3 units for the other polymers. By scaling the two photon absorption cross section of PTB7 polymer by the number of monomers in the conjugating unit, the contribution of the monomer to the two-photon absorption cross-section is found to be 1.60×10^4 GM. The contributions of the monomer of

PNSW, PNTPD, PNPDI and PECN to the two-photon-absorption cross-section were calculated to be 1.10×10^4 GM, 0.97×10^4 GM, 1.61×10^4 GM and 6.34×10^4 GM respectively. The results of the two-photon properties of the polymers are summarized in Table 4.3.

Table 4.3 TPA Properties of PTB7 and the polymers

Sample	**δ (× 10^4 GM)**	**δ/monomer (× 10^4 GM)**	**Calculated transition dipole of monomer (D)**
PTB7	9.60	1.60	6.77
PNSW	3.30	1.10	9.77
PNTPD	2.92	0.97	2.08
PNPDI	4.84	1.61	1.72
PECN	19.04	6.34	4.86

The TPA absorption cross-section is highly dependent on the transition dipole moment. The absorption cross-section is enhanced for conjugated systems possessing large transition dipole moment as well as large difference between the dipole moments in the ground and excited states. The transition dipole moments of the monomers in the building blocks of the polymers, given in Table 4.3, were obtained from the electronic structure calculations implemented in GAMESS software. The calculated transition dipole moment of PNSW was higher than the monomers of the other investigated polymers. The high transition dipole moment may be due to the good electron-withdrawing effect of the sulphonyl group in PNSW. However, similar trend was not observed in the experimentally determined two-photon absorption cross-section of the PNSW polymer compared with the other investigated polymers.

The steric hindrance of the sulphonyl group between monomers of PNSW may have limited the experimentally measured two-photon absorption cross-section. PECN and PTB7 with alternating donor-acceptor building blocks have the higher calculated transition dipole moment and two-photon absorption cross-section relative to the other investigated polymers.

4.4.5 Electronic structure calculations

The molecular orbital calculations indicated that the HOMO and LUMO were concentrated at the electron-donating and electron-withdrawing ends of the monomers respectively for organic polymers having alternating donor-acceptor alternating units. The localized effect of the HOMO and LUMO in different part of the copolymers of the alternating systems ensures that the HOMO and LUMO energy levels of the copolymers can be easily tuned independently. This provides the chance for further modification and improvement of the copolymers. Only monomers of PTB7 and PECN showed appreciable localization of HOMO and LUMO in different moieties. In the monomer of PTB7, the HOMO was localized on the BDT moiety while the LUMO was concentrated on the TT moiety. The presence of fluorine and esters on the TT ensures that the LUMO was effectively pulled towards the TT end. A similar scenario was observed in PECN in which the HOMO was localized in the EDOT moiety while the LUMO was localized in FDCPT-CN. However, the HOMO can also be seen to have extended to some part of FDCPT-CN. Therefore, the localization was not as evident as it was in PTB7. The localization of the energy levels in different moieties of the monomers ensures that electron delocalization and formation of quinoid mesomeric structures can take place through the push-pull driving force in the donor-acceptor system. The quinoid structure influences the carbon-carbon single bond between the electron-donating and electron-

withdrawing moieties to adopt more double bond character and the bond length alternation decreases. This improves the conjugation in the organic systems and enhances electron transfer. Effective conjugation and electron transfer in organic systems lead to red-shift of the absorption spectrum. This supports the results of the absorption spectra (see Figure 4.2) in which light harvesting in PTB7 and PECN extended to wavelengths of 800 nm and 900 nm respectively. This was the furthest absorption to the near infrared region of all the polymers investigated in this study. Good intermolecular coupling between two dipolar ends of PTB7 and PECN enhances the absorption of light in the near infrared region. In addition, good orbital mixing and redistribution of the HOMO and LUMO of the electron-withdrawing and electron-donating moieties in PTB7 and PECN also resulted in a narrow band gap as shown in Figure 4.3.

The HOMO and LUMO in PNSW and PNTPD were distributed throughout their entire monomers. The monomers of PNSW and PNTPD consist of two electron-withdrawing units. Therefore, the difference in the electron affinity between the two units in each of PNSW and PNTPD is not as significant as the difference in the electron affinity in the units contained in PTB7 and PECN. It can however be noticed that the HOMO has a slight bias for the TPTI unit because of its stronger electron affinity than the SW and TPD units. The push-pull concept cannot occur in PNSW and PNTPD because the HOMO and LUMO are not localized in different moieties of the monomers. These electronic results agree with the findings in the absorption spectra and bandgaps of PNSW and PNTPD as shown in Figure 4.2 and Figure 4.3 respectively. The light harvesting of PNSW and PNTPD only extended to ~ 700 nm which with the absorption peak being 626 and 537 nm respectively. Compared with the other

polymers, PNSW and PNTPD also had the largest bandgaps because the HOMO and LUMO could not redistribute effectively to reduce the bandgap. The slow fluorescence lifetimes of PNSW and PNTPD can also be explained from the HOMO and LUMO distribution in their monomers. Unlike in PTB7 and PECN where localization of HOMO and LUMO ensures effective electron transfer from the electron-donating to the electron-withdrawing units and eventually short fluorescence lifetimes, PNSW and PNTPD have distributed energy levels and cannot take advantage of the push-pull concept. Therefore, electron transfer rate is slower and the electrons are rather trapped within the monomer, hence the reason for the long fluorescence lifetimes observed in PNSW and PNTPD.

PNPDI is composed of two electron-withdrawing moieties in PDI and TPTI but the electron-withdrawing strength of PDI is greater. Thus, the LUMO was concentrated on the PDI moiety while the HOMO was more spread out in the PNPDI monomer. PNPDI had a spatial geometrical orientation which has TPTI lying in a parallel plane to PDI. The parallel nature of the HOMO and LUMO of TPTI and PDI in PNPDI must have contributed to the observed fluorescence quenching in the fluorescence lifetime measurements of PNPDI. Shown in Figure 4.7 are the HOMO and LUMO distribution of the repeating monomers in each of the polymers.

Polymer	**HOMO**	**LUMO**
PTB7	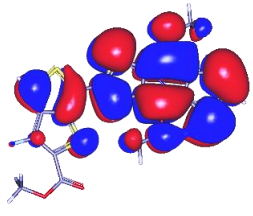	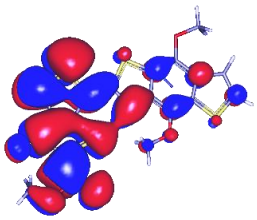

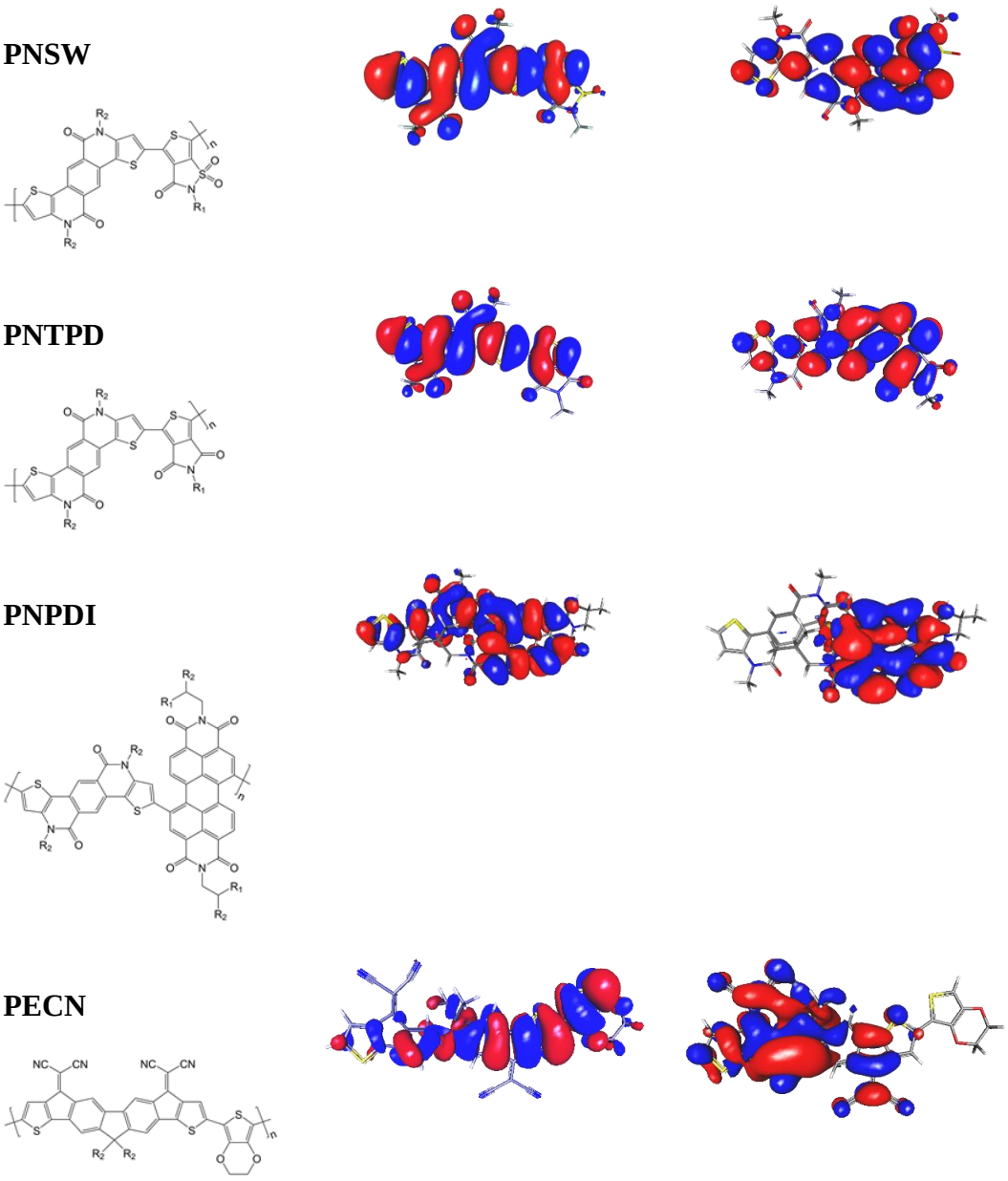

Figure 4.7 Molecular orbital energy level diagram of the repeating monomers in the polymers.

As shown in Table 4.4, PTB7 was estimated to have excitation energy of 4.16 eV. This energy was more than the excitation energies for all other monomers. However, the cyclic voltammetry results indicated that the bandgap of PTB7 was smaller than the bandgaps of PNSW and PNTPD. The bandgap of a polymer decreases as the number of monomers in the

conjugation length of the polymer increases. Therefore, the combined results of the cyclic voltammetry and the electronic structure calculations indicate that PTB7 has a conjugation length that extends beyond one monomer which was considered in the electronic structure calculation. This conclusion is consistent with the performance of PTB7 in solar cell device. Extended conjugation is essential for effective charge transfer and ultimately good solar cell performance. The trend in the excitation energies of the other monomers was consistent with the cyclic voltammetry results shown in Figure 4.3.

PECN, just like PTB7, has alternating donor-acceptor backbone. PECN showed a wide and intense absorption band, low quantum yield and high two-photon absorption cross-section. PECN also showed a localization of the HOMO and LUMO in different moieties of its monomer. These are properties that are essential for good solar cell performance. It will be worthwhile to investigate PECN as a donor material in a solar cell device. The results also confirm that the combination of electron-donating and electron-withdrawing moieties to form the backbone of organic solar cell materials is the best approach for the design of new solar cell materials.

Table 4.4 Electronic properties of the repeating monomers of the polymers obtained from electronic calculation using GAMESS

Monomer	Excitation energy (eV)	Ground state dipole (D)	Transition dipole (D)
PTB7	4.16	4.17	6.77
PNSW	3.66	4.23	9.77
PNTPD	3.80	3.28	2.08
PECN	2.32	3.52	1.72
PNPDI	2.33	3.83	4.86

4.5 Conclusions

PTB7, which is one of the best efficient organic solar cell materials, was investigated using linear, nonlinear and ultrafast spectroscopic techniques. The results were compared to those of new conjugated organic polymers which had different design motifs and electron-withdrawing substituents. The polymers with the donor-acceptor design motif had the most intense and widest spectral absorption band. Thus, PTB7 and PECN had absorption spectra that extended from 300 nm to 800 nm and 900 nm respectively. Only PNPDI showed absorption that extended to 800 nm out of the other polymers because of its extended conjugation. The nonlinear spectroscopic measurements indicated that PECN and PTB7 have high two-photon absorption cross-sections. Therefore, there will be effective charge transfer in PECN and PTB7 because of the direct correlation between two-photon absorption cross-section and effectiveness of charge transfer. The electronic structure calculations in the polymers indicate that the HOMO and LUMO are localized in different moieties contained in PTB7 and PECN which suggests that the polymers can take advantage of the push-pull concept to transfer charge. In the other investigated polymers, the HOMO and LUMO were distributed through the monomer. PECN showed photophysical properties similar to PTB7 and showed that it will be a good candidate as solar cell material. It will be suggested that PECN should be used to fabricate solar cell device in order to investigate its photovoltaic performance.

4.6 Supporting Information

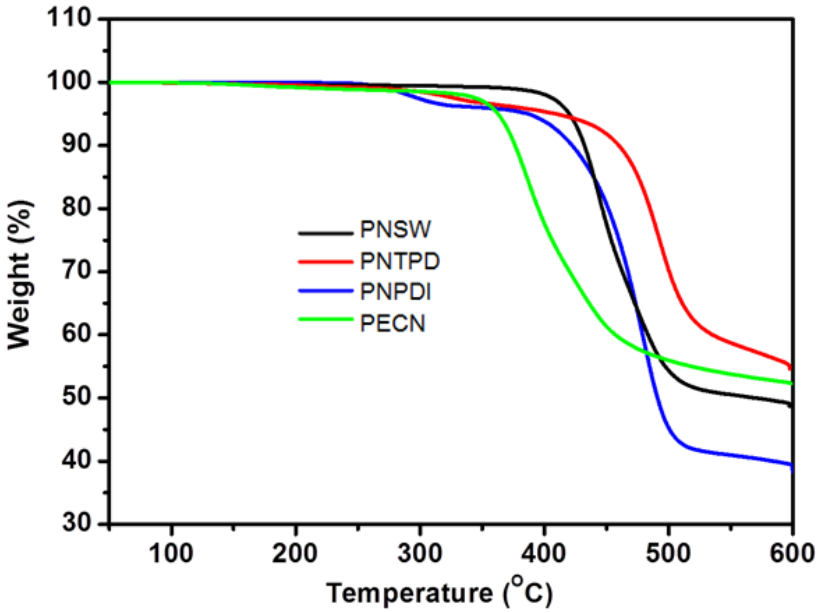

Figure S4.1 Thermogravimetric analysis (TGA) thermograms of the polymers were performed using a TA Q600 instrument. All polymers exhibited good thermal stability, showing less than 5% weight loss up to 381 - 420 °C.

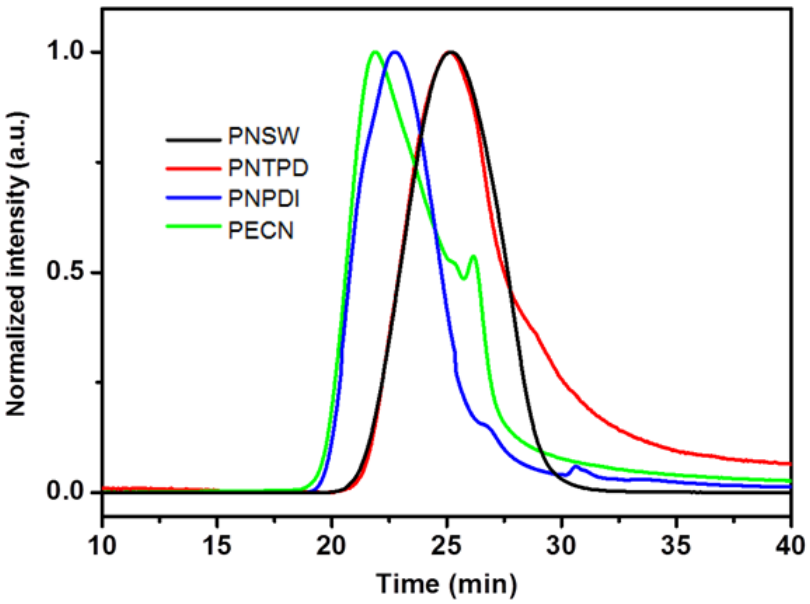

Figure S4.2 The number- and weight-averaged molecular weights of the polymers were determined by Gel-permeation chromatography (GPC) with a Waters Associates liquid chromatography instrument equipped with a Waters 510 HPLC pump, a Waters 410 differential refractometer, and a Waters 486 tunable absorbance detector. Tetrahydrofuran (THF) was used as the eluent and polystyrene as the standard.

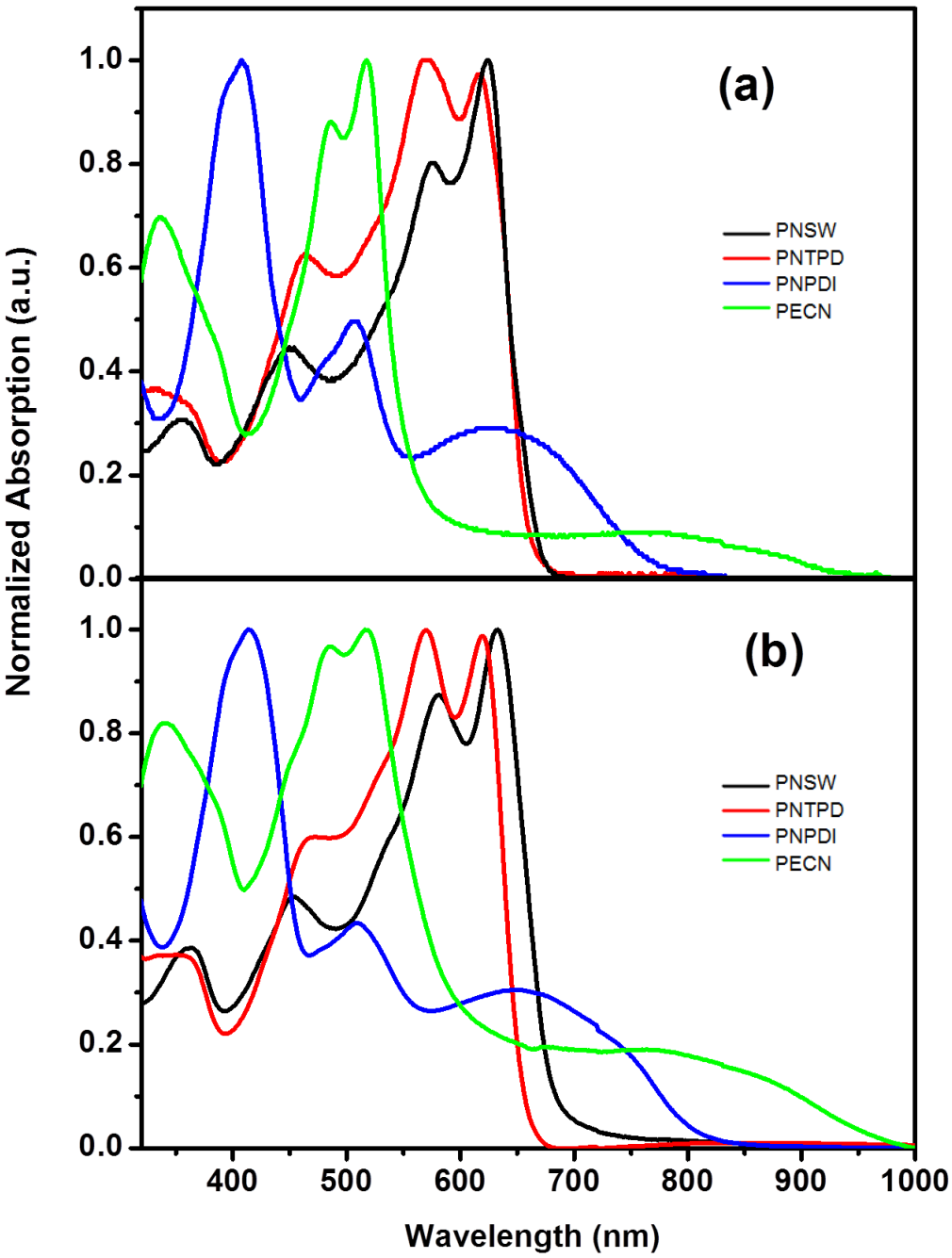

Figure S4.3 Normalized UV-visible absorption (a) in chloroform (CF) and (b) in film of the polymers

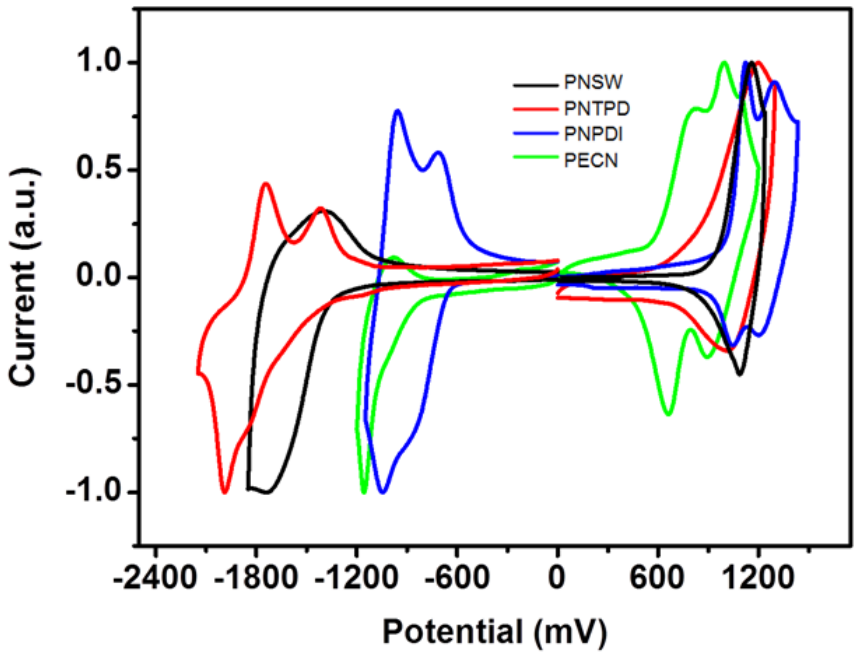

Figure S4.4 Cyclic voltammograms of the polymers were obtained from cyclic voltammetry, which was performed on an AUTOLAB/PG-STAT12 model system with a three-electrode cell in a 0.1 N Bu_4NBF_4 solution in acetonitrile at a scan rate of 50 mV/s. A film of each polymer was coated onto a Pt wire electrode by dipping the electrode into a polymer solution in chloroform. All measurements were calibrated against an internal standard of ferrocene (Fc), the ionization potential (IP) value of which is -4.8 eV for the Fc/Fc^+ redox system.

References

(1) Loferski, J. J. The First Forty Years: *Prog. Photovoltaics* **1993**, *1*, 67–78.

(2) Lodhi, M. A. K. PHOTOVOLTAICS AND HYDROGEN : FUTURE ENERGY OPTIONS. *Energy Convers. Manag.* **1997**, *38*, 1881–1893.

(3) Spanggaard, H.; Krebs, F. C. A Brief History of the Development of Organic and Polymeric Photovoltaics. *Sol. Energy Mater. Sol. Cells* **2004**, *83*, 125–146.

(4) Benanti, T. L.; Venkataraman, D. Organic Solar Cells: An Overview Focusing on Active Layer Morphology. *Photosynth. Res.* **2006**, *87*, 73–81.

(5) Hoppe, H.; Sariciftci, N. S. Organic Solar Cells: An Overview. *J. Mat. Res.* **2004**, *19*, 1924–1945.

(6) Goetzberger, A.; Hebling, C.; Schock, H.-W. Photovoltaic Materials, History, Status and Outlook. *Mater. Sci. Eng. R.* **2003**, *40*, 1–46.

(7) Brabec, C. J.; Sariciftci, N. S.; Hummelen, J. C. Plastic Solar Cells. *Adv. Funct. Mater.* **2001**, *11*, 15–26.

(8) Sariciftci, N. S. Plastic Photovoltaic Devices. *Mater. Today* **2004**, 36–40.

(9) Darling, S. B.; You, F. The Case for Organic Photovoltaics. *RSC Adv.* **2013**, *3*, 17633–17648.

(10) Nunzi, J. Organic Photovoltaic Materials and Devices. *C. R. Phys. 3* **2002**, *3*, 523–542.

(11) Scharber, M. C.; Sariciftci, N. S. Efficiency of Bulk-Heterojunction Organic Solar Cells. *Prog. Polym. Sci.* **2013**, *38*, 1929–1940.

(12) Shaheen, S. E.; Radspinner, R.; Peyghambarian, N.; Jabbour, G. E. Fabrication of Bulk Heterojunction Plastic Solar Cells by Screen Printing. *Appl. Phys. Lett.* **2001**, *79*, 2996–2998.

(13) Zhan, X.; Zhu, D. Conjugated Polymers for High-Efficiency Organic Photovoltaics. *Polym. Chem.* **2010**, *1*, 409–419.

(14) Xue, J. Perspectives on Organic Photovoltaics. *Polym. Rev.* **2010**, *50*, 411–419.

(15) You, J.; Dou, L.; Yoshimura, K.; Kato, T.; Ohya, K.; Moriarty, T.; Emery, K.; Chen, C.-C.; Gao, J.; Li, G.; et al. A Polymer Tandem Solar Cell with 10.6% Power Conversion Efficiency. *Nat. Commun.* **2013**, *4*, 1–10.

(16) Carsten, B.; Szarko, J. M.; Son, H. J.; Wang, W.; Lu, L.; He, F.; Rolczynski, B. S.; Lou, S. J.; Chen, L. X.; Yu, L. Examining the Effect of the Dipole Moment on Charge Separation in Donor-Acceptor Polymers for Organic Photovoltaic Applications. *J. Am. Chem. Soc.* **2011**, *133*, 20468–20475.

(17) Kalowekamo, J.; Baker, E. Estimating the Manufacturing Cost of Purely Organic Solar Cells. *Sol. Energy* **2009**, *83*, 1224–1231.

(18) Kwong, C. Y.; Choy, W. C. H.; Djurisic, A. B.; Chui, P. C.; Cheng, K. W.; Chan, W. K. Poly(3-hexylthiophene):TiO 2 Nanocomposites for Solar Cell Applications. *Nanotechnology* **2004**, *15*, 1156–1161.

(19) Berson, S.; De Bettignies, R.; Bailly, S.; Guillerez, S. Poly(3-Hexylthiophene) Fibers for Photovoltaic Applications. *Ad* **2007**, *17*, 1377–1384.

(20) Shakya, P.; Desai, P.; Kreouzis, T.; Gillin, W. P.; Tuladhar, S. M.; Ballantyne, a M.; Nelson, J. The Effect of Applied Magnetic Field on Photocurrent Generation in Poly-3-hexylthiophene:[6,6]-Phenyl C61-Butyric Acid Methyl Ester Photovoltaic Devices. *J. Phys. Condens. Matter* **2008**, *20*, 452203–452206.

(21) Ratcliff, E. L.; Jenkins, J. L.; Nebesny, K.; Armstrong, N. R. Electrodeposited, "Textured" Poly(3-Hexylthiophene) (e-P3HT) Films for Photovoltaic Applications. *Chem. Mater.* **2008**, *20*, 5796–5806.

(22) Lohwasser, R. H.; Bandara, J.; Thelakkat, M. Tailor-Made Synthesis of poly(3-Hexylthiophene) with Carboxylic End Groups and Its Application as a Polymer Sensitizer in Solid-State Dye-Sensitized Solar Cells. *J. Mater. Chem.* **2009**, *19*, 4126–4130.

(23) Lee, J. U.; Jung, J. W.; Emrick, T.; Russell, T. P.; Jo, W. H. Synthesis of C60-End Capped P3HT and Its Application for High Performance of P3HT/PCBM Bulk Heterojunction Solar Cells. *J. Mater. Chem.* **2010**, *20*, 3287–3294.

(24) Chen, L.; Wang, P.; Chen, Y. High Efficiency of poly(3-hexylthiophene)/[6,6]-Phenyl C61 Butyric Acid Methyl Ester Bulk Heterojunction Solar Cells through Precrystallining of poly(3-Hexylthiophene) Based Layer. *ACS Appl. Mater. Interfaces* **2013**, *5*, 5986–5993.

(25) Chen, L.; Yao, K.; Chen, Y. Can Morphology Tailoring Based on Functionalized Fullerene Nanostructures Improve the Performance of Organic Solar Cells? *J. Mater. Chem.* **2012**, *22*, 18768–18771.

(26) Guo, X.; Cui, C.; Zhang, M.; Huo, L.; Huang, Y.; Hou, J.; Li, Y. High Efficiency Polymer Solar Cells Based on poly(3-Hexylthiophene)/indene-C70 Bisadduct with Solvent Additive. *Energy Environ. Sci.* **2012**, *5*, 7943–7949.

(27) Jin, S.-H.; Vijaya Kumar Naidu, B.; Jeon, H.-S.; Park, S.-M.; Park, J.-S.; Chul Kim, S.; Wook Lee, J.; Gal, Y.-S. Optimization of Process Parameters for High-Efficiency Polymer Photovoltaic Devices Based on P3HT:PCBM System. *Sol. Energy Mater. Sol. Cells* **2007**, *91*, 1187–1193.

(28) Liu, Y.; Chen, C.-C.; Hong, Z.; Gao, J.; Michael Yang, Y.; Zhou, H.; Dou, L.; Li, G.; Yang, Y. Solution-Processed Small-Molecule Solar Cells: Breaking the 10% Power Conversion Efficiency. *Sci. Rep.* **2013**, *3*, 3356.

(29) Zhang, G.; Bala, H.; Cheng, Y.; Shi, D.; Lv, X.; Yu, Q.; Wang, P. High Efficiency and Stable Dye-Sensitized Solar Cells with an Organic Chromophore Featuring a Binary Π-Conjugated Spacer. *Chem. Commun.* **2009**, 2198–2200.

(30) Havinga, E. E.; ten Hoeve, W.; Wynberg, H. A New Class of Small Band Gap Organic Polymer Conductors. *Polym. Bull.* **1992**, *29*, 119–126.

(31) Heeger, A. J. Semiconducting Polymers: The Third Generation. *Chem. Soc. Rev.* **2010**, *39*, 2354–2371.

(32) Yuen, J. D.; Wudl, F. Strong Acceptors in Donor–acceptor Polymers for High Performance Thin Film Transistors. *Energy Environ. Sci.* **2013**, *6*, 392–406.

(33) Lei, T.; Wang, J.-Y.; Pei, J. Design, Synthesis, and Structure-Property Relationships of Isoindigo-Based Conjugated Polymers. *Acc. Chem. Res.* **2014**, *47*, 1117–1126, DOI**:** 10.1021/ar400254j.

(34) Zhuang, W.; Bolognesi, M.; Seri, M.; Henriksson, P.; Gedefaw, D.; Kroon, R.; Jarvid, M.; Lundin, A.; Wang, E.; Muccini, M.; et al. Influence of Incorporating Different Electron-Rich Thiophene-Based Units on the Photovoltaic Properties of Isoindigo-Based Conjugated Polymers: An Experimental and DFT Study. *Macromolecules* **2013**, *46*, 8488–8499.

(35) Owczarczyk, Z. R.; Braunecker, W. A.; Garcia, A.; Larsen, R.; Nardes, A. M.; Kopidakis, N.; Ginley, D. S.; Olson, D. C. 5,10-Dihydroindolo[3,2- B]indole-Based Copolymers with Alternating Donor and Acceptor Moieties for Organic Photovoltaics. *Macromolecules* **2013**, *46*, 1350–1360.

(36) Bronstein, H.; Frost, J. M.; Hadipour, A.; Kim, Y.; Nielsen, C. B.; Ashraf, R. S.; Rand, B. P.; Watkins, S.; Mcculloch, I. Effect of Fluorination on the Properties of a Donor − Acceptor Copolymer for Use in Photovoltaic Cells and Transistors. *Chem. Mater.* **2013**, *25*, 277–285.

(37) Kularatne, R. S.; Magurudeniya, H. D.; Sista, P.; Biewer, M. C.; Stefan, M. C. Donor-Acceptor Semiconducting Polymers for Organic Solar Cells. *J. Polym. Sci. Part A Polym. Chem.* **2013**, *51*, 743–768.

(38) Liang, Y.; Luping, Y. A New Class of Semiconducting Polymers for Bulk Heterojunction Solar Cells with Exceptionally High Performance. *Acc. Chem. Res.* **2010**, *43*, 1227–1236.

(39) Liang, Y.; Xu, Z.; Xia, J.; Tsai, S.-T.; Wu, Y.; Li, G.; Ray, C.; Yu, L. For the Bright Future-Bulk Heterojunction Polymer Solar Cells with Power Conversion Efficiency of 7.4%. *Adv. Mater.* **2010**, *22*, E135–E138.

(40) Liang, Y.; Feng, D.; Wu, Y.; Tsai, S.-T.; Li, G.; Ray, C.; Yu, L. Highly Efficient Solar Cell Polymers Developed via Fine-Tuning of Structural and Electronic Properties. *J. Am. Chem. Soc.* **2009**, *131*, 7792–7799.

(41) Liang, Y.; Wu, Y.; Feng, D.; Tsai, S.-T.; Son, H.-J.; Li, G.; Yu, L. Development of New Semiconducting Polymers for High Performance Solar Cells. *J. Am. Chem. Soc.* **2009**, *131*, 56–57.

(42) Jin, Z.; Gehrig, D.; Dyer-smith, C.; Heilweil, E. J.; Laquai, F.; Bonn, M.; Turchinovich, D. Ultrafast Terahertz Photoconductivity of Photovoltaic Polymer − Fullerene Blends: A Comparative Study Correlated with Photovoltaic Device Performance. *J. Phys. Chem. Lett.* **2014**, *5*, 3662–3668.

(43) Bhatta, R. S.; Perry, D. S.; Tsige, M. Nanostructures and Electronic Properties of a High-Efficiency Electron-Donating Polymer. *J. Phys. Chem. A* **2013**, *117*, 12628–12634.

(44) Ito, M.; Palanisamy, K.; Kumar, A.; Murugesan, V. S.; Shin, P.-K.; Tsuda, N.; Yamada, J.; Ochiai, S. Characterization of the Organic Thin Film Solar Cells with Active Layers of PTB7 / PC71BM Prepared by Using Solvent Mixtures with Different Additives. *Int. J. Photoenergy* **2014**, *2014*, 1–8.

(45) He, X.; Mukherjee, S.; Watkins, S.; Chen, M.; Qin, T.; Thomsen, L.; Ade, H.; Mcneill, C. R. Influence of Fluorination and Molecular Weight on the Morphology and Performance of PTB7:PC71BM Solar Cells. *J. Phys. Chem. C* **2014**, *118*, 9918–9929.

(46) Beatrup, D.; Wade, J.; Biniek, L.; Bronstein, H.; Hurhangee, M.; Kim, J.-S.; McCulloch, I.; Durrant, J. R. Polaron Stability in Semiconducting Polymer Neat Films. *Chem. Commun.* **2014**, *50*, 14425–14428.

(47) Lim, B.; Baeg, K.-J.; Jeong, H.-G.; Jo, J.; Kim, H.; Park, J.-W.; Noh, Y.-Y.; Vak, D.; Park, J.-H.; Park, J.-W.; et al. A New Poly(thienylenevinylene) Derivative with High Mobility and Oxidative Stability for Organic Thin-Film Transistors and Solar Cells. *Adv. Mater.* **2009**, *21*, 2808–2814.

(48) Hedström, S.; Henriksson, P.; Wang, E.; Andersson, M. R.; Persson, P. Light-Harvesting Capabilities of Low Band Gap Donor-Acceptor Polymers. *Phys. Chem. Chem. Phys.* **2014**, *16*, 24853–24865.

(49) Mola, G. T.; Abera, N. Correlation between LUMO Offset of Donor/acceptor Molecules to an Open Circuit Voltage in Bulk Heterojunction Solar Cell. *Phys. B* **2014**, *445*, 56–59.

(50) Servaites, J. D.; Ratner, M. A.; Marks, T. J. Practical Efficiency Limits in Organic Photovoltaic Cells: Functional Dependence of Fill Factor and External Quantum Efficiency. *Appl. Phys. Lett.* **2009**, *95*, 163302.

(51) Gondek, E.; Kityk, I. V.; Danel, A. Some Anthracene Derivatives with N,N-Dimethylamine Moieties as Materials for Photovoltaic Devices. *Mater. Chem. Phys.* **2008**, *112*, 301–304.

(52) Chi, C.-Y.; Chen, M.-C.; Liaw, D.-J.; Wu, H.-Y.; Huang, Y.-C.; Tai, Y. A Bifunctional Copolymer Additive to Utilize Photoenergy Transfer and to Improve Hole Mobility for Organic Ternary Bulk-Heterojunction Solar Cell. *ACS Appl. Mater. Interfaces* **2014**, *6*, 12119–12125.

(53) Jung, I. H.; Lo, W.-Y.; Jang, J.; Chen, W.; Zhao, D.; Landry, E. S.; Lu, L.; Talapin, D. V; Yu, L. Synthesis and Search for Design Principles of New Electron Accepting Polymers for All-Polymer Solar Cells. *Chem. Mater.* **2014**, *26*, 3450–3459.

(54) Maciejewski, A.; Steer, R. P. Spectral and Photophysical Properties of 9,10-Diphenylanthracene in Perfluoro-N-Hexane: The Influence of Solute-Solvent Interactions. *J. Photochem.* **1986**, *35*, 59–69.

(55) Furgal, J. C.; Jung, J. H.; Goodson III, T.; Laine, R. M. Analyzing Structure-Photophysical Property Relationships for Ssolated T8, T10, and T12 Stilbenevinylsilsesquioxanes. *J. Am. Chem. Soc.* **2013**, *135*, 12259–12269.

(56) Seybold, P. G.; Gouterman, M. Porphyrins XIII: Fluorescence Spectra and Quantum Yields. *J. Mol. Spectros.* **1969**, *31*, 1–13.

(57) Adegoke, O. O.; Ince, M.; Mishra, A.; Green, A.; Varnavski, O.; Mart, M. V.; Ba, P.; Goodson, T. Synthesis and Ultrafast Time Resolved Spectroscopy of Peripherally Functionalized Zinc Phthalocyanine Bearing Oligothienylene-Ethynylene Subunits. *J. Phys. Chem. C* **2013**, *117*, 20912–20918.

(58) Varnavski, O.; Samuel, I. D. W.; Pålsson, L.-O.; Beavington, R.; Burn, P. L.; Goodson, T. Investigations of Excitation Energy Transfer and Intramolecular Interactions in a Nitrogen Corded Distrylbenzene Dendrimer System. *J. Chem. Phys.* **2002**, *116*, 8893.

(59) Varnavski, O.; Yan, X.; Mongin, O.; Blanchard-Desce, M.; Goodson, T. Strongly Interacting Organic Conjugated Dendrimers with Enhanced Two-Photon Absorption. *J. Phys. Chem. C* **2007**, *111*, 149–162.

(60) Varnavski, O.; Leanov, A.; Liu, L.; Takacs, J.; Goodson III, T. Large Nonlinear Refraction and Higher Order Nonlinear Optical Effects in a Novel Organic Dendrimer. *J. Phys. Chem. B* **2000**, *104*, 179–188.

(61) Flynn, D. C.; Ramakrishna, G.; Yang, H.; Northrop, B. H.; Stang, P. J.; Goodson III, T. G. Ultrafast Optical Excitations In Supramolecular Metallacycles with Charge Transfer Properties. *J. Am. Chem. Soc.* **2010**, *132*, 1348–1358.

(62) Bhaskar, A.; Ramakrishna, G.; Lu, Z.; Twieg, R.; Hales, J. M.; Hagan, D. J.; Van Stryland, E.; Goodson, T. Investigation of Two-Photon Absorption Properties in Branched Alkene and Alkyne Chromophores. *J. Am. Chem. Soc.* **2006**, *128*, 11840–11849.

(63) Yau, S. H.; Abeyasinghe, N.; Orr, M.; Upton, L.; Varnavski, O.; Werner, J. H.; Yeh, H.-C.; Sharma, J.; Shreve, A. P.; Martinez, J. S.; et al. Bright Two-Photon Emission and Ultra-Fast Relaxation Dynamics in a DNA-Templated Nanocluster Investigated by Ultra-Fast Spectroscopy. *Nanoscale* **2012**, *4*, 4247–4254.

(64) Nag, A.; De, A. K.; Goswami, D. Two-Photon Cross-Section Measurements Using an Optical Chopper: Z -Scan and Two-Photon Fluorescence Schemes. *J. Phys. B At. Mol. Opt. Phys.* **2009**, *42*, 065103–065109.

(65) Schmidt, M. W.; Baldridge, K. K.; Boatz, J. A.; Elbert, S. T.; Gordon, M. S.; Jensen, J. H.; Koseki, S.; Matsunaga, N.; Nguyen, K. A.; Su, S.; et al. General Atomic and Molecular Electronic Structure System. *J. Comput. Chem.* **1993**, *14*, 1347–1363.

(66) Gordon, M. S.; Schmidt, M. W. Advances in Electronic Structure Theory: GAMESS a Decade Later. In *Theory and Applications of Computational Chemistry: The First Forty Years*; Dykstra, C. E.; Frenking, G.; Kim, K. S.; Scuseria, G. E., Eds.; Elsevier: Amsterdam, 2005; pp. 1167–1189.

(67) Hanwell, M. D.; Curtis, D. E.; Lonie, D. C.; Vandermeersch, T.; Zurek, E.; Hutchison, G. R. Avogadro: An Advanced Semantic Chemical Editor, Visualization, and Analysis Platform. *J. Cheminform.* **2012**, *4*, 1–17.

(68) Allouche, A. Software News and Updates Gabedit — A Graphical User Interface for Computational Chemistry Softwares. *J. Comput. Chem.* **2011**, *32*, 174–182.

(69) Zhang, J.; Fischer, M. K. R.; Bäuerle, P.; Goodson III, T. Energy Migration in Dendritic Oligothiophene-Perylene Bisimides. *J. Phys. Chem. B* **2013**, *117*, 4204–4215, DOI: 10.1021/jp302772y

(70) Huang, C.; Barlow, S.; Marder, S. R. Perylene-3,4,9,10-Tetracarboxylic Acid Diimides: Synthesis, Physical Properties, and Use in Organic Electronics. *J. Org. Chem.* **2011**, *76*, 2386–2407.

(71) Kozma, E.; Kotowski, D.; Catellani, M.; Luzzati, S.; Famulari, A.; Bertini, F. Synthesis and Characterization of New Electron Acceptor Perylene Diimide Molecules for Photovoltaic Applications. *Dye. Pigm.* **2013**, *99*, 329–338.

(72) Huo, E.-F.; Zou, Y.; Sun, H.-Q.; Bai, J.-L.; Huang, Y.; Lu, Z.-Y.; Liu, Y.; Jiang, Q.; Zhao, S.-L. Synthesis and Characterization of N-Type Conjugated Copolymers Bearing Perylene Diimide Moieties. *Polym. Bull.* **2011**, *67*, 843–857.

(73) Dinçalp, H.; Cimen, O.; Ameri, T.; Brabec, C. J.; Içli, S. Synthesis, Characterization and Optoelectronic Properties of a New Perylene Diimide-Benzimidazole Type Solar Light Harvesting Dye. *Spectrochim. Acta Mol. Biomol. Spectros.* **2014**, *128*, 197–206.

(74) Tilley, A. J.; Pensack, R. D.; Lee, T. S.; Djukic, B.; Scholes, G. D.; Seferos, D. S. Ultrafast Triplet Formation in Thionated Perylene Diimides. *J. Phys. Chem. C* **2014**, *118*, 9996–10004.

(75) Handa, N. V; Mendoza, K. D.; Shirtcliff, L. D. Syntheses and Properties of 1,6 and 1,7 Perylene Diimides and Tetracarboxylic Dianhydrides. *Org. Lett.* **2011**, *13*, 4724–4727.

(76) Kline, R. J.; McGehee, M. D.; Kadnikova, E. N.; Liu, J.; Fréchet, J. M. J. Controlling the Field-Effect Mobility of Regioregular Polythiophene by Changing the Molecular Weight. *Adv. Mater.* **2003**, *15*, 1519–1522.

(77) Kline, R. J.; McGehee, M. D.; Kadnikova, E. N.; Liu, J.; Fréchet, J. M. J.; Toney, M. F. Dependence of Regioregular Poly (3-Hexylthiophene) Film Morphology and Field-Effect Mobility on Molecular Weight. *Macromolecules* **2005**, *38*, 3312–3319.

(78) Zen, A.; Pflaum, J.; Hirschmann, S.; Zhuang, W.; Jaiser, F.; Asawapirom, U.; Rabe, J. P.; Scherf, U.; Neher, D. Effect of Molecular Weight and Annealing of Poly(3-

Hexylthiophene)s on the Performance of Organic Field-Effect Transistors. *Adv. Funct. Mater.* **2004**, *14*, 757–764.

(79) Johansson, L. B.-Å.; Langhals, H. Spectroscopic Studies of Fluorescent Perylene Dyes. *Spectrochim. Acta Mol. Biomol. Spectros.* **1991**, *47*, 857–861.

(80) El-daly, S. A.; Fayed, T. A. Photochemistry of N, Ń-Ditridecyl-3,4:9,10-Perylenetetracarboxylic Diimide in Chloromethane Solvents. *J. Photochem. Photobiol. A Chem.* **2000**, *137*, 15–19.

(81) Zhang, J.; Fischer, M. K. R.; Bäuerle, P.; Goodson III, T. Energy Migration in Dendritic Oligothiophene-Perylene Bisimides. *J. Phys. Chem. B* **2012**.

(82) Langhals, H.; Karolin, J.; Johansson, L. B. A. Spectroscopic Properties of New and Convenient Standards for Measuring Ñuorescence Quantum Yields. *J. Chem. Soc., Faraday Trans.* **1998**, *94*, 2919–2922.

(83) Würthner, F. Perylene Bisimide Dyes as Versatile Building Blocks for Functional Supramolecular Architectures. *Chem. Commun.* **2004**, 1564–1579.

(84) Fu, J.; Padilha, L. a.; Hagan, D. J.; Van Stryland, E. W.; Przhonska, O. V.; Bondar, M. V.; Slominsky, Y. L.; Kachkovski, A. D. Experimental and Theoretical Approaches to Understanding Two-Photon Absorption Spectra in Polymethine and Squaraine Molecules. *J. Opt. Soc. Am. B* **2007**, *24*, 67–76.

(85) Padilha, L. A.; Webster, S.; Przhonska, O. V.; Hu, H.; Peceli, D.; Rosch, J. L.; Bondar, M. V.; Gerasov, A. O.; Kovtun, Y. P.; Shandura, M. P.; et al. Nonlinear Absorption in a Series of Donor–π–Acceptor Cyanines with Different Conjugation Lengths. *J. Mater. Chem.* **2009**, *19*, 7503–7513.

(86) Kasatani, K.; Kawasaki, M.; Sato, H. Short-Wavelength Fluorescence Caused by Sequential Two-Photon Excitation of Some Cyanine Dyes: Effect of Solvent Viscosity on the Quantum Yields. *Chem. Phys.* **1984**, *83*, 461–469.

(87) Niklas, J.; Mardis, K. L.; Banks, B. P.; Grooms, G. M.; Sperlich, A.; Dyakonov, V.; Beaupré, S.; Leclerc, M.; Xu, T.; Yu, L.; et al. Highly-Efficient Charge Separation and Polaron Delocalization in Polymer-Fullerene Bulk-Heterojunctions: A Comparative Multi-Frequency EPR and DFT Study. *Phys. Chem. Chem. Phys.* **2013**, *15*, 9562–9574.

Chapter 5

Investigation of the Effect of Heteroatoms and Alkyl Side Chain on the Photophysical Performance of Donor-Acceptor Copolymers using Linear and Nonlinear Spectroscopic Techniques

5.1 Introduction

The design and development of new organic materials are central to the actualization of the commercialization of organic photovoltaic cells. Many organic compounds exist because of the ability of carbon to undergo catenation. In addition, other atoms and substituents like oxygen, sulphur, nitrogen among others can be incorporated to the main chain of these organic compounds. Organic polymers are important examples of organic compounds and they have been explored in the construction of organic photovoltaics.[1–5] Organic polymers based on repeating backbone unit of alternating electron-donating and electron-accepting moieties have been well investigated for organic photovoltaics because of their interesting optical and electronic properties especially wide spectral absorption and low bandgap.[6–11] The organic polymers having donor-acceptor backbone are able to lower the bandgap by making use of a "push-pull" mechanism where π electrons on the electron-rich donor moiety are drawn toward the neighboring electron-deficient moiety.[9,12,13] Electron delocalization and formation of mesomeric quinoid structures are achieved through the "push-pull" mechanism.[5,11,12,14–16]

Most high-performance polymers reported in the literature have thiophene and

thiophene heterocycles in their architectures.[11,17–23] Thiophene is a flat five-membered heterocyclic compound with the formula C_4H_4S. Thiophene has been explored in the development of organic photovoltaic materials because of its ability to increase conjugation along organic compounds through the stabilization of quinoidal structure.[24–26] Figure 5.1 shows the resonance stabilization effect of thiophene on polythiophene and poly(isothianaphthalene).[24] The early success in the development of efficient organic photovoltaics was observed in poly(3-hexylthiophene) which is a derivative of thiophene.[27–30] Other high-performing polymers, based on thiophene, have since been designed. One organic polymer that have been greatly explored in the development of organic photovoltaics is poly((4,8-bis[(2-ethylhexyl)oxy]benzo[1,2-b:4,5-b′]dithiophene-2,6-diyl)(3-fluoro-2-[(2-ethylhexyl)carbonyl]thieno[3,4-b]thiophenediyl)) (PTB7). The device with PTB7 as active material had an efficiency of 7.4%.[9,31]

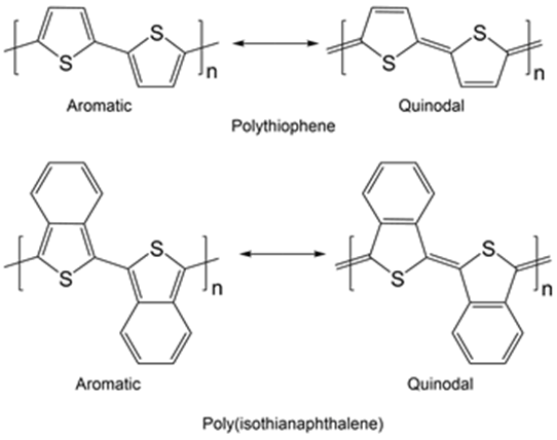

Figure 5.1 Resonance stabilization effect in thiophene-based compounds

Furan, which is an isoelectronic compound to thiophene, has several advantages over thiophene. Furan has an oxygen atom in place of sulphur of thiophene in a five-membered ring structure of thiophene. The smaller size of oxygen when compared to sulphur in thiophene

ensures that there is less steric repulsion between the heteroatom and the β-hydrogen atom in the adjacent ring. The small size of the oxygen heteroatom in furan ensures that the solution of furan-based polymers have better solubility than their thiophene-based analogs.[32–34] The improved solubility brought about by furan ensures that less bulky and shorter alkyl substituents are needed to improve solubility of furan-based organic polymers than in the case of their thiophene-based analogs.[34,35] Longer and bulky alkyl chains can help in the improvement of solubility of polymers but can also result in the distortion of intermolecular ordering and also affect the intermolecular charge transfer if they are not coplanar with the polymer backbone.[35,36] Therefore, incorporation of furan into the polymer chain can lead to enhancement of intermolecular charge transfer. Furan is less aromatic than thiophene and this property facilitates the ability of furan-based polymer to form quinoidal structure essential for stabilizing HOMO level.[37] Furan-based compounds are more rigid than their thiophene-based analogs. The rigidity in the backbone of furan-based compounds enhances planarity in their conjugated systems and contributes to good π-orbital overlap and effective electron delocalization.[33,37] These properties, in addition to biodegradability of furans, gives furan an edge over other competing building blocks of polymers.[37]

Although, furan has many advantages over thiophene as listed above, there have not been many synthesis of conjugated polymers from furan because of the difficulty involved in synthesizing furan-substituted conjugated compounds.[38] Furan has been used in place of thiophene in a number of dye-sensitized solar cells and results have been similar to those obtained for thiophene based compounds.[39,40] One of such dye-sensitized solar cells was designed with bis-dimethylfuorenyl amino benzo[b]furan by Jung *et al.* with a power conversion efficiency of 6.65%.[40] Furan-containing DPP-based polymers have been shown to

exhibit power conversion efficiency up to 5%.[34] Oligofuran-based organic solar cells have also been optimized to give open-circuit voltage of 0.73 V, a high short-circuit current of 9.1 mA cm^{-2} and a power conversion efficiency of 3.8%.[34]

In this study, the results of the spectroscopic study of conjugated polymers, based on 3,7-didodecyl-2,6-di(thiophen-2-yl)benzo[1,2-b:4,5-b′]difuran (BDF) as donor and either 3,6-di(2-furanyl)-1,4-diketopyrrolo[3,4-c]pyrrole (FDPP) or 3,6-di(2-thienyl)-1,4-diketopyrrolo[3,4-c]pyrrole (TDPP) as the acceptor, were presented. The synthesis of these conjugated polymers has earlier been reported by Kobilka *et al*.[38] As shown earlier, furan has some advantages over thiophene in the development of organic solar cell materials. Consequently, the building block of the donor group of these polymers was benzo[1,2-b:4,5-b′]difuran instead of the commonly used benzo[1,2-b:4,5-b′]dithiophene. Four different polymers with different linkages, which are either furan or thiophene, between BDF and DPP and different alkyl side chains to DPP were investigated. The alkyl side chains to DPP are 2-ethylhexyl and n-tetradecyl chains. The study gives insight to the effect of the replacement of thiophene by furan on the electronic and optical properties of conjugated polymers and ultimately the possible effect on the power conversion efficiency of organic solar cell. The influence of the size of the alkyl side chains on the intermolecular charge transfer of the polymers is also discussed. The structures of the investigated polymers are shown in Figure 5.2.

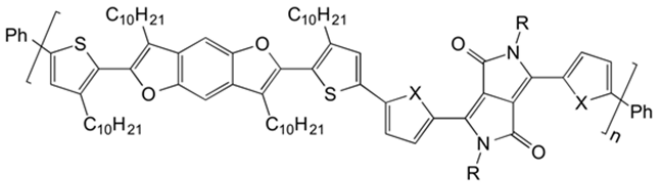

P1: X = O, R = 2-ethylhexyl
P2: X = O, R = *n*-$C_{14}H_{29}$
P3: X = S, R = 2-ethylhexyl
P4: X = S, R = *n*-$C_{14}H_{29}$

Figure 5.2 Structures of the investigated polymers based on BDF and DPP

5.2 Experimental Section

5.2.1 Materials

The synthesis of the four investigated polymers was carried out by Still cross-coupling reactions between benzodifuran and corresponding DPP and this has been reported by Kolbika *et al*.[38] The molecular weights were estimated using gel permeation chromatography with THF as eluent and the results are shown in Table 5.1. The samples were dissolved in spectroscopic grade choloroform (Sigma-Aldrich, spectrophotometric grade) before ultrafast measurements.

Table 5.1 Molecular weights for the polymers[38]

Polymer	M_w (kDa)	M_n (kDa)	PDI
P1	55.6	28.9	1.9
P2	44.2	19.9	2.2
P3	24.0	9.5	2.5
P4	8.1	6.1	1.3

5.2.2 Steady state measurements

The steady state measurements of the samples were carried out in solution phase. All

steady state measurements were carried out in 4 mm quartz cuvettes. The steady state absorption spectra were measurement with an Agilent 8432 UV-visible absorption spectrophotometer while the emission spectra measurements were carried out using Fluroromax-2 spectrophotometer. The steady state measurements were taken before and after each ultrafast measurement to confirm that there was no appreciable degradation during the measurements. The optical density was kept below 0.5 to avoid photon re-absorption.

5.2.3 Fluorescence lifetime measurements

The detail of the fluorescence set-up that was used to perform the time-resolved fluorescence measurements was provided in Chapter 2. The fluorescence lifetimes of the polymers were measured using the time-correlated single photon counting (TCSPC) method. The TCSPC method is capable of measuring fluorescence lifetimes in the time range of picosecond to nanosecond. Kapteyn Murnane (KM) Laboratories mode-locked Ti-sapphire laser pumped by Millenia V Nd:YVO_4 (Spectra Physics) was used to generate 800 nm pulsed beam. The output from KM laser had a pulse duration of 30 fs and a repetition rate of 90 MHz. The 800 nm output beam from the KM laser was frequency-doubled using β-barium borate crystal to obtain the 400 nm excitation beam. The excitation beam was directed to the polymer samples placed in a quartz cell with path length of 0.4 cm. The fluorescence beam is collected at right angle to the excitation beam. The detector is set such that only 1 photon per 100 excitation pulses can be measured. Once the excitation pulse gets to the sample, a signal is sent to the constant function discriminator (CFD) which measures the arrival time of the excitation beam. The signal sets up a voltage ramp which continues to rise until the fluorescence beam gets to the detector. The voltage signal is amplified and converted to a numerical value by the

analog-to-digital converter (ADC), which is stored in the appropriate time bin representing the time between the arrival of the excitation on the sample and arrival of the fluorescence beam on the detector. The process was repeated numerous times and the result was aggregated to generate the histogram of the decay process. The photomultiplier tube on the detector transmits the fluorescence to the computer through an interface card. The fluorescence result is displayed on the computer through the PicoQuant software. The PicoQuant Fluofit software is used to analyze and find the fluorescence decay times using exponential decay function.

5.2.4 Two-photon absorption measurements

The two-photon excitation fluorescence (TPEF) method was used to determine the two-photon absorption cross-sections of the polymers. The TPEF set-up consists of diode-pumped Mai Tai mode-locked Ti-sapphire oscillator (Spectra Physics) which was set to produce pulses at 860 nm and 100 fs duration. The average power from the laser was 2 W and the repetition rate was 80 MHz. The beam is directed through a variable neutral density filter into the polymer samples. The variable neutral density filter is used to control the power of the incident beam. The fluorescence is collected at the emission peak of each polymer sample at right angle direction to the excitation beam. The monochromator is used to select the desired fluorescence beam and the fluorescence is detected by a photomultiplier tube (R152P, Hamamatsu, Hamamatsu City, Japan). The detected photon is then sent to a computer for display via a photon-counting unit. The two-photon absorption cross-section of the polymer samples were calculated from the collected data by using a reference solution of Rhodamine B with known two-photon absorption cross-section.[41]

5.3 Results and Discussion

5.3.1 Steady state measurements

The steady state spectra of the polymers are shown in Figure 5.3 and the steady state properties are summarized in Table 5.2. All the four polymers had absorption spanning the visible spectrum. The polymers showed two distinct absorption bands. The high-energy band, which occurred at ~ 400 nm, can be attributed to localized π-π* transitions in the thiophene and furan rings present in the polymers. The broad, low energy band corresponds to intermolecular charge transfer between the BDF and the FDPP or TDPP. The absorption in the polymers containing FDPP (P1 and P2) had more intense absorption peaks than the polymers containing TDPP. The higher absorption intensity in FDPP-containing polymers can be attributed to reduced steric hindrance and repulsion in the FDPP compared to TDPP. Consequently, the conjugation in P1 and P2 containing FDPP is better than the conjugation in P3 and P4, resulting in a good intermolecular charge transfer from the donor to the acceptor. In addition, the size and bulkiness of the alkyl side chains can affect the spatial arrangement and ultimately the intermolecular charge transfer in the polymers. Long alkyl chains can contribute to improved solubility of polymers but can lead to poor intermolecular charge transfer due to poor π-π stacking. For both FDPP and TDPP-containing polymers, it was found that the polymers having 2-ethylhexyl side chain had more intense absorption than their corresponding polymers having n-tetradecyl side chain. Therefore, the maximum molar absorption coefficient of P1 was twice of the molar absorptivity coefficient of P2. Similar trend was also observed in P3 and P4 which contained the 2-ethylhexyl and n-tetradecyl side chains respectively. The switch between furan and thiophene as a linkage group was found to have a more significant effect on

the absorption properties of the polymers than the alkyl side chain. P1 with a furan linkage group had a maximum molar absorptivity coefficient that was five times greater than the maximum molar absorptivity coefficient of P3 having thiophene linkage group. Both P1 and P3 have 2-ethylhexyl side chain. On the other hand, the change in the alkyl side chain from 2-ethylhexyl to n-tertradecyl in P1 and P2 brought about only a reduction in the molar absorption coefficient by a factor of 2. There was a small red-shift in the absorption peak of the polymers as the linkage group in the polymers change from furan to thiophene. All four polymers exhibit shoulders in the absorption spectrum at the low-energy absorption bands at ~ 650 nm.

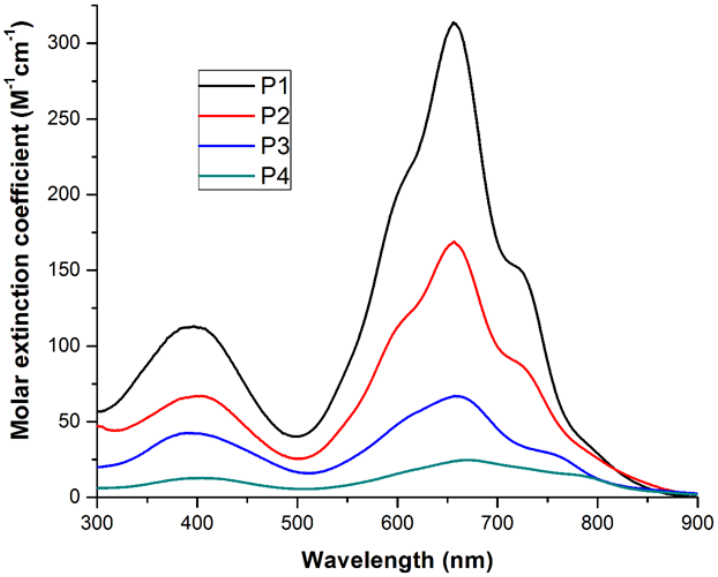

Figure 5.3 Absorption spectra of polymer samples

Table 5.2 Steady state properties of the polymers

Polymer	ε ($\times 10^4$) M^{-1} cm^{-1}	λ_{abs} (nm)	λ_{em} (nm)
P1	313	656	692
P2	168	656	692
P3	67	660	703
P4	24	670	695

The emission spectra of the polymers are shown in Figure 5.4. The primary emission peaks of the polymers occurred between 690 nm to 705 nm with the thiophene-based polymers having a slight red-shifted emission peaks relative to their furan-based analogs. There were secondary peaks at 525 nm and 550 nm for P3 and P4. There was no visible secondary emission peaks for the furan-based polymers. The absence of the secondary emission peaks in P1 and P2 may be an indication of an energy transfer between the BDF and FDPP. The difference in the emission behavior of FDPP- and TDPP- containing polymers can be attributed to the better conjugation in the FDPP-containing polymers which allow efficient electron delocalization and energy migration. The heteroatoms had more impact on the emission spectra than the alkyl side chains. The emission peak in P1 and P2, which contains FDPP but have different alkyl side chains, occurred at the same wavelength of 692 nm. On the other hand, there was a 10 nm red-shift between the emission peak of P1 and P3 having the same alkyl side chain of 2-ethylhexyl but different linkages of furan and thiophene.

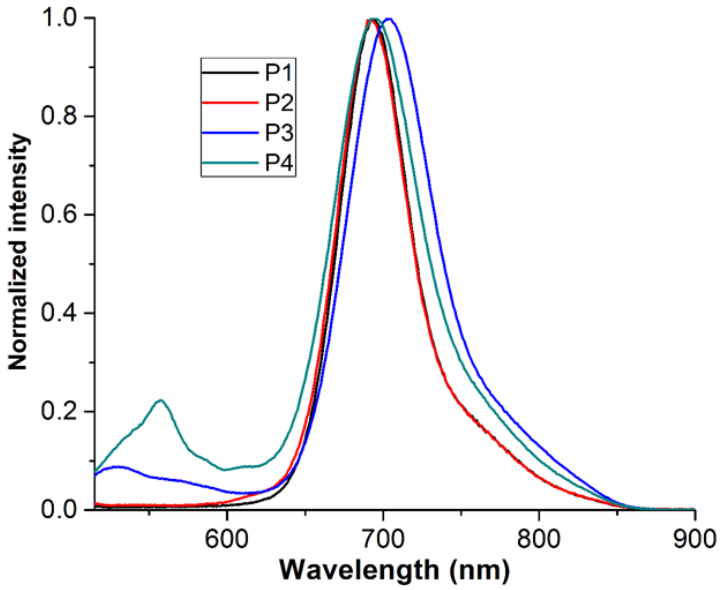

Figure 5.4 Emission spectra of the polymer samples

5.3.2 Time-resolved fluorescence measurements

The polymers samples were excited at 400 nm and the fluorescence dynamics were investigated at 700 nm. The fluorescence lifetimes were obtained by fitting the decay profile to an exponential decay function. As shown in Figure 5.5 and Table 5.3, the FDPP-containing polymers had longer fluorescence lifetimes than their TDPP-containing analogs. However, the effect of the heteroatoms on the fluorescence lifetimes is not as significant as the effect of the alkyl side chains. The relatively shorter lifetimes in polymers having n-tetradecyl side chain may be attributed to steric hindrance which distorts the π-π stacking in P2 and P4. This distortion in the π-π stacking provides a pathway for the depopulation of the excited states of P2 and P4.

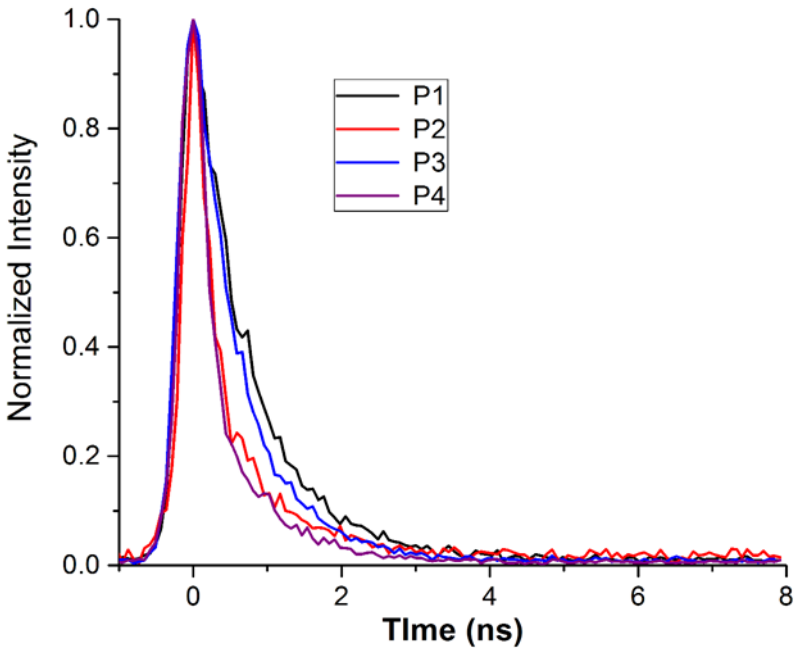

Figure 5.5 Decay dynamics of the polymer samples

Table 5.3 Fluorescence lifetimes of the investigated polymers

Polymer	Decay time (ps)
P1	757
P2	406
P3	628
P4	354

5.3.3 Two-photon absorption

The two-photon absorption cross-sections of the investigated polymers were measured using the two-photon emission fluorescence method. The method involves the comparison of the two-photon emission of the polymers samples with a reference standard with known two-photon properties. The reference sample used for the two-photon absorption study was

Rhodamine B.[41] The plot of the emission intensity to the power of the excitation beam was found to follow a quadratic dependence. The two-photon absorption cross-sections of P1, P2, P3 and P4 were 1405 GM, 1099 GM, 104 GM and 55 GM respectively. P1 was found to have significantly higher two-photon absorption than the other polymers. The high TPA of P1 can be attributed to the combined effect of low steric hindrance of 2-ethylhexyl (relative to n-tetradecyl) and better quinoid resonance structure-promoting qualities of furan over thiophene. The type of linkage between the electron-donating and electron-accepting units had a more significant impact on the two-photon absorption cross-section than the type of the alkyl side chain. As a result, P1 was found to have a greater TPA cross-section than P3 by more than a factor of 10. When only the alkyl side chain was changed in P1 from 2-ethylhexyl to n-tetradecyl to obtain P2, the TPA cross-section only decreased by less than a factor of 2.

Therefore, the two-photon absorption study on the polymers indicates that the replacement of thiophene by furan as linkage in organic polymers can bring about an enhancement in the two-photon absorption characteristic. The improvement is as a result of less steric hindrance between the oxygen heteroatom and the neighboring atoms when compared to the steric hindrance in thiophene. In addition, it was found that the longer the alkyl side chain to the DPP unit in the polymer, the lower the two-photon absorption cross-section. This can be attributed to the disruption of the π-π stacking by the alkyl group. Therefore, when adding alkyl side chain to improve solubility of polymers, it is essential to find the optimal size that will not significantly limits the two-photon absorption cross-section and ultimately the charge transfer ability of the polymer.

Table 5.4 Two-photon absorption cross-sections of the investigated polymers

Polymer	δ (GM)
P1	1405
P2	1099
P3	104
P4	55

5.4 Conclusions

Four polymers with BDF as electron donor and DPP as electron acceptor, with different linkages of thiophene and furan, were investigated to determine the effect of different heteroatoms and alkyl side chains on the optical and electronic properties of polymers. All the polymers were found to have a broad absorption that covered the visible spectrum. It was found that the replacement of thiophene by furan as linkage enhances the π-π stacking of the polymers. This was evident in the increase in the intensity of molar absorptivity coefficient and the two-photon absorption cross-section. The type of linkage (thiophene or furan) between the electron-donating BDF and electron-accepting DPP was found to have a more significant effect than the alkyl side chain on the DPP. The fluorescence lifetimes of the polymers were found to decrease as the size of the alkyl side chain increases. The effect of the furan or thiophene linkage was not as significant as that of the alkyl side chain on the fluorescence lifetimes. These results support the photovoltaic device performance of the polymers that was published by Kobilka *et al.*[38] P1 was found to have the best photovoltaic device performance, with a power conversion efficiency of 2.89 % with P2 not too far behind at 2.81%. P4 had the worst power conversion efficiency of 0.97%. Consequently, it can be concluded that the use of short

alkyl side chain and the use of furan to replace thiophene in organic polymers can improve photon absorption, two-photon-absorption ability and ultimately the photovoltaic performance of polymers.

References

(1) Bundgaard, E.; Krebs, F. Low Band Gap Polymers for Organic Photovoltaics. *Sol. Energy Mater. Sol. Cells* **2007**, *91*, 954–985.

(2) Zhan, X.; Zhu, D. Conjugated Polymers for High-Efficiency Organic Photovoltaics. *Polym. Chem.* **2010**, *1*, 409–419.

(3) Shrotriya, V. Organic Photovoltaics: Polymer Power. *Nat. Photon.* **2009**, *3*, 447–449.

(4) Dou, L.; You, J.; Hong, Z.; Xu, Z.; Li, G.; Street, R. A.; Yang, Y. 25th Anniversary Article: A Decade of Organic/Polymeric Photovoltaic Research. *Adv. Mater.* **2013**, *25*, 6642–6671.

(5) Li, G.; Zhu, R.; Yang, Y. Polymer Solar Cells. *Nat. Photon.* **2012**, *6*, 153–161.

(6) Cheng, W.; Wu, Z.; Wen, S.; Xu, B.; Li, H.; Zhu, F.; Tian, W. Donor–acceptor Copolymers Incorporating polybenzo[1,2-b:4,5-B′]dithiophene and Tetrazine for High Open Circuit Voltage Polymer Solar Cells. *Org. Electron.* **2013**, *14*, 2124–2131.

(7) Zhu, Z.; Waller, D.; Gaudiana, R.; Morana, M.; Muhlbacher, D.; Scharber, M.; Brabec, C. Panchromatic Conjugated Polymers Containing Alternating Donor / Acceptor Units for Photovoltaic Applications. *Macromolecules* **2007**, *40*, 1981–1986.

(8) Liu, Y.; Chen, C.-C.; Hong, Z.; Gao, J.; Michael Yang, Y.; Zhou, H.; Dou, L.; Li, G.; Yang, Y. Solution-Processed Small-Molecule Solar Cells: Breaking the 10% Power Conversion Efficiency. *Sci. Rep.* **2013**, *3*, 3356.

(9) Liang, Y.; Xu, Z.; Xia, J.; Tsai, S.-T.; Wu, Y.; Li, G.; Ray, C.; Yu, L. For the Bright Future-Bulk Heterojunction Polymer Solar Cells with Power Conversion Efficiency of 7.4%. *Adv. Mater.* **2010**, *22*, E135–E138.

(10) Xu, T.; Yu, L. How to Design Low Bandgap Polymers for Highly Efficient Organic Solar Cells. *Mater. Today* **2014**, *17*, 11–15.

(11) Liang, Y.; Feng, D.; Wu, Y.; Tsai, S.-T.; Li, G.; Ray, C.; Yu, L. Highly Efficient Solar Cell Polymers Developed via Fine-Tuning of Structural and Electronic Properties. *J. Am. Chem. Soc.* **2009**, *131*, 7792–7799.

(12) Duan, C.; Huang, F.; Cao, Y. Recent Development of Push–pull Conjugated Polymers for Bulk-Heterojunction Photovoltaics: Rational Design and Fine Tailoring of Molecular Structures. *J. Mater. Chem.* **2012**, *22*, 10416–10434.

(13) Kroon, R.; Lenes, M.; Hummelen, J. C.; Blom, P. W. M.; de Boer, B. Small Bandgap Polymers for Organic Solar Cells (Polymer Material Development in the Last 5 Years). *Polym. Rev.* **2008**, *48*, 531–582.

(14) Kleinhenz, N.; Yang, L.; Zhou, H.; Price, S. C.; You, W. Low-Band-Gap Polymers That Utilize Quinoid Resonance Structure Stabilization by Thienothiophene: Fine-Tuning of HOMO Level. *Macromolecules* **2011**, *44*, 872–877.

(15) Huang, Y.; Guo, X.; Liu, F.; Huo, L.; Chen, Y.; Russell, T. P.; Han, C. C.; Li, Y.; Hou, J. Improving the Ordering and Photovoltaic Properties by Extending Π-Conjugated Area of Electron-Donating Units in Polymers with D-A Structure. *Adv. Mater.* **2012**, *24*, 3383–3389.

(16) Liang, Y.; Luping, Y. A New Class of Semiconducting Polymers for Bulk Heterojunction Solar Cells with Exceptionally High Performance. *Acc. Chem. Res.* **2010**, *43*, 1227–1236.

(17) Goh, C.; Kline, R. J.; McGehee, M. D.; Kadnikova, E. N.; Fréchet, J. M. J. Molecular-Weight-Dependent Mobilities in Regioregular poly(3-Hexyl-Thiophene) Diodes. *Appl. Phys. Lett.* **2005**, *86*, 122110.

(18) Lu, Y.; Xiao, Z.; Yuan, Y.; Wu, H.; An, Z.; Hou, Y.; Gao, C.; Huang, J. Fluorine Substituted Thiophene–quinoxaline Copolymer to Reduce the HOMO Level and Increase the Dielectric Constant for High Open-Circuit Voltage Organic Solar Cells. *J. Mater. Chem. C* **2013**, *1*, 630–637.

(19) Umeyama, T.; Takamatsu, T.; Tezuka, N.; Matano, Y.; Araki, Y.; Wada, T.; Yoshikawa, O.; Sagawa, T.; Yoshikawa, S.; Imahori, H. Synthesis and Photophysical and Photovoltaic Properties of Porphyrin - Furan and - Thiophene Alternating Copolymers. *J. Phys. Chem. C* **2009**, *113*, 10798–10806.

(20) Ross, R. B.; Cardona, C. M.; Guldi, D. M.; Sankaranarayanan, S. G.; Reese, M. O.; Kopidakis, N.; Peet, J.; Walker, B.; Bazan, G. C.; Van Keuren, E.; et al. Endohedral Fullerenes for Organic Photovoltaic Devices. *Nat. Mater.* **2009**, *8*, 208–212.

(21) Brabec, C. J.; Durrant, J. R. Solution-Processed Organic Solar Cells. *MRS Bull.* **2008**, *33*, 670–675.

(22) Boudreault, P.-L. T.; Najari, A.; Leclerc, M. Processable Low-Bandgap Polymers for Photovoltaic Applications. *Chem. Mater.* **2011**, *23*, 456–469.

(23) Adegoke, O. O.; Ince, M.; Mishra, A.; Green, A.; Varnavski, O.; Mart, M. V.; Ba, P.; Goodson, T. Synthesis and Ultrafast Time Resolved Spectroscopy of Peripherally

Functionalized Zinc Phthalocyanine Bearing Oligothienylene-Ethynylene Subunits. *J. Phys. Chem. C* **2013**, *117*, 20912–20918.

(24) Cheng, Y.-J.; Yang, S.-H.; Hsu, C.-S. Synthesis of Conjugated Polymers for Organic Solar Cell Applications. *Chem. Rev.* **2009**, *109*, 5868–5923.

(25) Nithya, R.; Senthilkumar, K. Theoretical Studies on the Quinoidal Thiophene Based Dyes for Dye Sensitized Solar Cell and NLO Applications. *Phys. Chem. Chem. Phys.* **2014**, *16*, 21496–21505.

(26) Casado, J.; Ortiz, R. P.; Delgado, M. C. R.; Hernández, V.; Navarrete, J. T. L.; Raimundo, J.-M.; Blanchard, P.; Allain, M.; Roncali, J. Alternated Quinoid/aromatic Units in Terthiophenes Building Blocks for Electroactive Narrow Band Gap Polymers. Extended Spectroscopic, Solid State, Electrochemical, and Theoretical Study. *J. Phys. Chem. B* **2005**, *109*, 16616–16627.

(27) Urien, M.; Bailly, L.; Vignau, L.; Cloutet, E.; Cuendias, A. De; Wantz, G.; Cramail, H.; Hirsch, L.; Parneix, J.-P. Effect of the Regioregularity of Poly (3-Hexylthiophene) on the Performances of Organic Photovoltaic Devices. *Polym. Int.* **2008**, *57*, 764–769.

(28) Kim, Y.; Cook, S.; Tuladhar, S. M.; Choulis, S. A.; Nelson, J.; Durrant, J. R.; Bradley, D. D. C.; Giles, M.; McCulloch, I.; Ha, C.-S.; et al. A Strong Regioregularity Effect in Self-Organizing Conjugated Polymer Films and High-Efficiency Polythiophene:fullerene Solar Cells. *Nat. Mater.* **2006**, *5*, 197–203.

(29) Kline, R. J.; McGehee, M. D.; Kadnikova, E. N.; Liu, J.; Fréchet, J. M. J.; Toney, M. F. Dependence of Regioregular Poly (3-Hexylthiophene) Film Morphology and Field-Effect Mobility on Molecular Weight. *Macromolecules* **2005**, *38*, 3312–3319.

(30) Ma, W.; Kim, J. Y.; Lee, K.; Heeger, A. J. Effect of the Molecular Weight of Poly(3-Hexylthiophene) on the Morphology and Performance of Polymer Bulk Heterojunction Solar Cells. *Macromol. Rapid Commun.* **2007**, *28*, 1776–1780.

(31) Carsten, B.; Szarko, J. M.; Son, H. J.; Wang, W.; Lu, L.; He, F.; Rolczynski, B. S.; Lou, S. J.; Chen, L. X.; Yu, L. Examining the Effect of the Dipole Moment on Charge Separation in Donor-Acceptor Polymers for Organic Photovoltaic Applications. *J. Am. Chem. Soc.* **2011**, *133*, 20468–20475.

(32) Huo, L.; Zhang, S.; Guo, X.; Xu, F.; Li, Y.; Hou, J. Replacing Alkoxy Groups with Alkylthienyl Groups: A Feasible Approach to Improve the Properties of Photovoltaic Polymers. *Angew. Chem. Int. Ed.* **2011**, *50*, 9697–9702.

(33) Gidron, O.; Diskin-Posner, Y.; Bendikov, M. A-Oligofurans. *J. Am. Chem. Soc.* **2010**, *132*, 2148–2150.

(34) Woo, C. H.; Beaujuge, P. M.; Holcombe, T. W.; Lee, O. P.; Fréchet, J. M. J. Incorporation of Furan into Low Band-Gap Polymers for Efficient Solar Cells. *J. Am. Chem. Soc.* **2010**, *132*, 15547–15549.

(35) Yiu, A. T.; Beaujuge, P. M.; Lee, O. P.; Woo, C. H.; Toney, M. F.; Fréchet, J. M. J. Side-Chain Tunability of Furan-Containing Low-Band-Gap Polymers Provides Control of Structural Order in Efficient Solar Cells. *J. Am. Chem. Soc.* **2012**, *134*, 2180–2185.

(36) Piliego, C.; Holcombe, T. W.; Douglas, J. D.; Woo, C. H.; Beaujuge, P. M.; Fréchet, J. M. J. Synthetic Control of Structural Order in N-alkylthieno[3,4-C]pyrrole-4,6-Dione-Based Polymers for Efficient Solar Cells. *J. Am. Chem. Soc.* **2010**, *132*, 7595–7597.

(37) Gidron, O.; Bendikov, M. A-Oligofurans: An Emerging Class of Conjugated Oligomers for Organic Electronics. *Angew. Chem. Int. Ed.* **2014**, *53*, 2546–2555.

(38) Kobilka, B. M.; Hale, B. J.; Ewan, D.; Dubrovskiy, A. V.; Toby, L.; Ewan, M. D.; Nelson, T. L.; Duzhko, V.; Jeffries-EL, M. Influence of Heteroatoms on Photovoltaic Performance of Donor–acceptor Copolymers Based on 2,6-Di(thiophen-2-yl)benzo[1,2-b:4,5-B′]difurans and Diketopyrrolopyrrole. *Polym. Chem.* **2013**, *4*, 5329–5336.

(39) Li, R.; Lv, X.; Shi, D.; Zhou, D.; Cheng, Y.; Zhang, G.; Wang, P. Dye-Sensitized Solar Cells Based on Organic Sensitizers with Different Conjugated Linkers: Furan, Bifuran, Thiophene, Bithiophene, Selenophene, and Biselenophene. *J. Phys. Chem. C* **2009**, *113*, 7469–7479.

(40) Jung, I.; Lee, J. K.; Song, K. H.; Song, K.; Kang, S. O.; Ko, J. Synthesis and Photovoltaic Properties of Efficient Organic Dyes Containing the Benzo[b]furan Moiety for Solar Cells. *J. Org. Chem.* **2007**, *72*, 3652–3658.

(41) Xu, C.; Webb, W. W. Measurement of Two-Photon Excitation Cross Sections of Molecular Fluorophores with Data from 690 to 1050 Nm. *J. Opt. Soc. Am. B* **1996**, *13*, 481–491.

Chapter 6

Overall Summary and Future Direction

6.1 Overall summary

Researchers have spent enormous time and resources to develop new conjugated organic materials for solar cell applications. My dissertation focuses on using different spectroscopic techniques to understand the fundamental properties that can influence the performance of organic materials in photovoltaic devices. The dissertation sought answers to the effect of alteration of the structures of organic systems on their photophysical properties and ultimately their performance in organic photovoltaics. The effect of the alternation of substituent groups on ultrafast energy transfer and ultimately on performance in organic photovoltaics was investigated and presented in Chapter 3. Zinc phthalocyanine functionalized with oligothienylene-ethynylene subunits were studied to understand how the alteration of the substituents of an organic compound can lead to variation in the extent of ultrafast energy transfer. Zinc phthalocyanine with no attached substituents was used as a reference in the study. In Chapter 4, different organic polymers were studied to illustrate the effect of the alteration of conjugation and donor-acceptor groups on the photophysical properties of organic systems and ultimately performance of organic photovoltaics. PTB7 which is one of the most efficient polymers used in organic solar cell device was investigated using linear, nonlinear and ultrafast spectroscopic techniques and the results were compared to those of new conjugated

organic polymers based on thieno[2′,3′:5′,6′]pyrido[3,4-g]thieno[3,2-c]isoquinoline-5,11(4H,10H)-dione (TPTI) and fluorenedicyclopentathiophene dimalononitrile (FDCPT-CN) electron-accepting units. Chapter 5 highlighted the effect of alteration of heteroatoms and alkyl groups on the photophysical properties in organic systems and ultimately performance of organic photovoltaics. Donor-acceptor conjugated polymers based on electron-donating unit of 3,7-didodecyl-2,6-di(thiophene-2-yl)benzo[1,2-b:4,5-b′]difuran and electron-accepting unit of 1,4-diketopyrrolo[3,4-c]pyrrole were used for this study. The techniques that were used in the dissertation are the steady state spectroscopic method, two-photon absorption technique and time-resolved fluorescence technique. The steady state spectroscopic technique was able to reveal the absorption and fluorescence properties of the investigated organic materials. There were important properties that need to be met by organic compounds to be useful as solar cell active materials. Organic materials need to have good absorption over a wide spectral range of the visible spectrum, good charge transfer ability, low quantum yield, good charge carrier mobilities and good chemical and thermal stability. Important properties such as the absorption peak wavelength, molar extinction coefficient, and quantum yield were measured from the steady state measurements. The two-photon absorption technique provides information that can be processed to calculate the two-photon absorption cross-section. The magnitude of the two-photon absorption cross-section is related to the transition dipole moment. Large value of transition dipole moment is required for efficient charge transfer in organic molecule. The time-resolved fluorescence technique provides information about the dynamics of exciton decay and energy transfer between different states.

The background for the historical evolution of organic macromolecules for use as active materials in photovoltaic cell was presented in Chapter 1. The chapter focused on the

development of p-type and n-type semiconducting organic materials and how the efforts of the systematic design of new materials have led to an efficiency of ~ 12% in organic tandem solar cells.[1] The various spectroscopic techniques used in the dissertation were described comprehensively in Chapter 2. The theoretical background of concepts such as one-photon and two-photon absorption, and fluorescence process were provided. Chapter 3 contained the work on two dyads which consists of zinc phthalocyanine bearing oligothienylene-ethynylene subunits. Zinc phthalocyanine was selected because of its thermal and chemical stability. It has been widely investigated because of its usefulness in photodynamic and photovoltaic processes. Zinc phthalocyanine has a significant absorption in the near-infrared region of the solar spectrum. Zinc phthalocyanine, on the other hand, does not absorb photon significantly between 300 and 550 nm. Oligothiophenes are known to absorb light significantly in the region where zinc phthalocyanine does not absorb significantly. The two organic materials were combined through ethynylene linkage to produce two dyads. The dyads were synthesized to take advantage of complementary absorption in different spectral regions. The number of oligothiophene groups in each of the dyad was different, with one of the dyads having one group of oligothiophene and the other having three groups linked together by ethynylene linkages. The spectroscopic results of the dyads were compared with the results of the reference zinc phthalocyanine compound. The absorption spectra of the dyads indicated two bands – Q and Soret bands. The Q band was associated with the absorption from zinc phthalocyanine and oligothiophene in the dyads while the Soret band is a characteristic of the zinc phthalocyanine. The absorption of light by the dyads in the Q band was enhanced because of the attached oligothiophene to zinc phthalocyanine. Analysis of the absorption and fluorescence spectra of the dyads indicated an energy transfer from the oligothiophene group to

the zinc phthalocyanine. The energy transfer from the oligothiophene groups to zinc phthalocyanine in the dyads resulted in reduced fluorescence intensity between 300 and 550 nm and increased fluorescence intensity at the near-infrared region. The extent of the energy transfer was found to increase as the number of oligothiophene group increases. From the fluorescence lifetime measurements, it was found that the energy transfer took place within a time frame of 300 fs. Photovoltaic studies on the dyads, however, showed that the reference zinc phthalocyanine had a better solar cell performance than the dyads. The unexpected poor photovoltaic performance of the dyads can be due to a possible recombination of charge carriers in the dyads as was evidenced in a lower short circuit current compared to the device fabricated from reference zinc phthalocyanine. This study showed that addition of substituents to organic compounds can be used to influence ultrafast energy transfer process and possibly improve performance of the organic systems in organic photovoltaics if the problem of recombination can be overcome.

In Chapter 4, four promising organic polymers based on TPTI and FDCPT-CN monomers were studied to understand structure-function relationship in the polymers. The reference compound for the study was PTB7 which has been well-studied and still remains one of the best performing organic polymers for use as active material in solar cell device. For the TPTI-based polymers, the voltammetry study reveals that the HOMO was localized in the TPTI co-monomer of the polymer because similar values were obtained for the HOMO energy level of the TPTI-based organic polymers. The conclusion from the voltammetry result was confirmed by the electronic structure calculation implemented in GAMESS where the HOMO showed bias shift towards the TPTI moiety in the monomer of the organic polymers. PECN and PTB7 had absorption that extended to the near-infrared region of the solar spectrum. The

absorption band of PECN covered spectral window between 300 nm to 900 nm while the reference PTB7 had an absorption band that covered the spectral band between 300 nm to 800 nm. They were also the polymers with the most intense absorption peak. The maximum molar extinction coefficients of PTB7 and PECN were 3.40×10^6 and 1.38×10^6 $M^{-1}cm^{-1}$ while the other polymers (PNSW, PNTPD and PNPDI) had maximum molar extinction coefficients ~ 4.0×10^5 $M^{-1}cm^{-1}$. Among the investigated polymers, PECN and PTB7 had the greatest two-photon absorption cross section. The two-photon absorption cross-sections of PECN and PTB7 were measured as 19.0×10^4 and 9.6×10^4 GM respectively while the other polymers, PNSW, PNTPD and PNPDI, had two-photon absorption cross-sections of 3.3×10^4, 2.9×10^4 and 4.84×10^4 GM respectively. As a result of the study, it can be concluded that PECN and PTB7 were the best polymers for application in organic photovoltaics because of the good photon absorption and high two-photon cross-section which is related to effectiveness of charge transfer. PECN and PTB7 have alternating donor-acceptor repeating units as backbone unlike the other polymers which have electron-accepting units of different degrees coupled together as their backbones. The push-pull effect of the donor-acceptor backbone of PECN and PTB7 enhanced effective charge transfer and can be attributed for the observed wide spectral absorption band and two-photon absorption cross-section that were obtained in this study. Therefore, the results of this study suggest that PECN will be a good candidate as active material in organic photovoltaic system.

The effect of alteration of heteroatoms and alkyl group on the photophysical properties of organic polymers and ultimately performance of the organic systems in organic photovoltaics was investigated in Chapter 6. The photophysical properties of donor-acceptor

copolymers based on 3,7-didodecyl-2,6-di(thiophene-2-yl)benzo[1,2-b:4,5-b′]difuran (BDF) as electron donor and 1,4-diketopyrrolo[3,4-c]pyrrole (DPP) as electron-acceptors were investigated. BDF and DPP were connected together by different linkages of furan and thiophene to be able to study the effect of different heteroatoms of oxygen and sulphur on optical and electronic properties. Oxygen and sulphur are isoelectronic atoms with similar properties. In addition, different alkyl side chains of 2-ethylhexyl and n-tetradecyl were attached to the DPP. The different alkyl side chains was used to determine the trade-off between improvement of solubility of polymers and the distortion of π-π stacking as the length of the alkyl side chain increases. The results of the study show that the linear absorption and nonlinear absorption properties are enhanced when thiophene linkage in the polymers is replaced by furan. This can be attributed to the reduction of the steric hindrance due to the presence of a smaller oxygen atom in the furan relative to larger sulphur in thiophene. The rigidity and planarity of furan ensures that there is a better conjugation in the polymers containing furan which enhances charge transfer in the polymers. In addition to the effect of the different linkages, it was also found that the molar absorptivity and two-photon absorption cross-section decrease as the length of the alkyl side chain increases. These results were in agreement with the photovoltaic studies. The polymer with furan linkage and 2-ethylhexyl side chain had the highest power conversion efficiency of 2.89% while the polymer having thiophene linkage and n-tetradecyl side chain had the lowest power conversion efficiency of 0.97%. The result indicates the replacement of thiophene with furan can enhance the electronic and optical properties of polymers and ultimately the device photovoltaic performance. In addition, when adding alkyl side chain to enhance solubility, it is necessary to find the optical size of the alkyl group that will not distort the π-π stacking in the polymer backbone.

6.2 Future direction

The measurements in the dissertation were carried out in solution phase. Organic photovoltaic cells are made in thin films. In thin films, the molecules of the organic materials are tightly packed and there exists a better interaction between the molecules than in the liquid phase. It is therefore essential to study the spectroscopic behaviors of the organic materials in thin films. It had been reported previously that there could be a difference in the absorption spectra of organic molecules in film and in solution.[2,3] The method of preparation of thin films is crucial to the PCE in photovoltaic cells because of the influence of the morphology of the thin layer. The effect of the solvent used in making the film, annealing time and temperature can influence the PCE of the photovoltaic cell.[4–7] It is necessary to characterize the organic materials in solid state using the steady-state technique, the time-resolved fluorescence measurement and the two-photon absorption technique. The results obtained from the solid-state measurement will give a better indication of the performance of the organic materials when used on organic photovoltaic cells.

Solvent used in dissolving organic samples can be crucial to their photophysical behaviors. Organic materials behave differently in different organic solvents. Some organic materials can form aggregates when put in certain solvents and this can lead to a drastic change in photophysical performance.[8,9] In addition, the morphology of thin films in organic solar cells has been modified by using different solvents. It is therefore expedient to study solvent effect on the photophysical behavior of the investigated organic materials. Effect of the different solvents on the one-photon absorption, two-photon absorption and fluorescence properties can give indications of the best solvent that can ensure effect mobility and charge transfer properties in organic photovoltaic cells.

Molecular orbital calculation is fast becoming an essential tool in the development of new materials because of the rapid development in the computational technology over the years. The electronic structure calculation was carried out in this study but it was limited to only the monomers. The electronic and optical properties of organic molecules vary with the number of monomers. Therefore, it is essential to carry out the electronic structure calculation for larger number of monomers. This will require more computational memory space and power. The number of monomers making up the conjugation unit can be estimated from the electronic structure calculation. The length and the number of monomers in the conjugation unit play important role the in the linear and nonlinear properties of the polymers. More rigorous computational approach will be required in the modeling of electronic structure of the polymers. The density functional theory with Becke-Lee-Yang-Parr (B3LYP) functionality has been used in the literature for the study of complex molecules.[10,11] This can be the basis of further study on the investigated polymers.

References

(1) http://www.heliatek.com/newscenter/latest_news/neuer-weltrekord-fur-organische-solarzellen-heliatek-behauptet-sich-mit-12-zelleffizienz-als-technologiefuhrer/?lang=en#. Heliatek consolidates its technology leadership by establishing a new world record for organic solar technology with a cell efficiency of 12%.

(2) Hou, J.; Chen, H.-Y.; Zhang, S.; Li, G.; Yang, Y. Synthesis, Characterization, and Photovoltaic Properties of a Low Band Gap Polymer Based on Silole-Containing Polythiophenes and 2,1,3-Benzothiadiazole. *J. Am. Chem. Soc.* **2008**, *130*, 16144–16145.

(3) Carsten, B.; Szarko, J. M.; Son, H. J.; Wang, W.; Lu, L.; He, F.; Rolczynski, B. S.; Lou, S. J.; Chen, L. X.; Yu, L. Examining the Effect of the Dipole Moment on Charge Separation in Donor-Acceptor Polymers for Organic Photovoltaic Applications. *J. Am. Chem. Soc.* **2011**, *133*, 20468–20475.

(4) Kadem, B. Y.; Al-hashimi, M. K.; Hassan, A. K. The Effect of Solution Processing on the Power Conversion Efficiency of P3HT-Based Organic Solar Cells. *Energy Procedia* **2014**, *50*, 237–245.

(5) Etzold, F.; Howard, I. A.; Forler, N.; Cho, D. M.; Meister, M.; Mangold, H.; Shu, J.; Hansen, M. R.; Müllen, K.; Laquai, F. The Effect of Solvent Additives on Morphology and Excited-State Dynamics in PCPDTBT:PCBM Photovoltaic Blends. *J. Am. Chem. Soc*. **2012**, *134*, 10569–10583.

(6) Kumar, V.; Kumar, V.; Som, S.; Yousif, A.; Singh, N.; Ntwaeaborwa, O. M.; Kapoor, A.; Swart, H. C. Effect of Annealing on the Structural, Morphological and Photoluminescence Properties of ZnO Thin Films Prepared by Spin Coating. *J. Colloid Interface Sci.* **2014**, *428*, 8–15.

(7) Ray, B.; Nair, P. R.; Alam, M. A. Annealing Dependent Performance of Organic Bulk-Heterojunction Solar Cells: A Theoretical Perspective. *Sol. Energy Mater. Sol. Cells* **2011**, *95*, 3287–3294.

(8) Nguyen, T.-Q.; Doan, V.; Schwartz, B. J. Conjugated Polymer Aggregates in Solution: Control of Interchain Interactions. *J. Chem. Phys.* **1999**, *110*, 4068–4078.

(9) Luzio, A.; Criante, L.; D'Innocenzo, V.; Caironi, M. Control of Charge Transport in a Semiconducting Copolymer by Solvent-Induced Long-Range Order. *Sci. Rep.* **2013**, *3*, 3425.

(10) Wheeler, D. E.; Rodriguez, J. H.; McCusker, J. K. Density Functional Theory Analysis of Electronic Structure Variations across the Orthoquinone/Semiquinone/Catechol Redox Series. *J. Phys. Chem. A* **1999**, *103*, 6282–6282.

(11) Osikowicz, W.; Friedlein, R.; De Jong, M. P.; Sorensen, S. L.; Groenendaal, L.; Salaneck, W. R. Site-Specific Electronic Structure of an Oligo-Ethylenedioxythiophene Derivative Probed by Resonant Photoemission. *New J. Phys.* **2005**, *7*, 104.